UNIVERSITY OF GENOA
POLYTECHNIC SCHOOL

DIME – Department of Mechanical, Energy, Management and Transportation Engineering

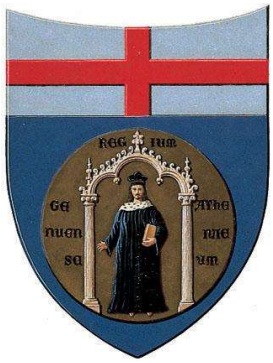

Ph.D. in Marine and Science Technologies
MACHINERY AND ENERGY SYSTEMS FOR THE SEA

PhD Thesis
XXXVI cycle

"Influence of pressurization for fuel cell systems fed with alternative fuels for maritime applications"

Supervisors:

Prof. Ing. Loredana Magistri

Prof. Ing. Aristide F. Massardo

Co-Supervisors:

Ing. Daria Bellotti

Candidate:

Federico Iester

June 2024

Abstract

The maritime sector, characterized by its reliance on conventional fossil fuels, is undergoing a decarbonization process towards cleaner and more sustainable energy sources. This thesis investigates the potential utilization of fuel cells as alternative energy power systems for maritime applications, with a particular emphasis on both low-temperature Proton Exchange Membrane Fuel Cells (PEMFC) and high-temperature Solid Oxide Fuel Cells (SOFC).

The study begins with a comprehensive review of the current composition of power energy systems in the maritime field, analysing existing propulsion systems and their environmental impact. To complete this first part, the software HELM (developed by the Thermochemical Power Group) was adopted to carry out a multicriteria analysis on few case studies to have a better understanding on the range of applicability of these innovative technologies.

The work includes the simulation of the fuel cells system through numerical models to evaluates the feasibility, advantages, and challenges associated with integrating PEMFC and SOFC systems into maritime vessels. Special attention is given to the study of pressurization of both PEMFC and SOFC systems. The performance of the system increases but the complexity of the BoP, the costs and the volumes and weights are influenced negatively. The pressurization is achieved for both cases, hybridizing the fuel cell with a turbocharger.

The PEMFC-TC system was analysed using the commercial software GT-Power while the SOFC was investigated with the use of TRANSEO which relies on MATLAB-Simulink.

The actual state of art for SOFC provides for the use of methane that is converted with a reforming process into hydrogen but in the recent years other hydrocarbons or hydrogen carriers are considered as alternative fuels. The last chapter of this thesis explores the potential of utilizing innovative fuels such as ammonia in SOFC systems. The feasibility and advantages of using ammonia

as a fuel source are examined, considering its potential for reducing greenhouse gas emissions relying on the fact that its production is widely diffused.

Overall, this thesis contributes to the research on alternative systems that will be part of the energy mix of the next years to reach the emissions limits imposed by regulations for a more sustainable maritime transportation by offering a comprehensive analysis of the opportunities and challenges associated with fuel cell technologies in this field.

Contents

Abstract II
Nomenclature VI
1 Introduction 10
1.1 Maritime transport sector 10
1.2 Alternative Fuels 17
Liquefied Natural Gas (LNG) 17
Methanol (CH_3OH) 19
Hydrogen (H_2) 21
Ammonia (NH_3) 25
1.3 Fuel Cells 28
1.4 Preliminary analysis: multi-criteria comparison 32
Algorithm description 34
Database implementation 41
Simulation results 48
1.5 Concluding remarks 59
2 Pressurization of a PEMFC 60
2.1 Commercialized models of PEMFC 62
2.2 Plant layout 63
PEMFC – TC system layout 66
Atmospheric PEMFC system layout 68
Control system 70
2.3 Commercial software for dynamic simulations: GT-Power 72
Custom component creation 74
2.4 Model description 79
PEMFC 80
Cathode circuit 81
Anode circuit 83
Cooling circuit 85
Modelling assumption for atmospheric PEMFC 86
2.5 Result and comparison 87
2.6 Concluding remarks 96
3 Pressurization of SOFC 98
3.1 Commercialized models of SOFC 102
3.2 Plant layout 104
3.3 TRANSEO tool for dynamic simulation 108
3.4 Model description 110
Fuel supply system 110
SOFC stack 112
Ejector 116
Air supply system 117
Control system 118
Power control system 119
Temperature control system 120

Storage system 121
Validation 122
3.5 Results 123
GT-Power results for pressurized SOFC model 127
4 Ammonia SOFC 136
4.1 Literature review 137
4.2 Layout analysis 141
4.3 Model description 147
4.4 Results 153
4.5 Ammonia compatibility with materials 160
4.6 Concluding remarks 161
5 Conclusions 163
Bibliography 165

Nomenclature

Abbreviations and Acronyms

AFC	Alkaline fuel cell
APH	Air pre-heater
BL	Blower
BoP	Balance of Plant
BV	Bleed valve
CBV	Cold bypass valve
CHP	Combined heat and power
DMFC	Direct methanol fuel cell
ECA	Emission control Area
EM	Electric Motor
EU	European Union
FPH	Fuel pre-heater
GHG	GreenHouse Gasses
HE	Heat Exchanger
HELM	Helper for Energy Layouts for Maritime applications
HFO/FO	Heavy Fuel Oil
HVO	Hydrotreated Vegetable Oil
ICE	Internal Combustion Engine
IMO	International Maritime Organization
LBG	Liquid Biogas
LNG	Liquefied Natural Gas
MCFC	Molten carbonate fuel cell
MDO	Marine Diesel Oil
MGT	Micro gas turbine
NZE	Net Zero Emission
OGB	Off-gas burner
PAFC	Phosphoric acid fuel cell
PEMFC	Proton exchange membrane fuel cell

REC	Recuperator
REF	Reformer
RV	Recirculation valve
SCB	Side Channel Blower
SCR	Selective Catalytic Reduction
SMR	Steam methane reforming
SOFC	Solid oxide fuel cell
TC	Turbocharger
TPG	Thermochemical power group
TRL	Technology Readiness Level
WGS	Water gas shift
WGV	Wastegate valve

Variables

A	Area [m^2]
$A_{HE,el}$	Discretization element heat exchange area [m^2]
C_{dis}	Ejector discharge coefficient (primary duct) [-]
c	Velocity [m/s]
c_p	Specific heat at constant pressure [J kg^{-1} K^{-1}]
$c_{p,mol}$	Molar specific heat [J mol^{-1} K^{-1}]
c_s	Specific heat of solid material [J kg^{-1} K^{-1}]
c_v	Specific heat at constant volume [J kg^{-1} K^{-1}]
D	Gas diffusivity [m^2 s^{-1}]
D_h	Hydraulic diameter [m]
E	Energy [J mol^{-1}]
F	Faraday constant [C mol^{-1}]
FO	fractional opening [-]
f	Friction factor [-]
ΔG	Gibbs free energy change on overall reaction [J mol^{-1}]
ΔG^0	Standard Gibbs free energy change on overall reaction [J mol^{-1}]
H	Enthalpy [J kg^{-1}]

ΔH	Overall reaction enthalpy change [J mol^{-1}]
h	Convective heat coefficient [W m^{-2} K^{-1}]
i_{cell}	Fuel cell electric current [A]
j_0	Exchange electric current density [A m^{-2}]
j_{cell}	Fuel cell electric current density [A m^{-2}]
K^{eq}	Reaction equilibrium constant [-]
K_p	Surge margin [-]
L	Length [m]
LHV	Lower heating value [J kg^{-1}]
l	Pressure loss coefficient [-]
M	Mass [kg]
$\dot{m}$	Mass flow rate [kg/s]
N_{cells}	Number of cells in the SOFC stack [-]
Nu	Nusselt number [-]
n_e	Number of electrons transferred in the electrochemical reaction [-]
P	Power [W]
p	Pressure [Pa]
p_X	Partial pressure of the substance X [Pa]
Pr	Prandtl number [-]
Δq	Heat exchange [W]
$\dot{q}$	Heat flux [W]
R	Overall reaction rate [mol s^{-1}]
Re	Reynolds number [-]
R_g	Gas constant [J mol^{-1} K^{-1}]
R_{sg}	Specific gas constant [J kg^{-1} K^{-1}]
RR	Recirculation ratio [-]
r	Reaction rate [mol m^{-3} s^{-1}]
S/C	Steam to carbon ratio [-]
T	Temperature [K]
ΔT	Temperature gradient [K]
t	Thickness [m]

U_f	Fuel utilization factor [-]
V_{Nernst}	Nernst ideal electric potential [V]
V_{real}	Fuel cell real electric potential [V]
ΔV	Fuel cell electric potential loss [V]
X	Molar fraction [-]
x	Cell coordinate [m]
ß	Pressure ratio [-]
ɣ	Activation losses coefficient [A m^{-2}]
η	Efficiency [-]
κ	Concentrated pressure losses coefficient [-]
Λ	Volume [m^3]
λ	Thermal conductivity [W m^{-1} K^{-1}]
ν	Stoichiometric coefficient [-]
μ	Dynamic viscosity [Pa·s]
ρ	Density [kg/m^3]
τ	Time [s]
Ψ	Concentrated pressure losses coefficient [-]
Ω	Section area [m^2]

1 Introduction

1.1 Maritime transport sector

The maritime industry plays a pivotal role in global trade and transportation, connecting nations and facilitating the movement of goods worldwide. However, this essential sector is also a significant contributor to environmental challenges, particularly through emissions that impact air quality and climate change. In recent years, there has been a growing recognition of the urgent need to address these environmental impacts by reducing emissions and transitioning towards decarbonization.

Lots of efforts to reduce emissions are in progress in all the fields of application. The ambitious aim of the European Green Deal, a package of policies introduced by the European Commission in 2019, is to replace fossil fuel power plants with renewable energy sources to achieve zero net greenhouse gas emissions inside the EU by 2050 [1]. The EU will move toward a circular, climate-neutral, and sustainable economy thanks to the Green Deal [2]. Regarding maritime transport, it has experienced extremely rapid growth in recent decades. Since the 1990s, the slope of the curve describing the mass of goods transported has become extremely important, having almost tripled in thirty years, with a consequent increase in emissions produced by maritime transport (*Figure 1*). It can be noted that the CO_2 emissions produced currently represent approximately 2% of the total emissions produced by humans throughout the world (*Figure 2*).

The most recent data indicates that it is having an increasing influence as well, with GHG emissions rising from 977 million tons in 2012 to over 1.1 billion tons in 2018 (+9.6%) [3]. In 2022, CO_2 emissions from transport in general increased by 3%, driven by a rebound from the COVID-19 pandemic [4]. To achieve Net

Zero Emissions (NZE) by 2050, transport emissions need to decrease by over 3% annually until 2030, requiring strong regulations, fiscal incentives, and infrastructure investment [5].

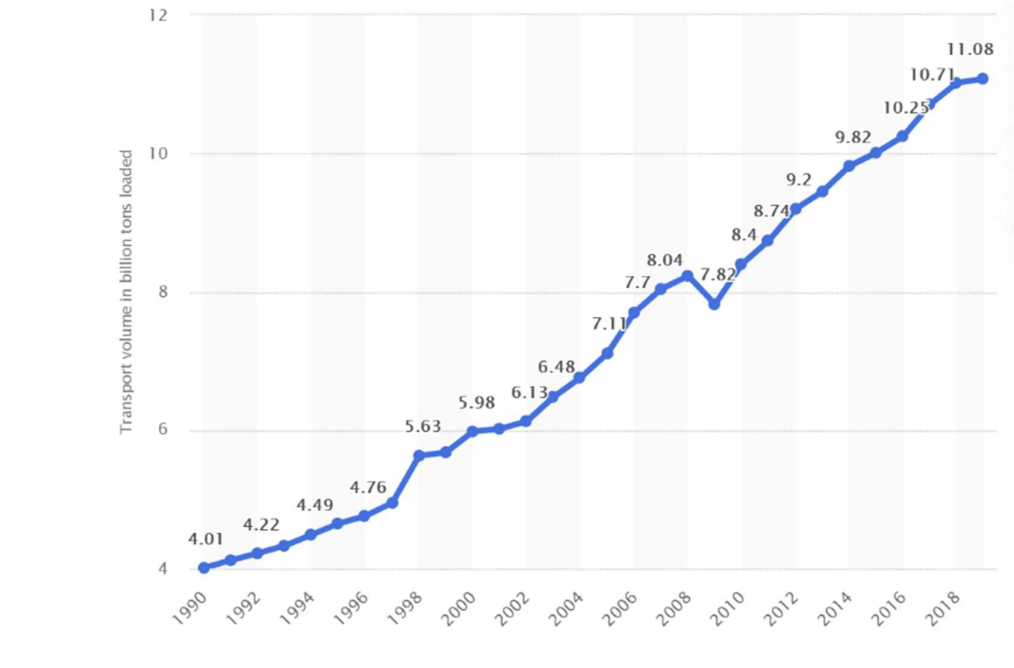

Figure 1. *Volume of goods transported annually by sea in billions of tons* [6].

Shipping, historically reliant on oil-based fuels, needs to transition to alternative fuels like biofuels, hydrogen, and electricity. Internal combustion engines (ICEs), powered by high-polluting fuel oils (heavy fuel oil, or MDO), account for nearly all (99.5%) of operating maritime vessels today [7]. Maritime shipping must maintain emissions until 2025 and then decrease them to meet NZE by 2050. Targets include the need for legally binding measures to achieve net zero emissions by 2050, technological innovation, and collaborative efforts of the main producers of the sector. International shipping accounted for 2% of global energy-related CO_2 emissions in 2022. The International Maritime Organization's revised targets align with the Paris Agreement, but enforceable measures are necessary for implementation to meet NZE goals [8].

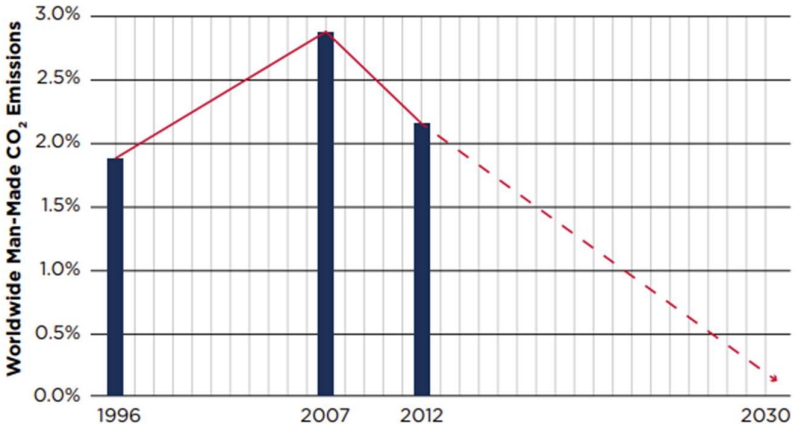

Figure 2. *Emissions due to maritime transport expressed as a percentage of total emissions produced by man* [6].

Given the high cost and limited availability of carbon-neutral fuels, the maritime sector must explore every possibility to achieve its decarbonization objectives. The 2020s are fundamental for the shipping industry's efforts to reduce emissions, with regulations from organizations such as the IMO and EU. Industry stakeholders are thus compelled to take action now, shaping the trajectory of decarbonization for years to come. The latest Maritime Forecast to 2050 delves into the implications of recent regulatory developments while outlining the potential evolution of a carbon-neutral fuel ecosystem.

In July 2023, the International Maritime Organization (IMO) finalized the first update to its greenhouse gas (GHG) strategy (*Figure 3*), significantly elevating the targets for global shipping in comparison to the original objective of achieving a 50% reduction in GHG emissions by 2050. Using 2008 as a reference point, the revised strategy now sets forth goals to decrease well-to-wake GHG emissions by 20% by 2030, by 70% by 2040, and ultimately achieve net-zero emissions by 2050 [3].

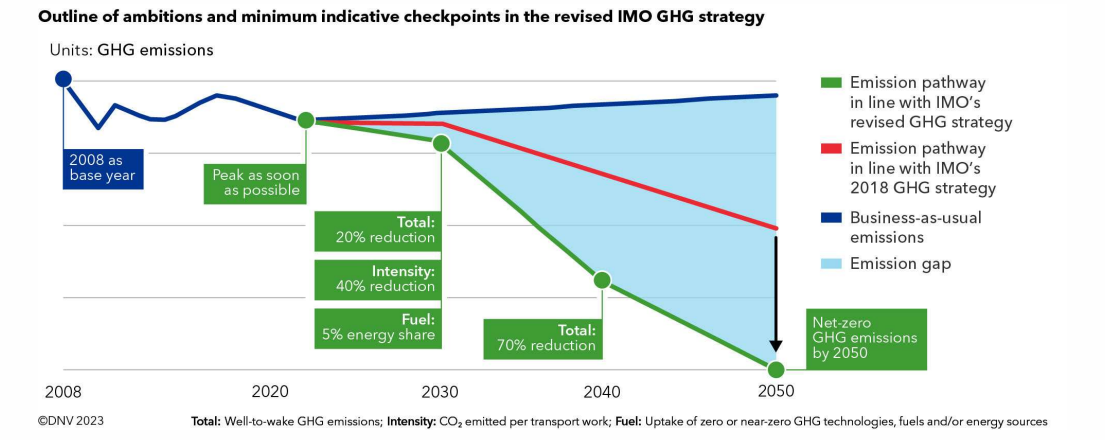

Figure 3. *Outline of ambitions and minimum indicative checkpoints in the revised IMO GHG strategy* [3].

To meet this requirement, the use of alternative fuels is mandatory, and in this direction, the production of carbon-neutral fuel should follow the goal reported in Figure 4. The statistics reveal that shipping would need 30-40% of the estimated global supply of carbon-neutral fuels to meet expected demand of 17 Mtoe per year by 2030, considering the IMO's current GHG strategy [3].

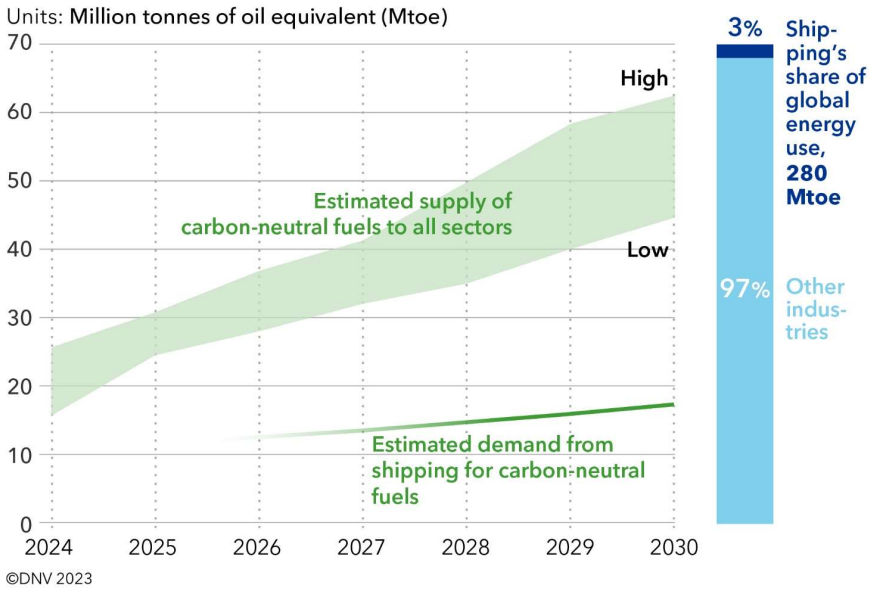

Figure 4. *Cross-sector supply of carbon-neutral fuels vs. total shipping demand* [3].

Forecasts regarding the mix of alternative fuels used in the maritime sector indicate that more and more vessels will use systems with reduced polluting emissions as shown in *Figure 5*.

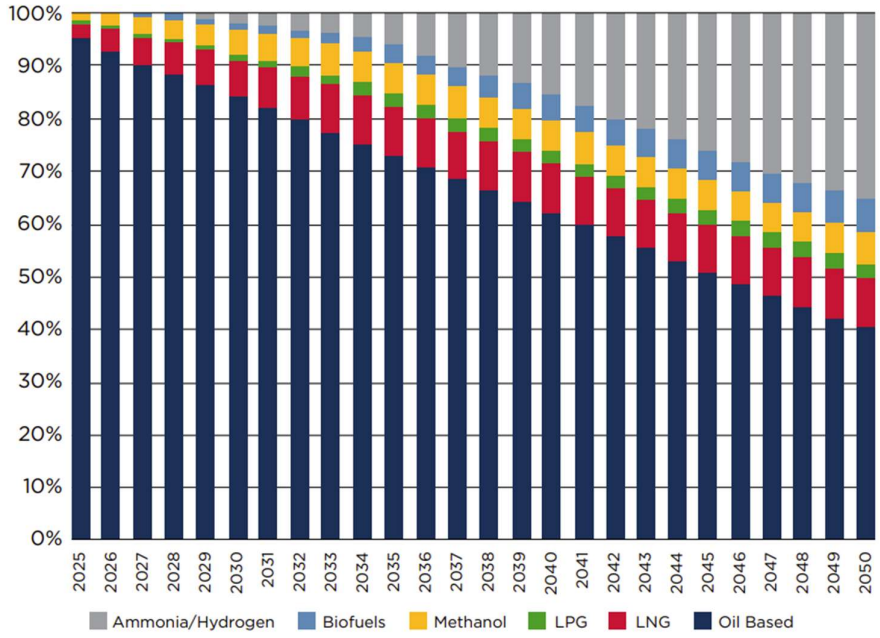

Figure 5. *Forecast on the use of each fuel in the maritime sector until 2050* [6].

LNG is undoubtedly the most widespread alternative technology now, with costs that are not excessive when compared to traditional generation technologies. Methanol and biofuels, on the other hand, have the great advantage of being a fuel for which relatively low-cost retrofits are possible for conventionally powered ships. For this reason, these two fuels are expected to grow in the maritime sector as fuel oil vessels are converted.

Finally, ammonia and hydrogen represent a technology that is currently under development but is extremely promising for the future. Undoubtedly, the need

to review the distribution network and engines to exploit these fuels makes their adoption slower. Currently, dual fuel engines are establishing themselves on the market: generally, these engines can operate by burning FO (Fuel Oil) or natural gas, or, in some cases, methanol.

In addition, to adopting carbon-neutral fuels, it's important to keep improving energy power systems in terms of efficiency and to develop new innovative technologies for fuel production and carbon capture systems. Furthermore, in the last year, fuel cells have aroused lot of interest since they can operate at zero emissions [9]. This feature is fundamental for the maritime sector since the transport of after-treatment systems can take wide volume and weight.

Moreover, the IMO has imposed limits on NO_x and SO_x emissions. Three Tiers have been defined for NO_x based on the maximum operating speed of the engine according to *Table 1*. In *Figure 6* the three Tiers are plotted as a function of the rated engine speed. For SO_x, however, the limit imposed in 2020 provides for a maximum of 0.5% of SO_x and particulate matter in the exhaust fumes for non-ECA areas, and 0.1% for ECA (Emission Control Area) areas [8].

Table 1. *MARPOL Annex VI NO_x emission limits.*

Tier	Date	NOx Limit, g/kWh		
		n < 130	130 ≤ n < 2000	n ≥ 2000
Tier I	2000	17.0	$45 \cdot n^{-0.2}$	9.8
Tier II	2011	14.4	$44 \cdot n^{-0.23}$	7.7
Tier III	2016†	3.4	$9 \cdot n^{-0.2}$	1.96
† In NOx Emission Control Areas (Tier II standards apply outside ECAs).				

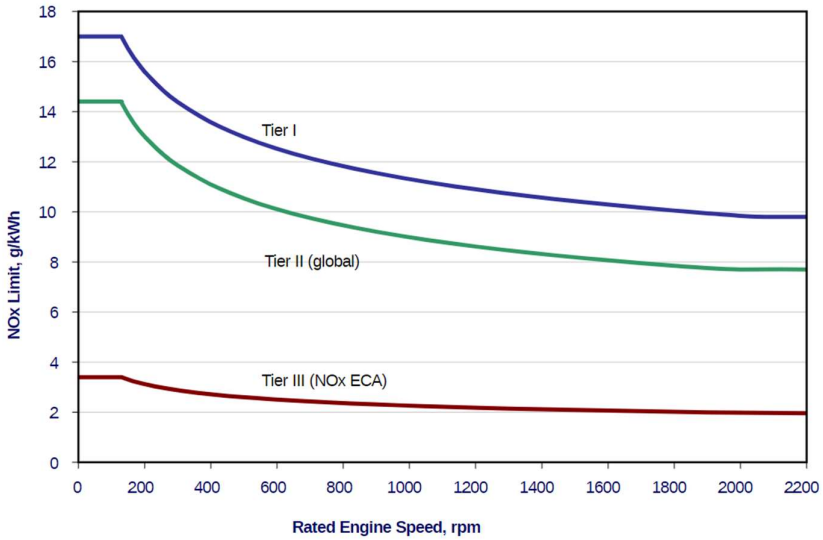

Figure 6. *NO_x emissions limits for the different Tiers.*

There are currently four ECA zones defined:

- **Baltic Sea** (limits on SO_x only)
- **North Sea** (limits on SO_x only)
- **North American area** (limits on SO_x, NO_x and PM)
- **US Caribbean area** (limits on SO_x, NO_x and PM)

Figure 7. *Actual and possible future ECA* [3].

1.2 Alternative Fuels

The energy transition to the use of alternative fuels is a key point for decarbonisation of the maritime sector. The fuels that are being studied for ship application include Liquefied Natural Gas (LNG), Liquid Biogas (LBG), Hydrogen, Ammonia, Methanol, Ethanol and hydrotreated vegetable oil (HVO) [10]. Some of these are intended for use in traditional energy production systems, i.e. internal combustion engines (ICE), while some are possible solutions for fuel cell use.

Liquefied Natural Gas (LNG)

Liquefied natural gas is mainly composed of methane (CH_4), the hydrocarbon with the lowest carbon content, for a percentage between 70% and 99%, and in smaller quantities ethane, propane, butane and traces of nitrogen.

Nowadays, liquefied natural gas is used by a small fraction of the world's fleet, amounting to 182 ships, but this number is expected to grow rapidly. Using natural gas as a fuel allows to reduce NO_x emissions, (almost) eliminate SO_x and particulate emissions, and reduce carbon dioxide emissions by up to 21% compared to HFO.

Generally, transportation takes place in cryogenic form, refrigerated at -162 °C, reducing its volume up to 1/600 of the volume of the gas, as well as being considerably safer. The density of LNG is approximately half the HFO one, with an energy density, on the contrary, 20% higher. For this reason, it requires approximately 1.8 times the volume for the same amount of chemical energy transported, also taking into account the equipment needed to keep it in a cryogenic state. The list of properties is reported in *Table 2*.

The use and transport of this fuel has specific requirements but since the LNG has been transported for lots of years in tankers, the safety rules and systems have partially been established. From the moment that the fuel is transported it makes sense to also use it in the engine. For this reason, among the main ships using LNG as fuel there are LNG tankers, 525 worldwide at the end of 2018 [6]. These use boil-off of natural gas as fuel, so the pressure inside the tanks is regulated, but at the same time the part that would otherwise be dispersed into the atmosphere is not wasted. In the past, the boil-off amounted to 0.15% daily, which has since been reduced to 0.08% over the last two decades thanks to the development of better thermal insulation for LNG tanks.

In the past, the engine most used by these boats was a steam turbine connected to an LNG boiler, while more recently the use of dual fuel diesel engines has become established.

Table 2. *LNG chemical properties.*

Chemical Composition	**CH_4**	
LHV	48	[MJ/kg]
Boiling Point[1]	-162	[°C]
Auto Ignition Temperature	650	[°C]
Flammable Range[2]	5-15	[%]
Energy Density	21.6	[MJ/l]
Density	450-550[3]	[kg/m^3]
Carbon Content	0.75	[-]
CO_2 Emissions	0.2061	[kg(CO_2)/kWh]

Methanol (CH_3OH)

Methanol is available globally and has been used in industry for decades. It is generally produced from LNG, but can also originate from biomass, in which case the impact of its life cycle is drastically reduced. At ambient temperature and pressure, it appears as a transparent and odorless liquid, much easier to transport and handle than fuels that require transport in cryogenic form such as LNG.

Among the positive characteristics of methanol, it can be highlighted that the hydrogen/carbon ratio is the highest of all fuels in liquid form, thus allowing carbon dioxide emissions to be reduced. Furthermore, since methanol dissolves

[1] Evaluated at 1 bar pressure.
[2] Volumetric percentage in air
[3] The value is influenced by the composition of the natural gas that is not only CH_4

very quickly in water, if it accidentally was to be discharged into marine or lake environments the effects would be less impactful than conventional FO. In addition, some properties make it suitable for spark ignition engine: low stochiometric air/fuel ration, high flame speed, low combustion temperature, high heat of vaporization [11].

However, the energy density of methanol is much lower than that of FO, and therefore requires approximately 2.54 times its volume to store the same amount of chemical energy. In *Table 3* the main properties of methanol are reported.

Table 3. *Methanol chemical properties* [11]

Chemical Composition	**CH_3OH**	
LHV	19.9	[MJ/kg]
Boiling Point[4]	65	[°C]
Auto Ignition Temperature	440	[°C]
Flammable Range[5]	6-36	[%]
Energy Density	15.7	[MJ/l]
Density	792	[kg/m^3]
Carbon Content	0.375	[-]
CO_2 Emissions	0.2486	[$kg(CO_2)/kWh$]

[4] Evaluated at 1 bar pressure.
[5] Volumetric percentage in air

The production of methanol is quite varied, it can start from different raw materials and is already fairly produced on large scale.

LNG is currently the most used, although the production process is very expensive in terms of energy and it emits between 0.5 and 1.4 tons of CO_2 per ton of methanol produced, respectively in the case of Steam Reforming or partial oxidation [12], [13], and it requires three different steps: creation of syngas, synthesis of methanol, and finally distillation of the same.

$$CO + 2H_2 \rightarrow CH_3OH \quad (1)$$

Starting from biomass, the process is similar, since it also starts from the preliminary production of syngas by treating the biomass at very specific temperatures and pressures. The reaction of the process changes from (1) to (2) and the steps are water electrolysis, carbon dioxide capture, methanol synthesis and separation of methanol. In terms of emissions during the production phase, however, starting from biomass makes the process itself neutral with regards to greenhouse gas emissions, but does not guarantee that the energy produced to make it is also neutral.

$$CO_2 + 3H_2 \rightarrow CH_3OH + H_2O \quad (2)$$

Compared to LNG, storage is less expensive, and therefore more attractive, especially for vessels that do not need to carry fuel for very long journeys, for which the volume of the tanks could be too high to be profitable compared to conventional FO.

Hydrogen (H_2)

Hydrogen as an energy carrier has by far the highest gravimetric energy density, 120.1 MJ/kg, compared to liquid hydrocarbon. The higher heating value

is 141.88 MJ/kg. The hydrogen has the disadvantage of having a very low power density, it occupies about 3 times the space of the traditional fuels. This fuel can be transported in different ways to reduce its volume:

- Liquid Hydrogen (LH2): guarantees a fuel density around 72 kg/m3 using cryogenic tanks (at -252 °C).
- Compressed Hydrogen (CH2): stored in tanks with different density depending on the chosen pressure (i.e. 12 kg/m3 at 200 bar, 35 kg/m3 at 700 bar).
- Metal Hydrides: allow storing large amounts of Hydrogen at ambient pressure, but on the other hand imply a disadvantage in terms of weights and thermal management.
- Cold- and cryo-compressed Hydrogen (CcH2): in addition to separate compression or cooling, the two storage methods can be combined. Hydrogen is cooled first. Depending on how much the hydrogen is cooled, it is referred to as cold-compressed hydrogen (above 150 K) or cryo-compressed hydrogen (CcH2). Cryo-compressed hydrogen is cooled to temperatures close to the critical temperature, but it still remains gaseous. The cooled hydrogen is then compressed. CcH2 is a further development of hydrogen storage for mobility purposes.

Although hydrogen is an extremely common element in nature, it tends to form compounds with other elements, therefore requiring its separation in order to be used as fuel. Once separated, this can be used both as fuel for ICE and to power fuel cells for power generation.
About 95% of hydrogen produced today comes from fossil fuels, such as oil and LNG.

Hydrogen is the "cleanest" fuel for marine applications currently on the market, thanks to the zero amount of particulate matter and SO_x emitted, and due to the relatively low percentage of NO_x produced. Moreover, when produced using renewable energy, greenhouse gas emissions are almost zero.

Nowadays, the applications of hydrogen in the maritime field are limited and characterized by low powers. Moreover, the production of this fuel is extremely costly in terms of energy, and the necessary technology is not yet available on a large scale.

Table 4. *Hydrogen chemical properties* [14], [15], [16].

Chemical Composition	**H_2**	
LHV	120.2	[MJ/kg]
Boiling Point[6]	-253	[°C]
Auto Ignition Temperature	535	[°C]
Flammable Range[7]	4-74	[%]
Carbon Content	0	[-]
CO_2 Emissions	0	[kg(CO_2)/kWh]

Chemical Composition	**H_2**	**LH_2**	**CH_2 (350-700bar)**	**CcH_2**	
Density	0.09	70.8	23-38	80	[kg/m^3]

[6] Evaluated at 1 bar pressure.
[7] Volumetric percentage in air

There are many methods for the production of hydrogen, at present 95% is produced by thermal treatment of LNG. This treatment uses high-temperature steam, which induces the separation of carbon atoms from hydrogen atoms.
Another useful process to produce hydrogen is the gasification of coal (which may have been produced from biomass). The process involves combustion at very high temperatures (between 1200 and 1500 °C), so that the coal releases gas then separated and reformed to produce hydrogen and carbon monoxide.
Hydrogen, moreover, can be produced by electrolysis using electricity and water, and thus obtaining oxygen and hydrogen. Compared to production from fossil fuels, it produces lower emissions even if powered by energy produced from non-renewable sources.
Related to the production method there are different hydrogen type:

- **Green hydrogen**: made by using clean electricity from surplus renewable energy sources, such as solar or wind power, to electrolyse water. Electrolysers use an electrochemical reaction to split water into its components of hydrogen and oxygen, emitting zero-carbon dioxide in the process.
- **Blue hydrogen**: produced mainly from natural gas, using a process called steam reforming, which brings together natural gas and heated water in the form of steam. The output is hydrogen, but carbon dioxide is also produced as a by-product. So, the definition of blue hydrogen includes the use of carbon capture and storage (CCS) to trap and store this carbon.
- **Grey hydrogen**: created from natural gas, or methane, using steam methane reforming but without capturing the greenhouse gases made in the process. Grey hydrogen is essentially the same as blue hydrogen, but without the use of carbon capture and storage.
- **Black and brown hydrogen**: using black coal or lignite (brown coal) in the hydrogen-making process, these black and brown hydrogen are the

absolute opposite of green hydrogen in the hydrogen spectrum and the most environmentally damaging.

- **Pink hydrogen**: generated through electrolysis powered by nuclear energy. Nuclear-produced hydrogen can also be referred to as purple hydrogen or red hydrogen.
- **Turquoise hydrogen**: made using a process called methane pyrolysis to produce hydrogen and solid carbon. In the future, turquoise hydrogen may be valued as a low-emission hydrogen, dependent on the thermal process being powered with renewable energy and the carbon being permanently stored or used.

Ammonia (NH_3)

Ammonia is considered one of the possible future players in the new energy scenario for the maritime systems [17]. Ammonia is a compound of hydrogen and nitrogen commonly found in nature in the form of a colourless gas at ambient temperature and pressure (with a density of 0.717 kg/m^3). Although it has been used as a fuel for ICE for 75 years on land, in the maritime sector there is still very little development, but it has chemical properties that suggest the application both with internal combustion engines and fuel cells.

Its lower heating value (LHV) is 18.8 MJ/kg, while its higher heating value (HHV) is 22.5 MJ/kg. It is comparable with other fossil fuels as methane and kerosene, which have LHVs of 50 MJ/kg and 43 MJ/kg, respectively. During transport it is stored liquid (with a density of 684.015 kg/m^3) at a temperature of -33 °C ambient pressure or to be transported at 20 °C it must be pressurized at 0.8 MPa relative. From the point of view of flammability, it isn't critical for

shipping even though the real challenge is its toxicity that adds significant complications from safety aspects to avoid leakage [18].
The combustion process of ammonia is greenhouse gases free and the emissions generated during its production and life cycle make it only slightly better than traditional fuels. The oxidation of ammonia produces only nitrogen and water as waste[8], according to the following chemical reaction (3).

$$4NH_3(g) + 3O_2(g) \rightarrow 2N_3(g) + 6H_2O(l) \quad \Delta H = -634\ kJ \tag{3}$$

Under certain conditions, NO can be found in the exhaust, for which the strict limiting normative leads to a detailed projectual phase in order to avoid high temperature, leading to a partial oxidation of ammonia[7] (4):

$$2NH_3(g) + 2O_2(g) \rightarrow NO(g) + 3H_2O(l) \quad \Delta H = -454\ kJ \tag{4}$$

Furthermore, the energy required during production increases the cost, and combustion generally does not occur unless an additional pilot fuel is used, which therefore reduces the benefits in terms of reducing carbon dioxide emissions. The transport of ammonia is less expensive than that of H_2 and for this reason could be used as a hydrogen carrier and then be converted through a cracking process on board. The volume required for storage, however, is approximately 2.5 times higher than FO.
The dissociation of the ammonia (5) with the cracking process occurs following the equation and is better explained in chapter 4.3.

[8] The heat of the reaction is taken from the literature [125]

$$NH_3 \leftrightarrow N_2 + 3H_2 \quad \Delta H = 94\ kJ \tag{5}$$

Table 5. *Ammonia chemical properties.*

Chemical Composition	**NH_3**	
LHV	22.5	[MJ/kg]
Boiling Point[9]	-33	[°C]
Auto Ignition Temperature	630	[°C]
Flammable Range[10]	15-33.6	[%]
Energy Density	15.7	[MJ/l]
Density	682	[kg/m^3]
Carbon Content	0	[-]
CO_2 Emissions	0	[$kg(CO_2)/kWh$]

Ammonia is the second most used chemical in the world for the production of fertilizers, medicines and numerous other products. It can be produced both from fossil fuels such as LNG and using renewable sources.

One of the ways to produce ammonia without carbon dioxide emissions involves the use of renewable electricity to extract hydrogen, which is then combined with nitrogen present in the atmosphere via the Haber-Bosch process.

As for the hydrogen, also in the ammonia case, depending on the source adopted for the production we can distinguish green, blue, turquoise, grey and brown, ammonia.

[9] Evaluated at 1 bar pressure.
[10] Volumetric percentage in air

1.3 Fuel Cells

Fuel cells are electrochemical devices that can convert hydrogen and oxygen into water producing electric power in direct current. The basic equation of functioning is (6). The main feature of this energy system is the possibility of reaching very high efficiency, which can theoretically attain values >75% [19], since the reaction isn't an oxidation, so the performance is not limited by the Carnot limit cycle.

$$H_2 + \frac{1}{2} O_2 \leftrightarrow H_2O \tag{6}$$

There are different types of fuel cell but in every case the cell is made by one electrolyte and two electrodes, the anode, fed with the fuel, and the cathode, fed with the oxidizer, as could be seen in *Figure 8*. The production of current is accomplished by the electrons that after the H_2 is split in ions, are collected and sent to an external circuit. The ions (depending on the type of fuel cell the ions are H^+ or O^-) pass through the electrolyte and with the electron they react forming water on cathode or anode side.

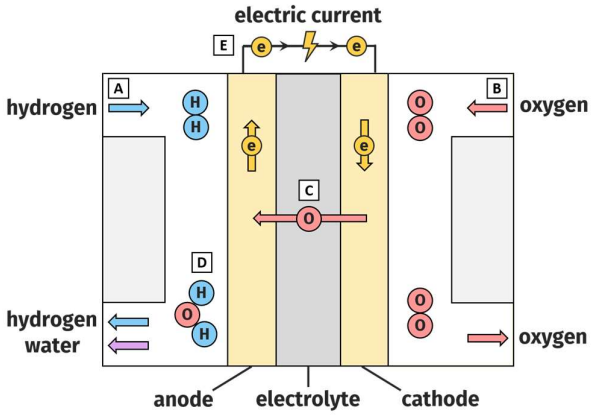

Figure 8. *Main structure and basic working principles of a solid oxide fuel cell.*

The advantages of using fuel cells, other than the emission and the efficiency aspect, are that having no mechanical or mobile parts increases durability and reliability, the almost total silence [20], low operating temperatures (depending on the FC type) and the almost linear size scalability thanks to their modularity. On the other hand, they have quite high costs and lower volume power density compared to ICEs (in terms of gravimetric power density, however, fuel cells have equal or better performance than the other two solutions). In *Figure 9* and *Figure 10* below are shown different technologies and fuels are shown and compared according to their volumetric and gravimetric power density. The most significant problem, however, remains fuel management, from the production to distribution and storage.

Many reports highlight the strong growth of fuel cell applications during the last two decades [21], [22], [23], [24], [25], [26], [27], [28]. The most relevant applications of fuel cells are in the transportation field. The main advantages of fuel cells with respect to internal combustion engines regard efficiency, size, noise and pollutant emissions [29]. Various automotive companies, such as Honda, Toyota and Volkswagen, presented vehicles powered by fuel cells during the last years [30]. They are generally powered entirely by a fuel cell or by a fuel cell – battery hybrid system and use hydrogen as energy source. For this application PEMFC are usually used, due to their low temperature, high power density and slow corrosion. The interest towards fuel cells has been growing also in the naval sector, for vessels of various sizes. Many research projects, investigating maritime applications of fuel cells, have been carried out over the last few decades [27]. One of the latest accomplishments in this field is the creation by the Italian shipbuilding company Fincantieri of the ZEUS experimental vessel, equipped with a 130 kW fuel cell system powered by hydrogen. In order to reduce CO_2 emissions, also the aviation sector has shown interest in fuel cells, mainly PEMFC and SOFC [28], [31]. Some of the main

manufacturers, such as Boeing and Airbus, are developing hydrogen fuel cell systems to provide electrical power to non-propulsion systems on the airplane. Regarding propulsion applications, fuel cells have been installed mainly on unmanned aerial vehicles and small manned aircrafts. One of the latest accomplishments in this field is the successful test of the HY4 aircraft by the DLR German Aerospace Center in 2016. The HY4 is equipped by a hydrogen PEMFC and a lithium battery to assist during peak power loads, has space for four passengers and can reach a speed of about 200 km/h [32].

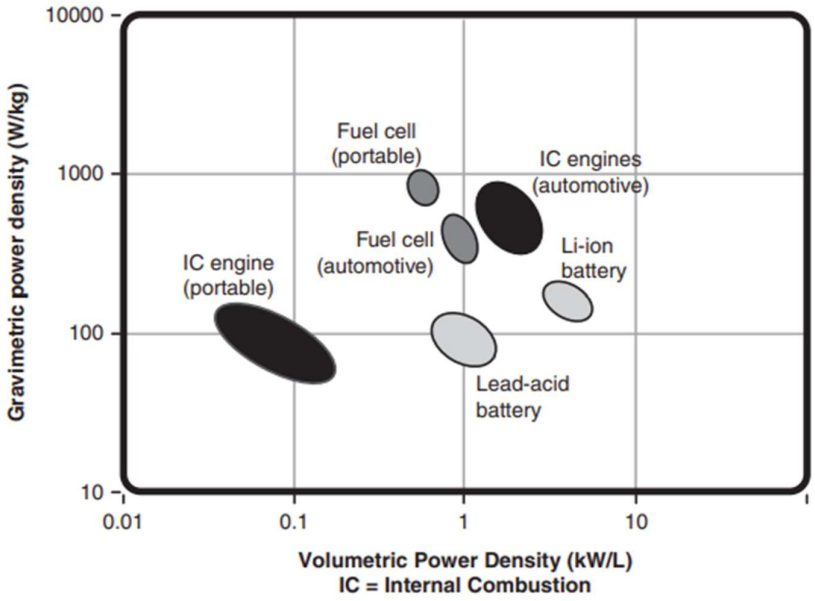

Figure 9. *Comparison of volumetric and gravimetric power densities of different technologies* [33].

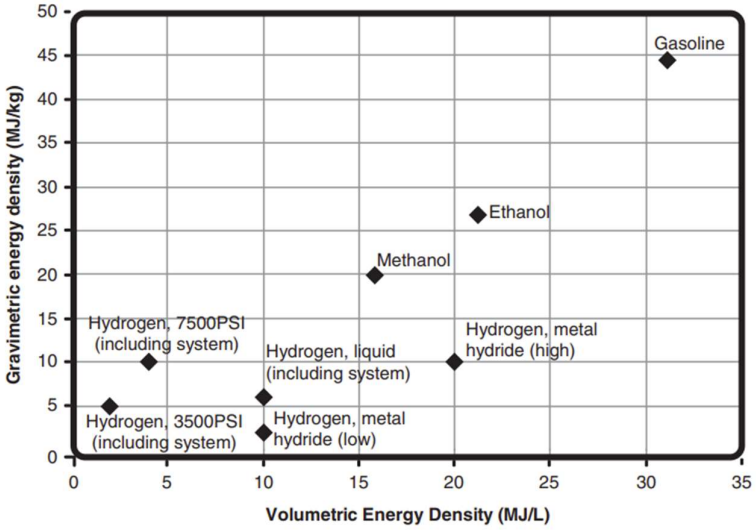

Figure 10. *Comparison of volume and gravimetric power densities of different fuels* [33].

There are currently six main types of fuel cells, which are by their electrolyte type [34]:

- Sulphuric Acid Fuel Cell (PAFC)
- Polymer Electrolyte Membrane Fuel Cell (PEMFC)
- Alkaline Fuel Cell (AFC)
- Molten Carbonate Fuel Cell (MCFC)
- Solid Oxide Fuel Cell (SOFC)

The different types of fuel cells differ also for material, operating temperature, fuel to be fed in, chemical process details, etc… In *Table 6* the main differences among fuel cells are briefly described. The main classification is made using the operating temperature, we have low and high temperature fuel cell. Beside the material that must change since the temperature difference is strong, the fuel is for sure an important characteristic. Low temperature fuel cell requires high purity hydrogen (higher than 99.9 %) otherwise the cell could be damaged. On

the other hand, high temperature fuel cell could be fed with hydrocarbons or hydrogen carriers, which can be send directly in the cell and, thanks to the high temperature, react and produce H_2.

Table 6. *Fuel cell properties* [35].

Fuel Cell Type	Operating Temperature	Typical Electrical Efficiency (LHV)	Typical power range (kW)	Applications	Advantages	Challenges
Polymer Electrolyte Membrane (PEM)	<120°C	60% direct H_2; 40% reformed fuel	1 – 100	Backup power Portable power Distributed generation Transportation Specialty vehicles Grid support P2P	Solid electrolyte reduces corrosion & electrolyte management problems Low temperature Quick start-up and load following	LT PEM: Expensive catalysts Sensitive to fuel impurities
Alkaline (AFC)	<100°C	60%	1 – 100	Military Space Backup power Transportation	Wider range of stable materials allows lower cost components Low temperature Quick start-up	Sensitive to CO_2 in fuel and air Electrolyte management (aqueous) Electrolyte conductivity (polymer)
Phosphoric Acid (PAFC)	150 - 200°C	40%	5 – 400	Distributed generation	Suitable for CHP Increased tolerance to fuel impurities	Expensive catalysts Long start-up time Sulfur sensitivity
Molten Carbonate (MCFC)	600 - 700°C	50%	300 – 3000	Electric utility Distributed generation	High efficiency Fuel flexibility Suitable for CHP Suitable for Hybrid/gas turbine cycle Suitable for Carbon Capture	High temperature corrosion and breakdown of cell components Long start-up time Low power density
Solid Oxide (SOFC)	500 - 1000°C	60%	1 – 2000	Auxiliary power Electric utility Distributed generation	High efficiency Fuel flexibility Solid electrolyte Suitable for CHP Potential for reversible operation Suitable for Hybrid/gas turbine cycle	High temperature corrosion and breakdown of cell components Long start-up time Limited number of shutdowns

1.4 Preliminary analysis: multi-criteria comparison

The maritime sector includes different sizes and different applications, so the best solution for GHG emissions reduction could change according to the case study and for this reason part of this work included a study through the use of

a multi criteria analysis done with HELM (Helper for Energy Layouts for Maritime applications), a software for the preliminary design of ships that aims to identify the best solution among different types of propulsion depending on the project requirements [36].

Figure 11. *HELM Logo*

HELM was developed by the TPG (Thermochemical Power Group) research group of the University of Genoa, and over the years it has been implemented with new technologies and new data to offer a simulation tool that is always up to date and in step with the different solutions that have emerged over the years.

The software compares technologies on different parameters, such as masses, volumes, costs and emissions. The importance of each of these parameters will depend on the type of ship, on the use that this ship will have and in some cases on the location of the routes that it will have to travel. The tool will highlight, based on the different relevance given to each parameter, the best solution among those implemented in the software that are reported in Table 7.

Table 7. *Technologies implemented in HELM.*

Power generation system	Storage system
PEM Fuel Cells (PEMFC)	Liquid H_2 (LH_2)
PEM Fuel Cells (PEMFC)	Compressed H_2 (CH_2)
Solide Oxyde Fuel Cells (SOFC)	Liquid Natural Gas (LNG)
microGT (mGT)	Liquid Natural Gas (LNG)
Int. Comb. Engine (ICE)	methanol
Int. Comb. Engine (ICE)	ammonia
Int. Comb. Engine (ICE)	Liquid Natural Gas (LNG)
Int. Comb. Engine (ICE)	Marine Diesel Oil (MDO)

Algorithm description

The software algorithm works using of a database easy to be updated. From these data the tool creates maps to carry out the evaluation, an example is proposed in *Figure 12*. In particular, it represents the storage of FO: on the x axis we have the fuel capacities, from which the masses, volumes and costs are obtained. As can be seen from the figure, the map represents curves with different analytical shapes: this is because different functions are used to best describe the trend of the data collected, reducing the error to a minimum, but without neglecting coherence of the predictions given by the function outside the range of the data collected.

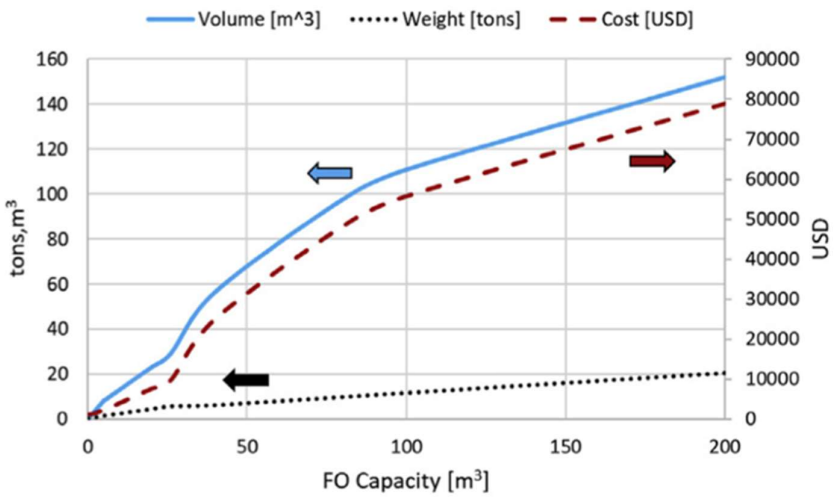

Figure 12. *FO storage costs, volumes, and masses are an example of a function that HELM has implemented* [37].

The user can freely enter all the details of his case study in the interface, including the significance of the four performance parameters (cost, volume, weight, emissions) and the two operating parameters for ship sizing, that are maximum power required and operating hours, which affect energy system size and fuel volumes to be stored respectively. Actually, during navigation, the ship's real power requirements will typically be less than the maximum power specified as an operating parameter.

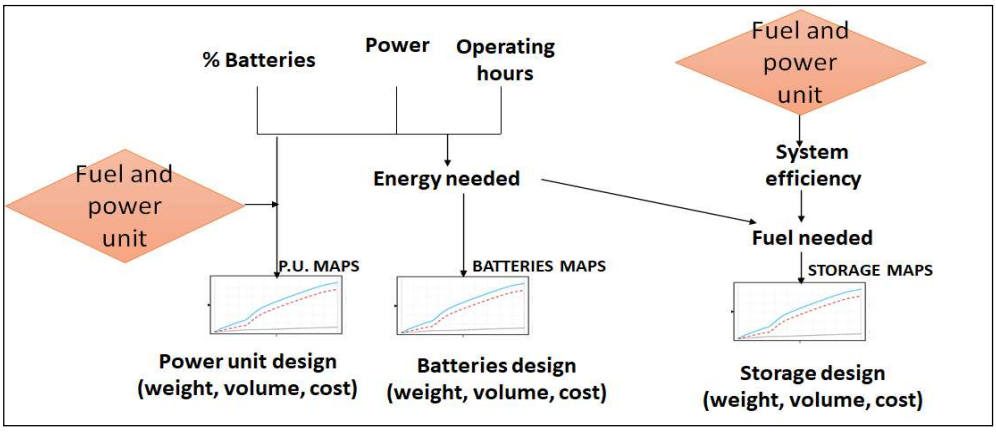

Figure 13. *Logic implemented in HELM* [38].

In the software were implemented additional features such as a percentage of batteries used to fulfil the power load for systems with lower response like high temperature fuel cell. As result, *Figure 13* illustrates the logical scheme performed by the software for the calculations. The energy required during navigation is calculated from the product between the required power and the operating hours entered. The dimensions, costs and mass of the thrusters are calculated directly from the required power. By dividing the mechanical energy required by the efficiency of the various technologies, the software evaluates the properties of the storage. The efficiency is set as an average among the different models of the same technologies, but it can be modified from the user.

The HELM was created with the *app designer* of MATLAB and the graphical interface is shown in *Figure 14*. The max power and the operational hours inputs for the simulation are in the higher part of the window. These two information items give the result previously discussed. In the lower part the software shows the other part of the tool, the relevance for the technology comparison. Inserted on the page with various colors there are buttons. By pressing the Calculate button, the data are processed, and the simulation is displayed on the screen in the windows: the calculated values are in white, and the score of the technology is in blue.


HELM
Tool for innovative solutions in maritime applications
Medium
Small
Large
Size
Max. Power Required [kW] 0
Operational hours 0
PEM Fuel Cells + LH2
PEM Fuel Cells + CH2
SOFC + LNG
mGT + LNG
Internal Combustion Engine + MeOH
Internal Combustion Engine + LNG
Internal Combustion Engine + FO
Internal Combustion Engine + NH3
PEM Efficiency 45
H2 Weight [tons] 0.000
Tot Weight [tons] 0.00
Tot Volume [m3] 0.00
Tot Fix Cost [kUSD] 0
CO2 [tons] 0.00
NOx [kg] 0.00
Batteries % 0.00
SOFC Efficiency 50
LNG Weight [tons] 0.000
mGT Efficiency 30
ICE Efficiency 35
MeOH Weight [tons] 0.000
FO Weight [tons] 0.000
NH3 Weight [tons] 0.000
SCORE 0
Volume Relevance 1
Weight Relevance 1
Costs Relevance 1
Emissions Relevance 1
Calculate
Generate simulation report
Calculate and export dataset with current relevance values
Calculate and export batteries dataset
Show dataset 3D map
Show batteries 3D map
Developed by

Figure 14. *HELM graphic interface.*

Each technology is given a score: the higher the score, the more convenient the technology is for the application considered. The score displayed is the total of the sum of the individual scores obtained in the four categories (volume, mass, cost and emissions) corresponding to the respective relevance. In each category the score is assigned on a scale from 1 to 10: 1 corresponds to the lowest value, 10 the maximum score. Max scores are awarded to the winning technology among all, and the other technologies get a score according to the equation (7).

$$X = \frac{V_i}{V_{best}} \tag{7}$$

According to the X value, using *Table 8*,

Table ***9*** and *Table 10* each energy system receives a score for all the 4 performance parameters.

Table 8. *Score for X ranges used for costs, weights and volumes.*

X Range	***Score***
1.1<X	*10*
1.1<X<1.3	*9*
1.3<X<1.6	*8*
1.6<X<2	*7*
2<X<3	*6*
3<X<4	*5*
4<X<6	*4*
6<X<8	*3*

8<X<10	*2*
X>10	*1*

Table 9. *Score for X ranges used for CO_2 emissions (PEMFC are not included).*

X Range	***Score***
1.1<X	*3*
1.1<X<1.3	*2.5*
1.3<X<1.8	*2*
1.8<X<2.2	*1.5*
2.2<X<3	*1*
X>3	*0.5*

Table 10. *Score for X ranges used for NO_X emissions (PEMFC and SOFC are not included).*

X Range	***Score***
1.5<X	*3*
1.5<X<2	*2.5*
2<X<6	*2*
6<X<15	*1.5*
15<X<30	*1*
X>30	*0.5*

The total result is influenced by the relevance values that have been set previously: in particular, each score of the single category is multiplied by the relevance score that has been given to it.

Database implementation

This section explains the methodologies using which the maps implemented within the software are created. As already explained above, the simplicity of the software is a fundamental point that allows quick and frequent updates, depending on availability on the market. Each map is created from datasheet on the market for different sizes. From the specifics, a linear trend line fits the data minimizing the error in the range of size with data availability. Whether there are no data for a certain range, the map is filled simulating a prediction of the expected behavior. Some examples for the liquid and compressed hydrogen are reported below, for both the power generation system and the storage system.

Liquid hydrogen, being transported in cryogenic form, requires IMO Type 7 storage systems, i.e. transportable tanks thermally insulated and structurally suitable for the transport of liquefied refrigerated gases.

Data available are collected from manufacturers such as Linde, Cryofab, CryoTherm [39], [40], [41].

It is worth underlining that some of the solutions are not tanks specifically intended for naval use: the technology is in fact still too immature to be able to generate a significant dataset in such a new field of application, and the choice to enlarge the range of solutions studied is justified by the probable future availability of solutions currently offered for road transport or industrial storage also for the naval sector.

The chosen solutions have capacities ranging from 100 l up to 2.300.000 l (industrial storage).

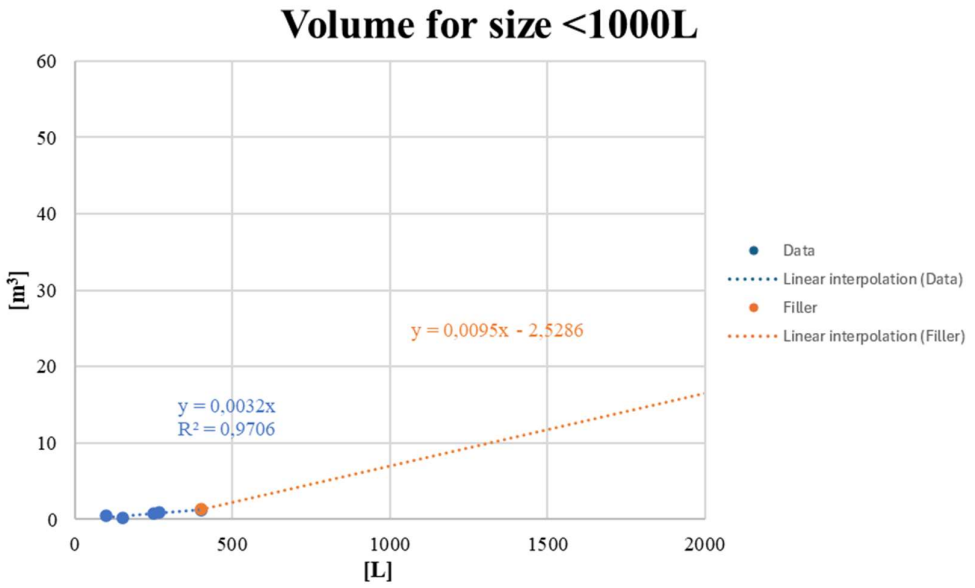

Figure 15. *Volume of liquid hydrogen in storage for size < 1000L.*

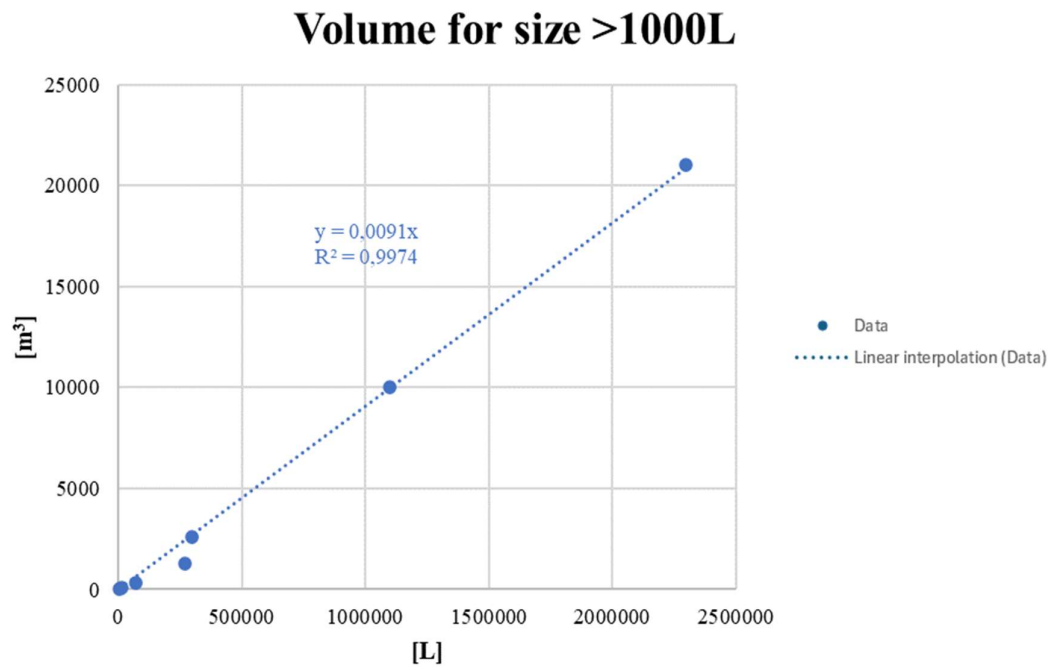

Figure 16. *Volume of liquid hydrogen in storage for size > 1000L.*

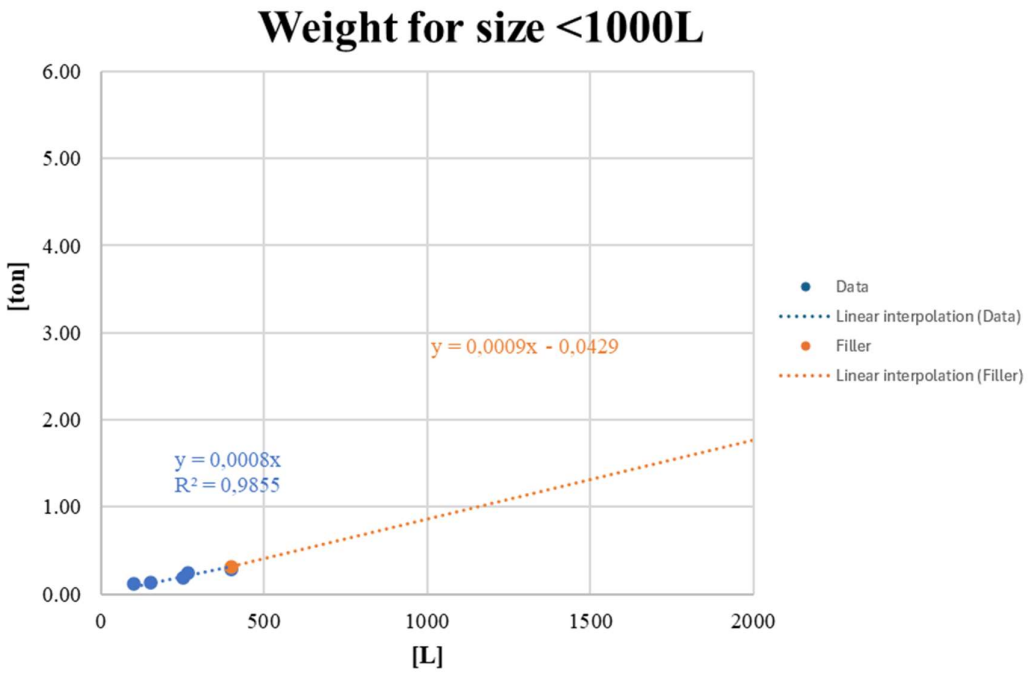

Figure 17. *Weight of liquid hydrogen storage for size < 1000L.*

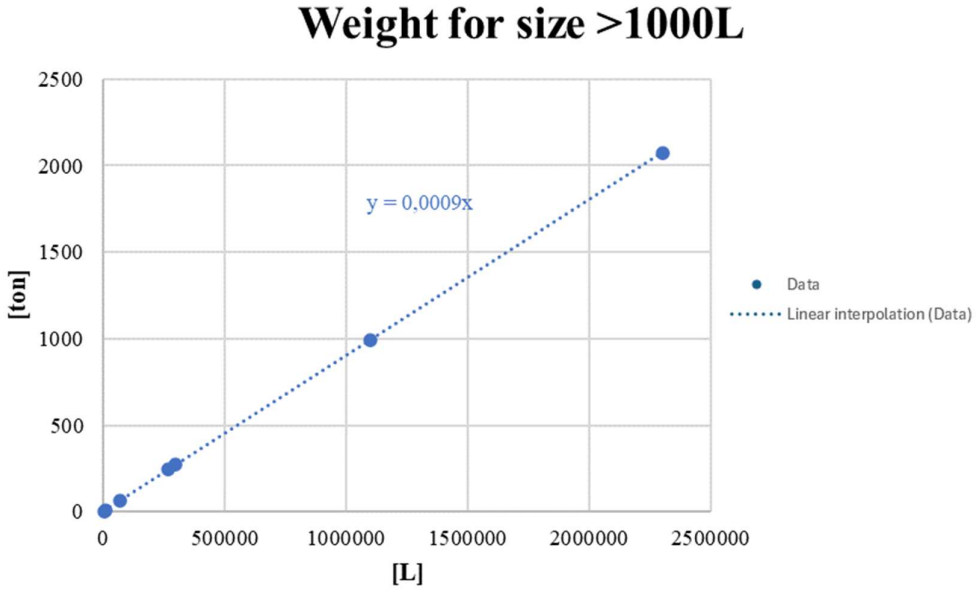

Figure 18. *Weight of liquid hydrogen storage for size > 1000L.*

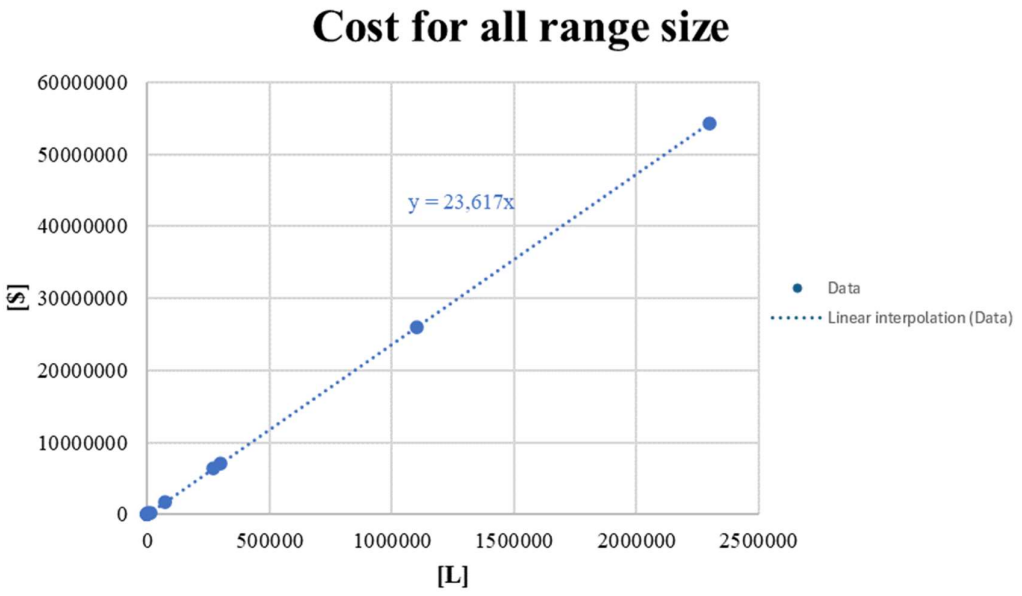

Figure 19. *Cost of liquid hydrogen storage.*

Compressed hydrogen, being transported in cryogenic form, requires IMO Type 5 storage systems, i.e. transportable tanks with pressure release devices and suitable for the transport of class 2 non-refrigerated gases.

Data from manufacturers such as Faber, Hexagon, Luxfer, Mahytec, Worthington were collected.

The chosen solutions have capacities ranging from 10 l up to 50.000 l.

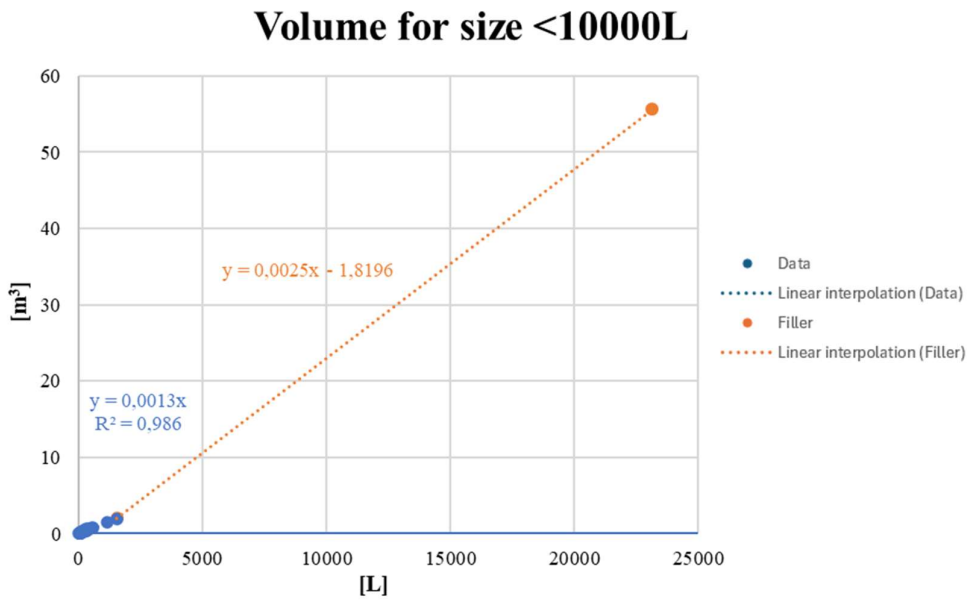

Figure 20. *Volume of compressed hydrogen storage for size < 10000L.*

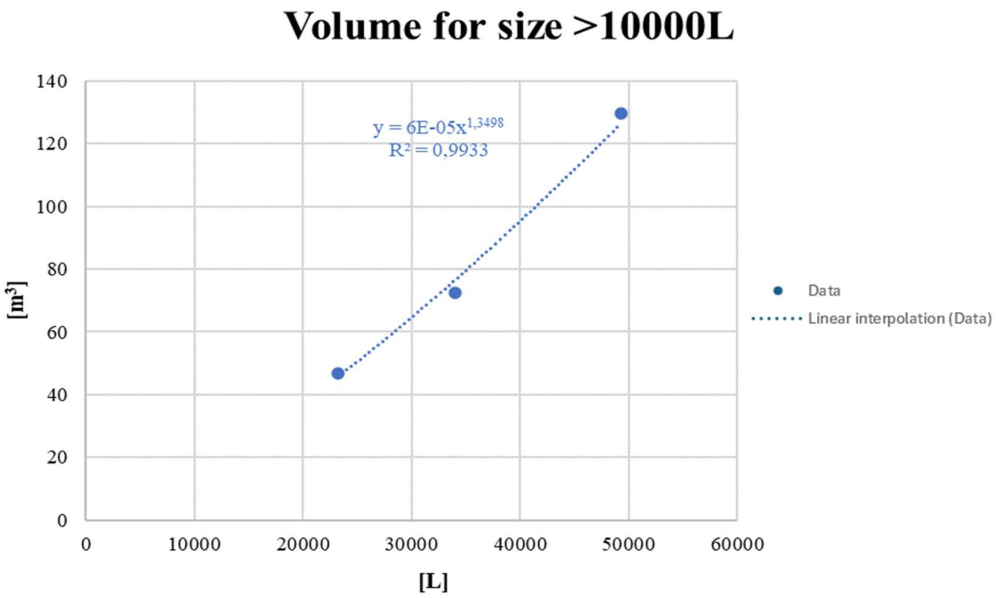

Figure 21. *Volume of compressed hydrogen storage for size > 10000L.*

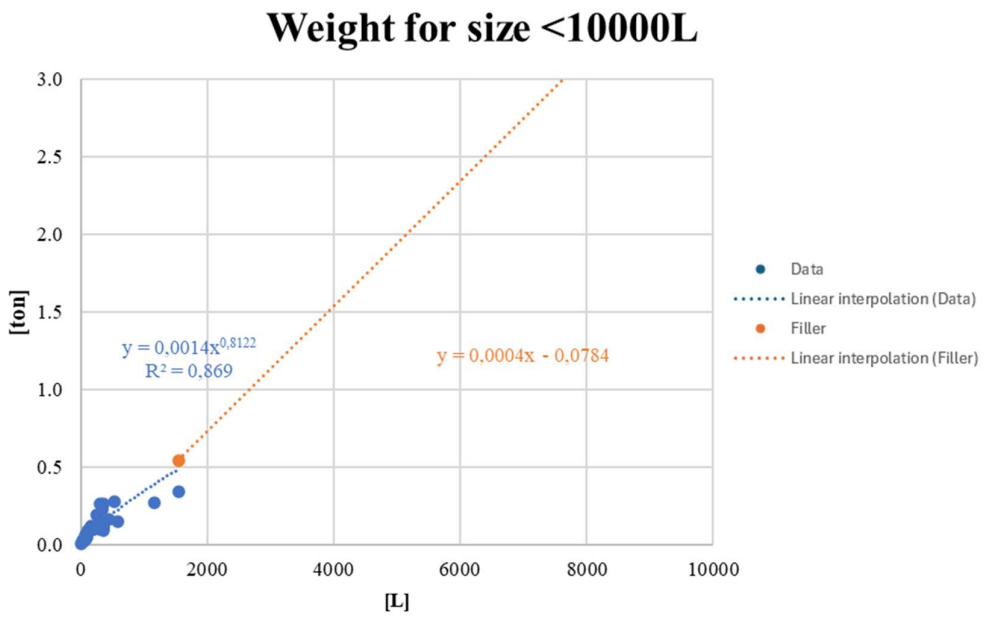

Figure 22. *Weight of compressed hydrogen storage for size < 10000L.*

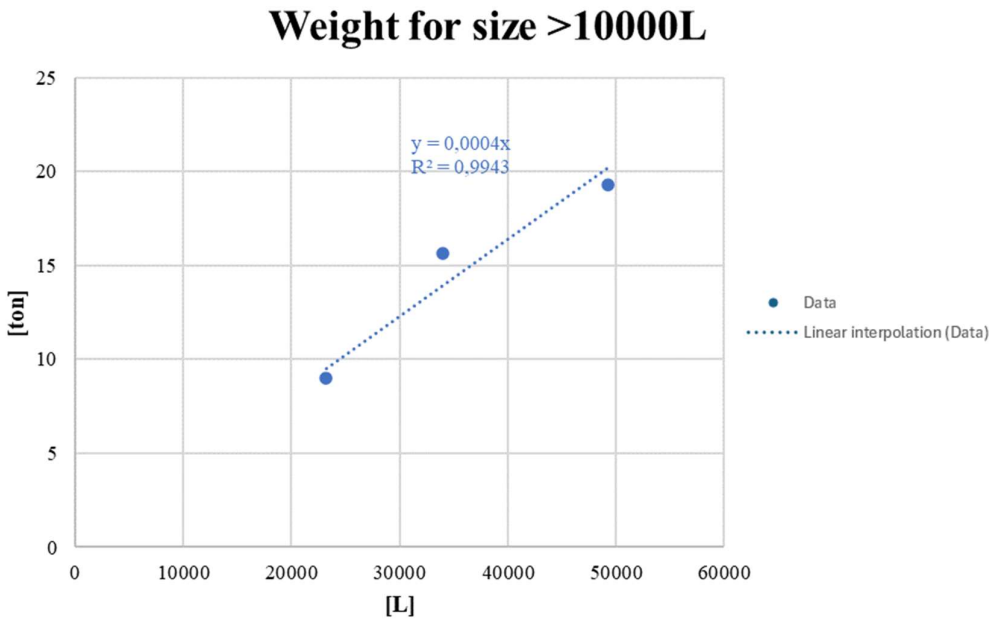

Figure 23. *Weight of compressed hydrogen storage for size > 10000L.*

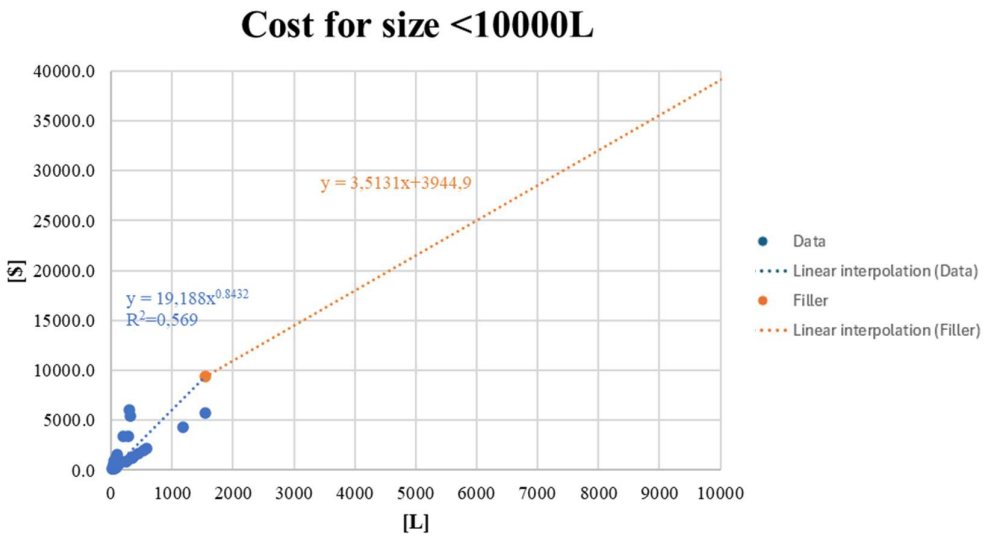

Figure 24. *Cost of compressed hydrogen storage for size < 10000L.*

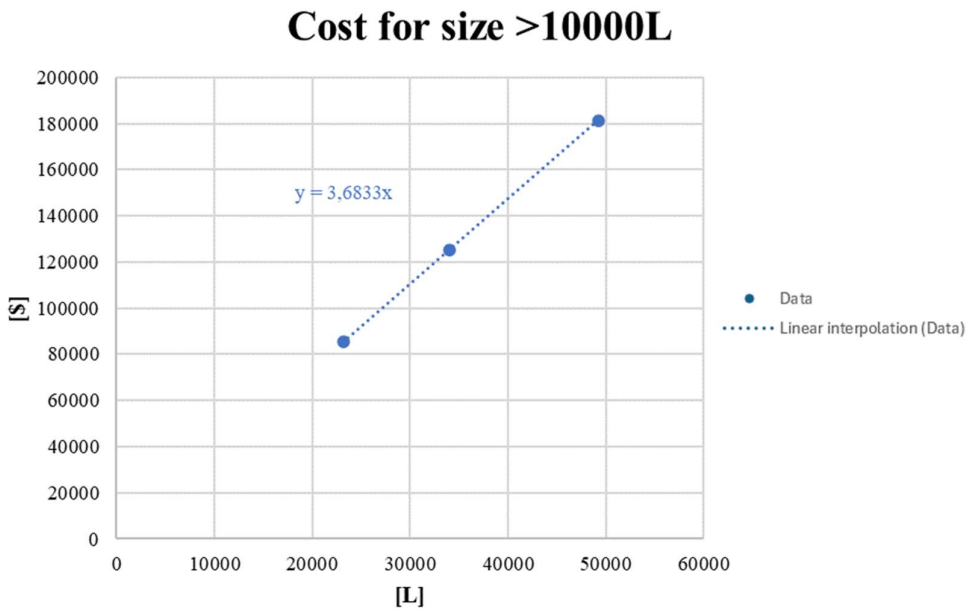

Figure 25. *Cost of compressed hydrogen storage for size > 10000L.*

Simulation results

As already explained, the simulations in HELM require some starting information, including the relevance of the four parameters, the maximum power required and the operating hours. Starting from the discussion on the need to use equivalent hours to obtain a simulation more consistent with reality, it is necessary to use the hours of autonomy of the ship as the value of operating hours requested by the software. These equivalent hours are calculated because, during navigation, the ship will not require constant power from the thruster. In fact, by directly using the hours of autonomy of the vessel, a request equal to the maximum power for all hours of operation would be simulated, making the quantity of fuel needed by the ship much greater than the actual need. From the analysis of the load profiles, a weighted average was carried out on the hours of use for the different powers (expressed as a percentage of maximum power) required, thus obtaining a percentage that can be used to transform the navigation hours into equivalent hours (at maximum power). For this work we analysed the operating profile taken from *VesselFinder* [42]. Some of the data found and analysed are shown in *Figure 26* and *Figure 27*.

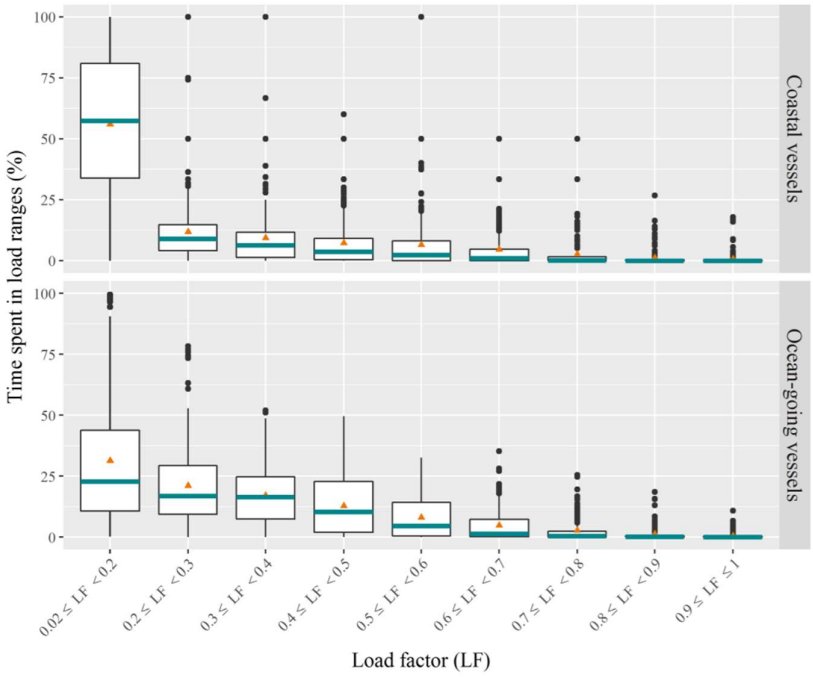

Figure 26. *Load profile for passenger transport ships* [43].

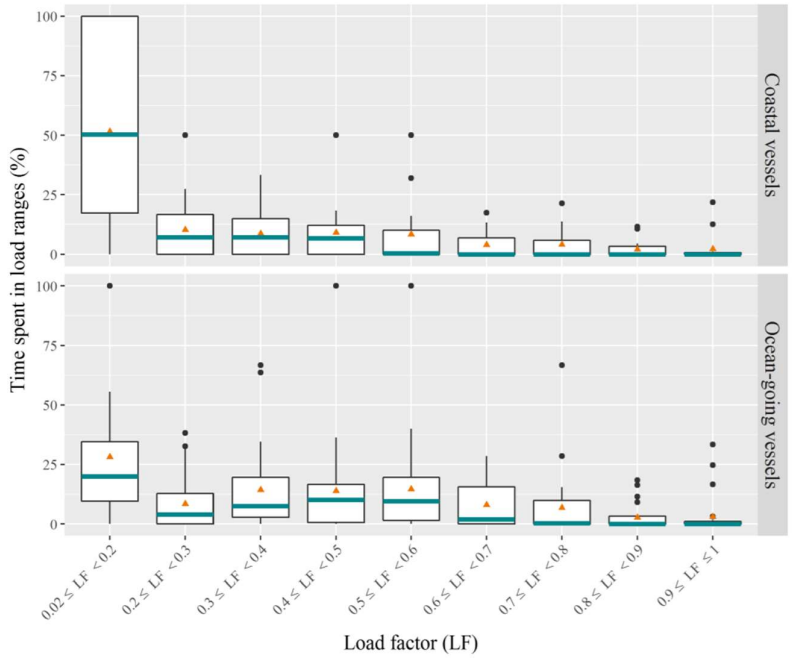

Figure 27. *Load profile of Ro-Ro ship* [43].

From these values a percentage of equivalent operational hours was evaluated. Furthermore, to obtain a value that is more in line with the greatest number of boats, it was decided to use the median and not the average as a percentage of hours. The following formula is then used to calculate the actual load utilization percentage:

$$\bar{P} = \frac{\sum_{i=1}^{9} T_i P_i}{\sum_{i=1}^{9} T_i} \tag{8}$$

Where:

T are the hours spent at the given power

P is the average value of each power range

For each type of ship, a percentage of load utilization was evaluated and then reported in ***Table 11***.

Table 11. *Load percentage for different type of ship.*

	Costal Vessels	***Ocean-going Vessels***
Tankers	20 %	47 %
Bulk Carriers	27 %	46 %
General Cargo Ships	38 %	47 %
Container Ships	25 %	35 %
Ro-Ro ships	22 %	33%
Reefers	41 %	50 %
Off-Shore Vessels	19 %	25 %
Passenger Ships	19 %	28 %

To increase the reliability of the tool, we considered some case study, and we analysed the results with HELM [38]. The two cases are:

- The motor vessel F.A. Gauthier, a ferry over 130 meters long and almost 25 meters wide. It was the first liquefied natural gas ferry used in North America, and the first of its kind to be built in Italy. Four Wartsila 12V34 Dual Fuel LNG/MDO engines are installed on board with a total power of 20,880 kW and three 250 cubic meter tanks to contain the LNG necessary for the thrusters [27].
- The second case study is a very small boat for public river transport in Nantes, France, and is among the first ships of this type to be powered by hydrogen. The ship uses an electrical power of 10 kW produced by two hydrogen fuel cells, its hydrogen consumption is approximately 1.3 kg per day. The shuttle is ten meters long and almost four meters wide with a capacity of twelve passengers and eight bicycle spaces [20].

For the first case study the F.A. Gauthier vessels was considered as Ro-Ro Ships for Oceanic purpose and the load percentage was set at 33% of a 48 hour travel. Furthermore, the reference for this application, considering the purpose of the type of ship, were set as:

- Volume: 4
- Weight: 2
- Costs: 3
- Emissions: 2

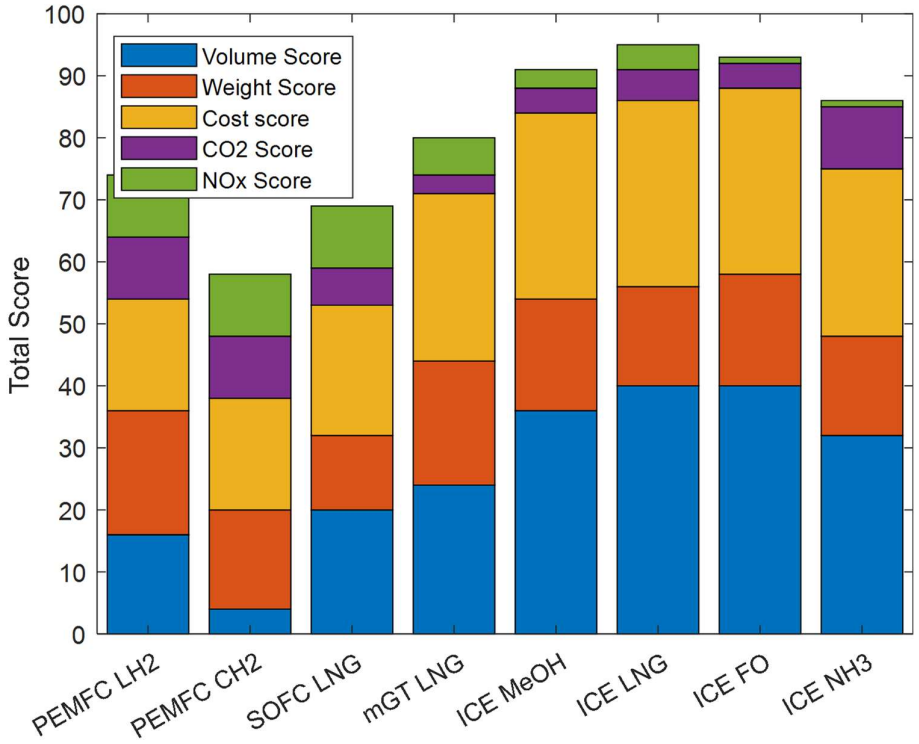

Figure 28. *Score of the different technologies for first case scenario simulation.*

From the result of the simulation, the output of the tool is in agreement with the actual power system adopted for this application, in fact the highest score in *Figure 28* is the one for LNG fed ICE. In ***Table 12*** the outputs of the simulation that better explain the score results are listed.

Table 12. *Results of the different technologies for first case scenario simulation.*

Technology	Total Volume [m^3]	Total Weight [tons]	Total Cost [k$]	CO2 [kg]	NOx [kg]	Efficiency [%]
PEMFC LH2	3260.06	443.19	27116.05	0.00	0.00	45
PEMFC CH2	53451.81	670.21	25705.56	0.00	0.00	45
SOFC LNG	2404.22	1117.31	21089.73	140740.09	0.00	50
mGT LNG	2026.53	467.66	14965.55	266061.31	81.95	30
ICE MeOH	920.73	568.08	11964.47	188603.35	1093.35	44
ICE LNG	852.92	631.82	12296.48	159931.91	488.52	44
ICE FO	788.55	565.67	11534.41	219080.55	2581.53	44
ICE NH3	1105.89	608.44	14588.64	0.00	2565.49	44

It is worth mentioning that for this application, characterized by medium-high power and low operating hours, internal combustion solutions present similar scores for all the fuel options. In this case, in fact, the advantages given by the absence of SCR (Selective Catalytic Reduction) systems for LNG systems cancels the advantage in terms of storage volumes for fuel oil ICEs. Furthermore, the lower weight of the solution itself is an advantage which, together with the reduced emissions, makes LNG more competitive than other internal combustion solutions.
Finally, methanol solutions are more competitive than ammonia ones thanks to their lower volume and costs, although the difference is not extremely marked.

For the second case study, the load profile is in the Passenger Ship, Coastal vessel application and 19% as load percentage is chosen, over a 24 hour navigation.
The relevance adopted for this case study are:

- Volume: 3
- Weight: 2
- Costs: 1
- Emissions: 5 and 3

The same case study was also evaluated even in the hypothesis in which emissions have a less significant impact. The results are presented in *Figure 29* and *Figure 30*.

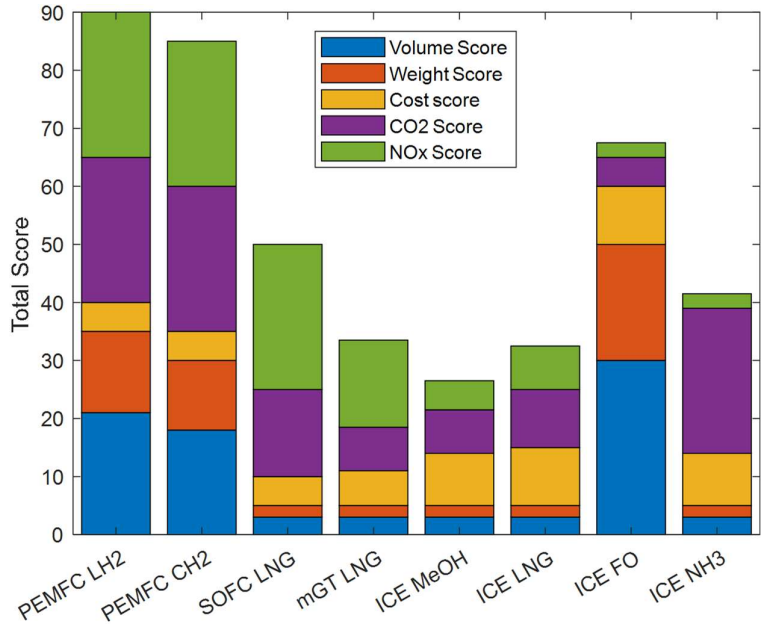

Figure 29. *Score of the different technologies for second case scenario simulation with emission relevance = 5.*

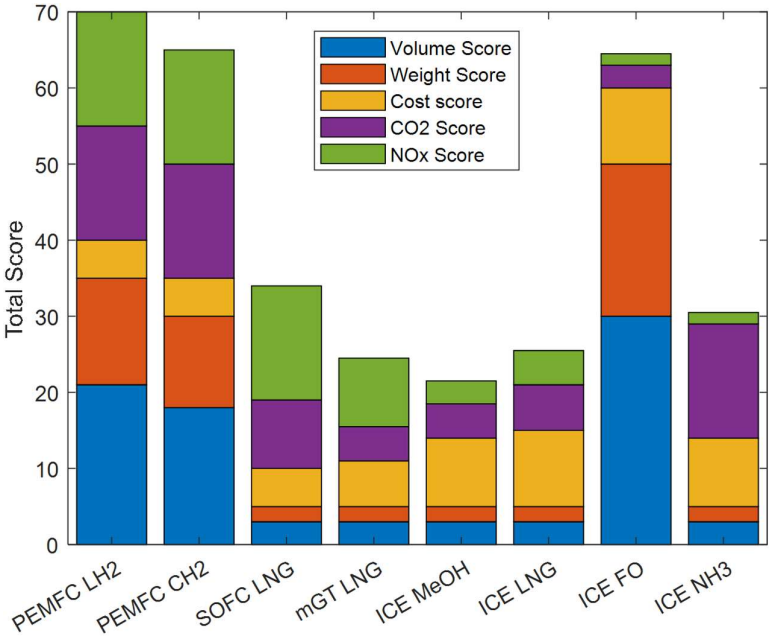

Figure 30. *Score of the different technologies for second case scenario simulation with emission relevance = 3.*

In *Table 13,* once again the results of the simulation are shown for all the technologies included in the comparison.

Table 13. *Results of the different technologies for second case scenario simulation with emission relevance = 5.*

Technology	Total Volume [m^3]	Total Weight [tons]	Total Cost [k$]	CO2 [kg]	NOx [kg]	Efficiency [%]
PEMFC LH2	0.32	0.13	58.39	0.00	0.00	45
PEMFC CH2	0.42	0.21	58.31	0.00	0.00	45
SOFC LNG	5.38	5.67	61.96	21.06	0.00	50
mGT LNG	4.78	4.24	38.86	39.82	0.01	30
ICE MeOH	2.75	0.92	18.05	42.83	0.25	29
ICE LNG	2.99	3.81	16.05	36.32	0.11	29
ICE FO	0.16	0.08	16.32	49.75	0.59	29
ICE NH3	4.42	0.95	20.70	0.00	0.58	29

In this simulation, although the relevance of the emissions varies from 5 to 3, the relationships between the scores remain similar. Therefore, there is an excellent competitiveness of PEMFC solutions for low operating hours and reduced powers, regardless the importance assigned to emissions. This result, very significant and indicating a certain maturity of fuel cell solutions, must be compared with the high score obtained by internal combustion engines running on fuel oil, which, in the case of reduced emissions relevance, still represents one of the best solutions, thanks to the very high score in terms of weight and volume.

In conclusion, for large powers combined with significant quantities of operating hours, FO technology obtains significantly higher scores than any other technology. This is due to the obvious advantages of a technology that is more mature and to the excellent energy density of the fuel, which allows storage of reduced dimensions and masses. However, it cannot go unnoticed that, generally, such conditions of high power and numerous operating hours are

accompanied by very low emission relevance. This is due to the routes generally followed by these ships, often transoceanic, not passing through protected areas.

Furthermore, decreasing the operating hours, make the alternative technologies of LNG, MeOH and NH_3 systems more valuable, even if the powers remain high. This trend is due to the intrinsic disadvantage in terms of storage of these fuels, due to their lower energy density.

For high relevance of emissions, obviously, technologies using PEMFC have clear advantages in terms of scoring. Their zero emissions in all fields considered by the simulator (CO_2, SO_x, NO_x) make the comparison with any other technology extremely advantageous for these solutions, which, however, due to the very high investment costs, require cost relevance rather low to have scores significantly higher than those of other technologies.

To have a general view of the technologies for all ranges of power requirement and operating hours, we plotted in 3D graph the score for some relevance cases. FO is at the moment the best solution for most of the range. The emission relevance makes new alternative solution valuable choice like in the aforementioned examples.

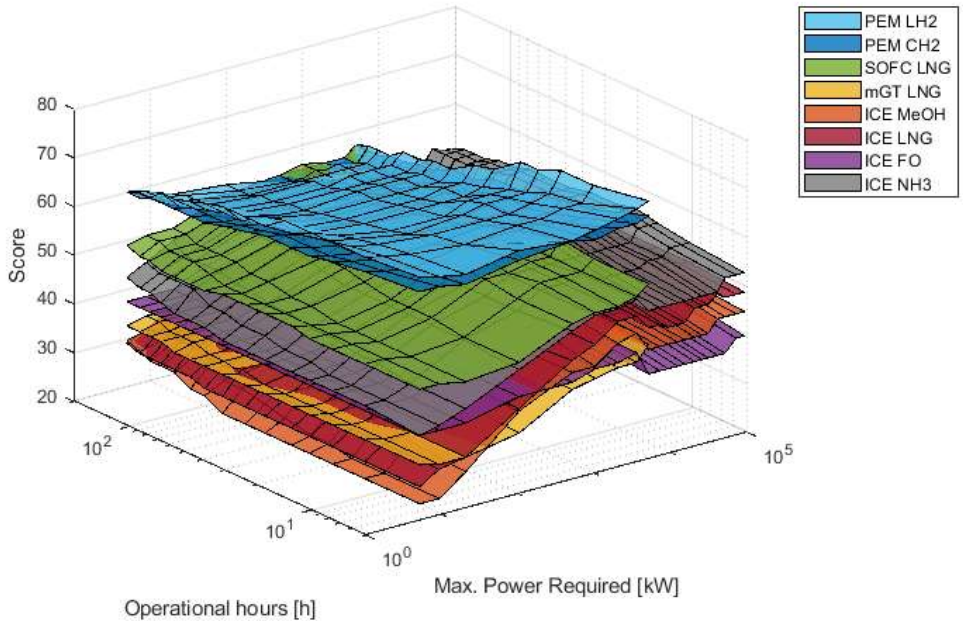

Figure 31. *3D representation of dataset for relevance equal to 1 for volume, mass and cost, and 5 for emissions.*

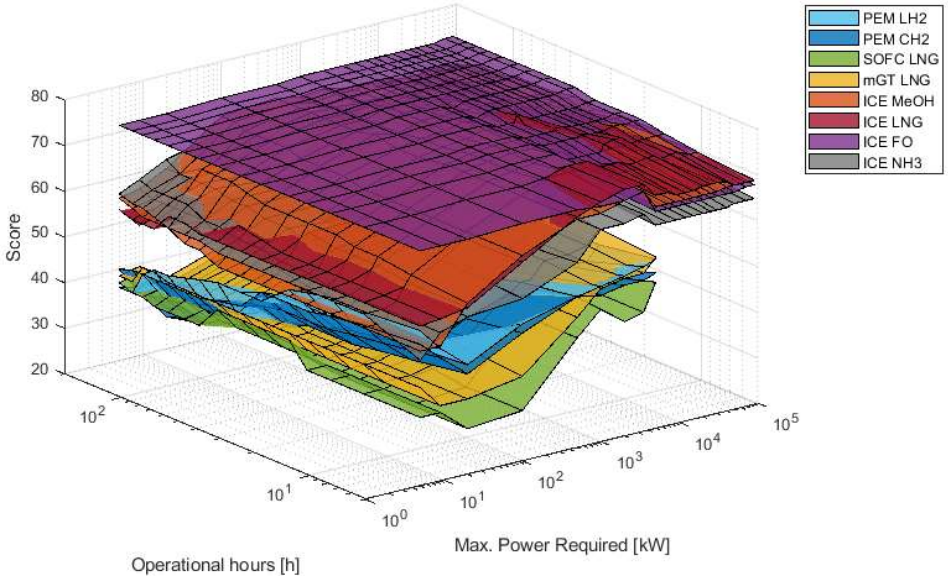

Figure 32. *3D representation of dataset for relevance equal to 1 for volume, mass and emissions, and 5 for cost.*

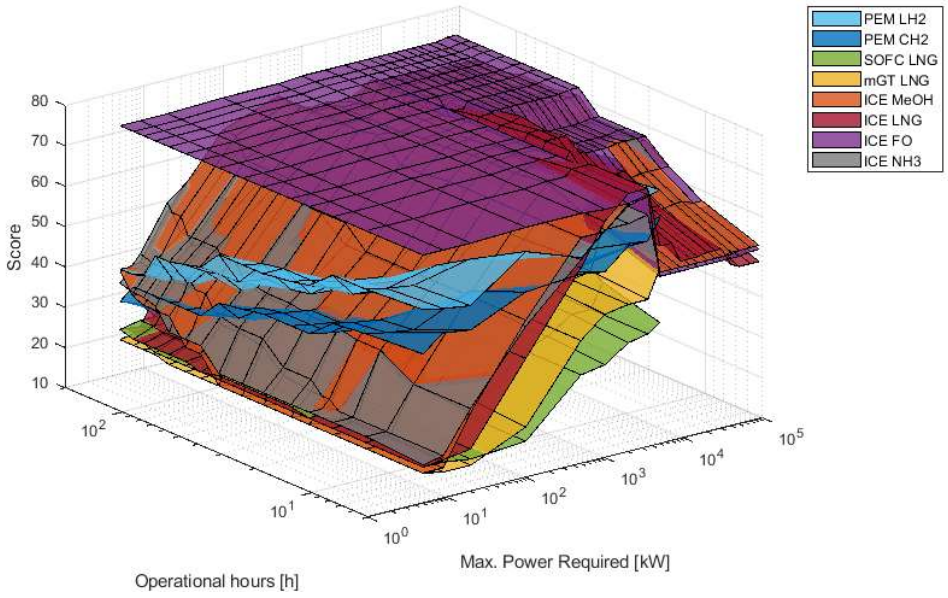

Figure 33. *3D representation of dataset for relevance equal to 1 for volume, cost and emissions, and 5 for mass.*

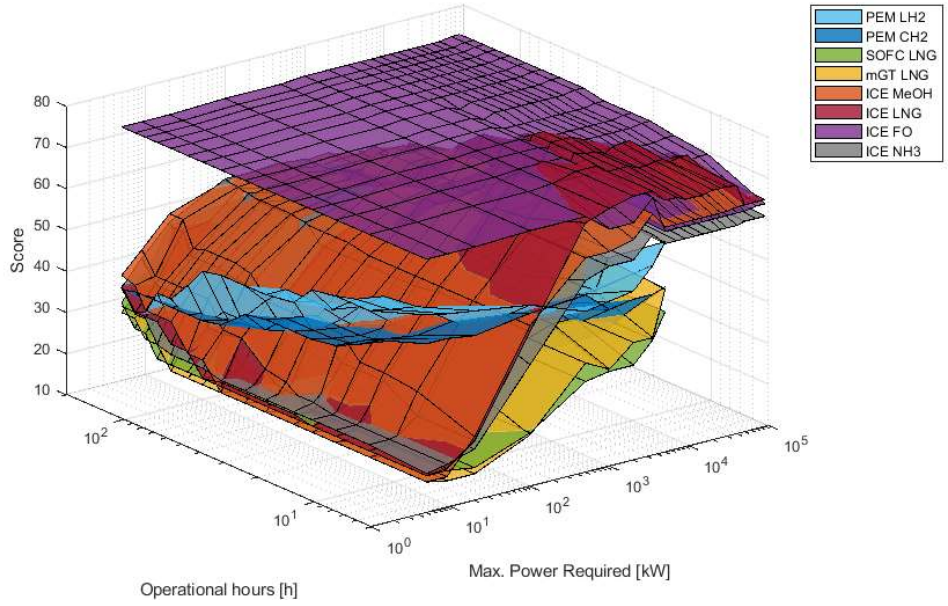

Figure 34. *3D representation of dataset for relevance equal to 1 for mass, cost and emissions, and 5 for volume.*

1.5 Concluding remarks

In conclusion, form the first analysis of the maritime field, we can firstly appreciate the adherence of the simulations with the two real cases, meaning that the tool is reliable and could be used to investigate other case study.
Through the two case study presented, the competitiveness of fuel oil engines has been highlighted in most applications requiring large powers and abundant operating hours, while, as this decrease, a growing competitiveness of alternative engine fuels, in particular LNG, has been highlighted, even in medium-high ranges of power and operating hours. In the lower ranges of these parameters, however, numerous solutions present similar scores, and for high emission relevance values, very high scores were obtained for alternative technologies such as fuel cells, demonstrating their competitiveness, despite their limitations in terms of costs and volumes, that could be the result of their low TRL (Technology Readiness Level).
From this starting point, we investigated the fuel cell solution as a clean energy system. Furthermore, in the next chapters there is an analysis in detail of these systems and the pressurization is described as a way of increasing efficiency and reducing volumes.

2 Pressurization of a PEMFC

Polymeric Electrolyte Membrane Fuel Cells (PEMFCs) are one of the most advanced fuel cell typologies. They are considered a promising technology due to their high performance [9], [44], [45] and clean energy generation. They also have a high power density [46] which makes them a valid alternative to the internal combustion engine for the propulsion of ships. PEMFCs belong to low temperature fuel cell class and this feature allows quick start-ups and shutdowns, making this system able to achieve dynamic responses following load variations and they can be scaled up to total nominal power of 1 MW [37], [47], [48], [49]. The TRL of this technology is not the same as traditional energy systems but is already commercialized. The possibility of improving this technology suggests a likely future use, however now, there are some challenges to be overcome that are related to the use of hydrogen that implies safety-related problems, the infrastructure not yet existing and the complicated transport. Moreover, these systems are currently quite expensive for the material adopted and the constrains for the supply. This type of system, in fact, uses extremely pure hydrogen as fuel and air or oxygen as combustion that must be fed with precise values of concentration and humidity to ensure the correct functioning of the system. In addition, air and hydrogen treatment systems are often used to control these levels of the flow into the cells. Electrolytes are composed of catalysts to promote reactions, hydrogen that splits (9) and then goes to bind with oxygen producing water (10) and at the same time energy in the form of direct current. In *Figure 35* is represented a traditional pattern of operation of a PEMFC.

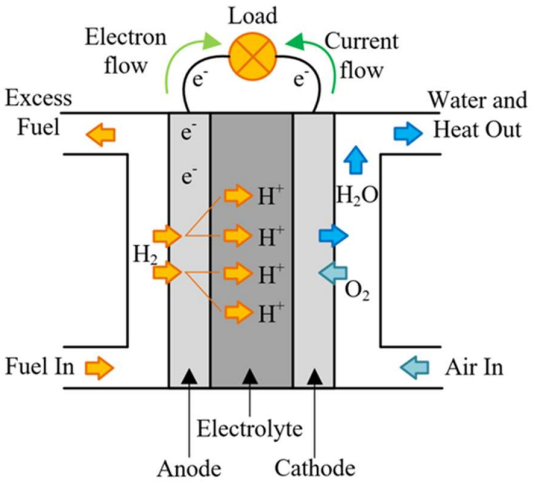

Figure 35. *Schematic functioning of a generic PEMFC*

A PEMFC normally produces 0.6÷0.7 V and currents ranging from 0.2 to 2 A/cm^2. Therefore, to produce significant powers it is necessary to dispose more cells in series related to bipolar plates. The operating temperature of the traditional LT-PEMFC varies between 50-100 °C [50] and pressures ranging from 1-4 bar absolute.

$$H_2 \rightarrow 2H^+ + 2e^- \tag{9}$$

$$\frac{1}{2}O_2 + 2H^+ + 2e^- \rightarrow H_2O \tag{10}$$

The electrochemical transformation is accompanied by a certain production of heat which requires the system to be efficiently cooled to maintain the temperature of the cell as constant as possible. Generally, the coolant consists of a mixture of water and glycols to minimize the electrical conductivity of the refrigerant while avoiding the formation of electrical bridges that would lead to short circuit and emergency shutdown of the entire system.

2.1 Commercialized models of PEMFC

Some characteristics of the main manufacturers of medium/large fuel cells are collected in this chapter, they are intended for applications in the transport sector.. A single PEM fuel cell can develop a power range between 0.1 and 1.2 W/cm^2; therefore, they are appropriately grouped into sets called stacks; each of them can develop a power proportional to the number of cells installed in it and by their performance. It is important to emphasize that operating conditions, in terms of temperature and/or pressure, determine performance that can vary even significantly from standard ones. The design choices of the fuel cell system layout is not unique, but each manufacturer assumes degrees of freedom and optimizes the auxiliary circuits by evaluating the benefits on the performance of the modules and the disadvantages due to the loops. *Table 14* contains data from the main manufacturers of hydrogen-powered polymer membrane fuel cells. All manufacturers offer solutions of individual stacks of size 30-100 kW. Some suppliers, such as Ballard and PowerCell, offer multi-stack cell systems in series for a total installed power of approximately 200 kW and sizes optimized for naval application.

Table 14. *PEMFC commercialized solutions.*

	Model	Power Range min-max [kW]	Stack Dimensions W x H x L [mm]	Stack Weight [kg]
Proton Motor	HyRange 38	5.1-35.5	436x279x768	64
	HyRange 68	9.2-64	436x279x1141	100
Ballard	FC wave	30-200	738x2200x1220	875
	FCgen-HPS	21-140	555x195x484	55 (empty)

	FCgen-ICS	9.5-63.4	443x110x675	39 (empty)
Nuvera	E-45-HD	7-45	600x500x1000	187
	E-60-HD	9-59	600x500x1000	190
PowerCell	MarineSystem200	30-200	900x2000x700	700
	PowerGeneration100	15-100	606x696x674	170
	PowerGeneration30	5-30	462x696x665	<150

2.2 Plant layout

In this section we will be dealing with a plant layout for a PEMFC. In addition to the cell itself, a series of auxiliaries that allow the correct operation of the system and that increase the cost and the complexity of the overall system are required. The traditional PEMFC system requires the basic components represented in the *Figure 36*. As could be seen, the components can be divided into three main circuits: anodic supply circuit, cathodic supply circuit and cooling system. The configuration of the installation may vary depending on the design choices of the manufacturer but mostly the components are those listed below:

- **Fuel supply system**: includes a tank containing high-purity hydrogen which, depending on the application, can be at other pressures, at cryogenic temperatures, or through metallic hydrides. On the line connecting the tank to the cell adjustment valves are placed to obtain the desired pressures in the cell input and then often the system includes an anodic recirculation loop in which the outgoing result from the cell anode

is recircled with a blower or with an ejector in order to get higher utilization factors.

- **Air supply system:** includes all the heating, humidification and compression systems necessary to obtain the required target at the cathode inlet. Included components can be a compressor, a humidifier, heat exchangers and an expander in case of higher pressures to recover energy to possibly supply to the compressors mechanically.

- **Coolant system**: serves to maintain the temperature of the cell at a fixed objective value.

Another circuit to be represented is the electrical one, that deals with managing the electrical power generated by the system and at the same time supplying energy to auxiliary systems that require a certain amount of electric power.

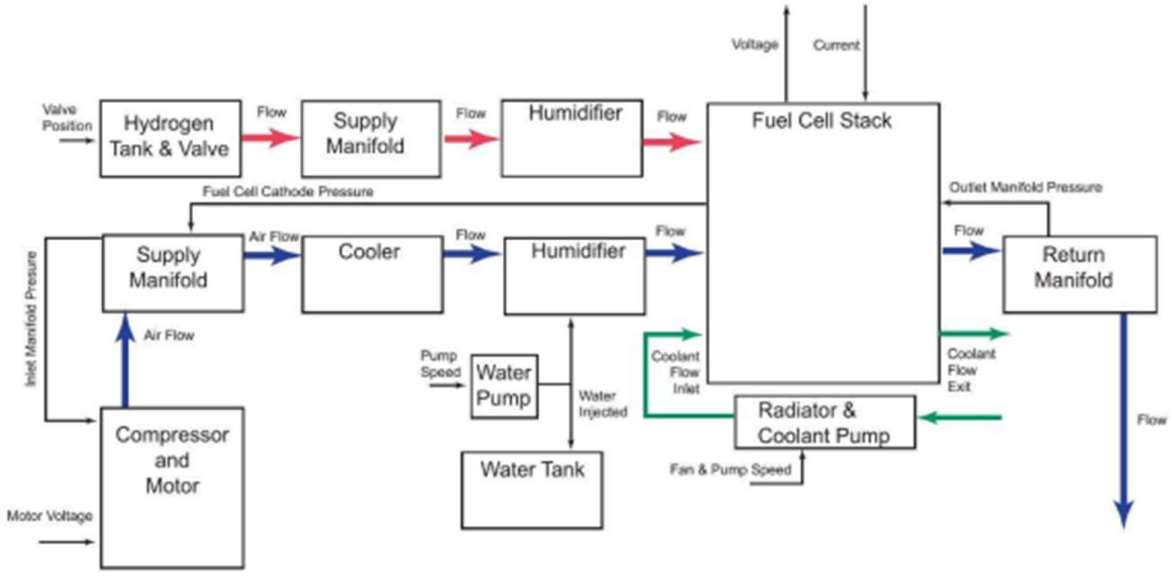

Figure 36. *Traditional plant layout of PEMFC with stack and auxilliaries.*

The traditional scheme of a PEMFC feeds reactants inside the cell at a pressure slightly higher than ambient pressure to overcome the pressure loss of the piping and the components. However, to improve efficiency, it is possible to increase the operating pressure of the system to influence the Nernst balance of the cell. In fact, in the equation that describes the maximum efficiency that a cell can reach, the so-called Open Circuit Voltage (OVC), the maximum voltage is directly proportional through a logarithm to the partial pressure of the supplied hydrogen and oxygen in the flows. Thus, pressurising the inlet flows is a way of increasing efficiency, but this choice influences the BoP complexity with the need for a component such as a compressor that requires a significant power to compress the required air flow [51]. From the hydrogen side pressurization is necessary unless lamination valves are used, and hydrogen comes from a pressurized storage. Not using the pressure solution is possible but still a blower must be included to move the air inside the circuit resulting in a lower power peak [52]. The temperature of the exhaust gases could reach more than 100 °C, so the enthalpy of exhaust gases could be expanded in a turbine mechanically connected to the compressor [53]. Since the enthalpy difference between turbine inlet and outlet can't provide the needed power to compressor in all working condition, a power surplus could be provided by an electric motor. The solution with turbocharger has already been studied previously by our research group [54], [55], [56] and by others [53], [57].

In this section we present the advantages about pressurizing a PEMFC through model simulation [58], using a commercial software, GT-Power by Gamma Technologies, and the code developed by our research group in MATLAB-Simulink ambient. For the comparison we modelled two systems, one

pressurized and one atmospheric with most of the components in common to appreciate the advantages of the pressurization with a TC (Turbocharger).

PEMFC – TC system layout

The first layout is shown in Figure 37: the air flow is pressurized by the compressor (C) and pre-heats the PEMFC exhausts through a gas-to-gas heat exchanger (GTG) installed in counter-flow configuration. The system is designed to work with a cathode inlet pressure of 2.5 bar in nominal conditions. To guarantee the correct operation of the PEMFC, it is necessary to maintain the polymeric electrolyte membranes wet and to feed the cell with a properly humid cathode flow. For this reason, a nafion membrane crossflow humidifier (HUM) is installed on the cathode loop. The pressurized air coming from the GTG enters the dry side of the HUM, while the PEMFC cathode outlet flow enters the wet side. In fact, in a PEMFC the H+ ions migrate from the anode to the cathode, where they react with oxygen to form H2O. The fuel cell stack also includes condensation traps to avoid presence of liquid water in the outlet flows. However, the cathode outlet flow of the PEMFC has high relative humidity. Within the HUM, part of the water contained in the flow is transferred to dry side through the nafion membranes, increasing the humidity of the cathode inlet flow to the correct values. Then, the cathode outlet flow enters the GTG and expands in the turbine (T), providing part of the mechanical power necessary to drive the compressor. The remaining part is supplied by an electrical motor (EM) connected to the shaft of the turbocharger. The GTG has been specifically designed and sized to guarantee correct operation of the turbine and prevent the flow from condensing for any operating condition. Finally, the cathode flow is discharged into the ambient.

The cathode loop also includes a set of valves, which can be used to control the system in various conditions and improve its flexibility. Part of the air flow can be diverted from the HUM dry inlet to the wet outlet through the fuel cell bypass valve (FCB). This can be useful at low electrical loads, to limit the reduction of air mass flow and avoid fluid-dynamic instabilities in the turbocharger. Moreover, both sides of the HUM can be partially bypassed through the wet side bypass valve (WSB) and the dry side bypass valve (DSB). In this way, it is possible to control the humidity of the cathode inlet air in many different conditions and meet the requirements of the PEMFC.

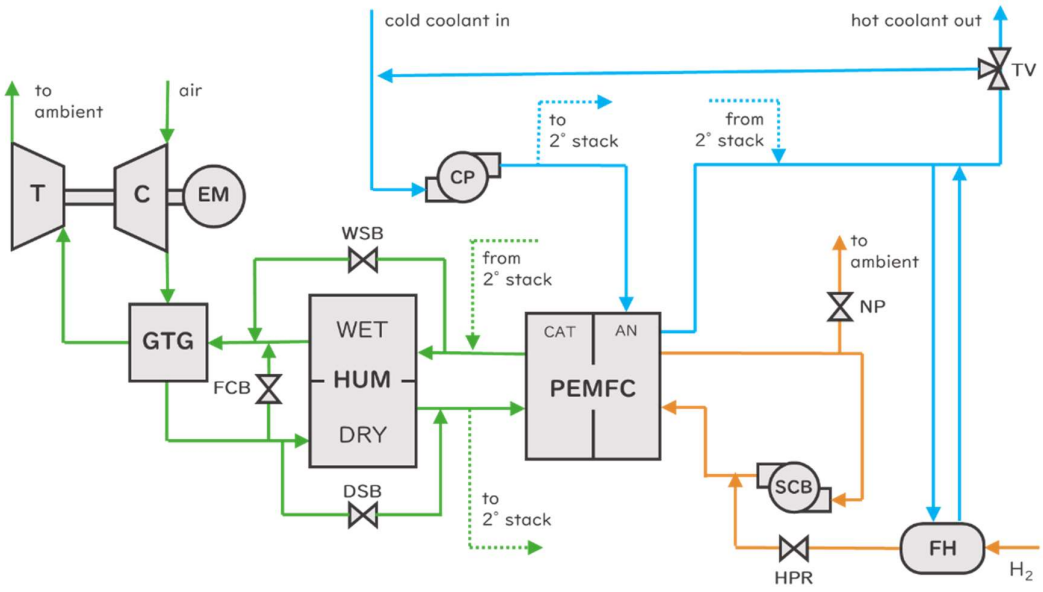

Figure 37. *Layout of the turbocharged PEMFC system (in green the cathode loop, in orange the anode loop, in blue the cooling circuit).*

The fuel used to power the PEMFC is pure H2, which is assumed to be available at 10 bar. The H_2 flow is first pre-heated by a fuel heater (FH) and then its pressure is reduced by the hydrogen pressure reducer valve (HPR) before entering the anode loop. Then the hydrogen enters the anode side of the PEMFC,

where it is consumed to generate electric power. However, not all the H_2 reacts within the cell and the hydrogen content at the anode outlet is still significant. For this reason, the anode outlet flow is recirculated by a side channel blower (SCB) and mixed with the pure H_2. The choice of this component is dictated by design reasons. Unlike an ejector, which has a fixed geometry, the SCB gives the possibility of adding a degree of freedom to the system by varying its rotational speed. Furthermore, compared to other types of blowers, it is the optimal choice for flow rates of this magnitude, both in terms of performance and maintenance requirements.

The anode loop also includes a nitrogen purge valve (NP). In fact, because of diffusion effects, small quantities of N_2 can go from the cathode to the anode side of the PEMFC. Since the anode loop is closed, the amount of N_2 would increase over time, reducing the concentration of H_2 and negatively affecting the performance of the fuel cell. A periodic discharge of the anode flow to the ambient through the NP prevents this phenomenon.

The main purpose of the cooling circuit is to control the temperature of the PEMFCs. To do this, a water-glycol mixture is used as refrigerant fluid. The refrigerant is supplied to the cooling circuit at a certain temperature (71°C in nominal conditions). If this temperature were too low, the flow could be mixed with part of the hot refrigerant, which is diverted from the main line through the thermostat valve (TV). Then, the fluid is pressurized by a centrifugal pump to overcome the pressure losses of the circuit and used to cool down the stacks. The refrigerant at the stack outlet is significantly hotter than the H_2 supplied to the system, which is assumed to be at 25°C. Therefore, it is possible to use the hot coolant to pre-heat the fuel flow in the FH.

Atmospheric PEMFC system layout

The atmospheric PEMFC system considered for this comparison includes most of the components used for the TC-PEMFC plant. The small changes implemented lead to the layout described in *Figure 38*, which shows:

- The cathode circuit, including a compressor driven by an electric motor, a charge air cooler (CAC), a humidifier, and an orifice (BPO) that keeps the system pressure slightly above the ambient condition (the geometry was fixed to obtain 1.5 bar at the cathode inlet in nominal condition).
- The anode circuit, which includes a fuel preparation system, a nitrogen purge valve and an ejector-based anode recirculation system. Being a static component with a fixed geometry, the ejector does not require any electric power.
- The cooling system, which has the same layout of the one in the turbocharged system. It includes a centrifugal pump that circulates the refrigerant and a thermostat valve to control the pump inlet temperature.

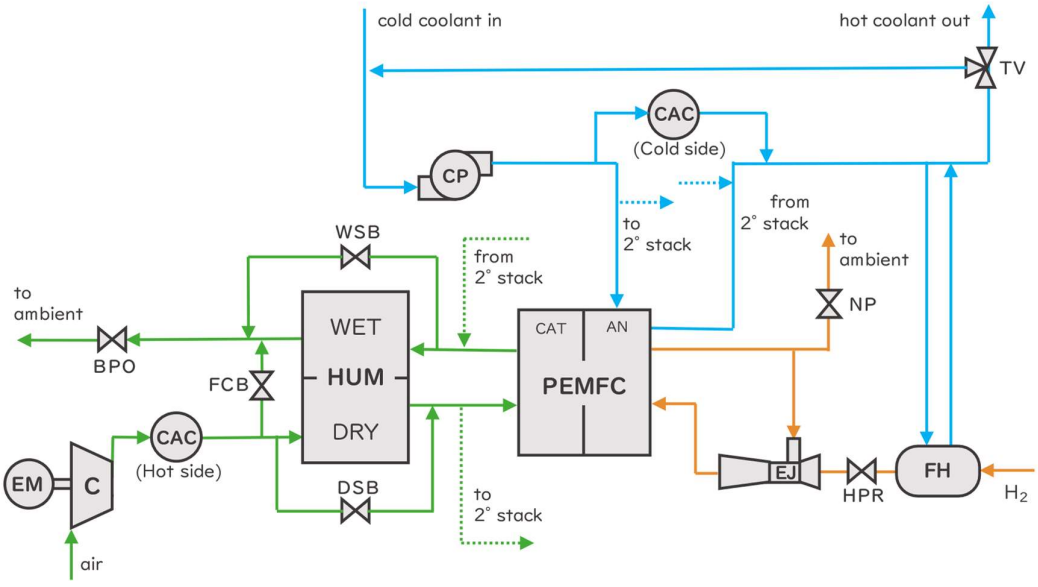

Figure 38. *Layout of the traditional atmospheric PEMFC system (in green the cathode loop, in orange the anode loop, in blue the cooling circuit).*

Control system

As previously mentioned, many of the BoP components are used to guarantee the correct functioning of the PEMFCs and to comply with their operative constraints. Therefore, it was necessary to design a control system devoted to the regulation of these components.
Having many parameters to be controlled, the system relies on simple and reliable controllers. In details, the two following types of controllers were adopted:

- *Feed-forward*: the control variable is modified according to a pre-determined relationship, as a function of the PEMFC electric current. Such relationship (typically an interpolated 1D table) was previously defined in stationary conditions, in order to obtain the desired value of the controlled parameter.
- *Proportional-Integral-Derivative (PID)*: the control variable is modified depending on the error between the controlled parameter and its setpoint value.

The controllers considered for this work and implemented on the dynamic model are described below.

- *Excess of oxygen* – The PEMFC should work with a proper excess of oxygen λ_{O2} (i.e., the ratio between supplied and consumed O_2). A feed-forward controller changes the rotational speed of the turbocharger N_{TC} to obtain the desired value of λ_{O2} that should be 1.8 in all operating conditions except for low rotational speed where the value increases due to compressor map limits.
- *Cathode inlet humidity* – The relative humidity of the cathode inlet air $R_{cat,in}$ (computed at the coolant inlet temperature) is controlled by

acting on the DSB. The opening of the valve FO_{DSB} is determined by a feed-forward controller.

- *Anode inlet pressure* – The pressure difference between anode and cathode must be limited not to stress the membranes. A PID controller acting on the HPR opening FO_{HPR} modifies the fuel pressure to maintain this difference constant.

- *Nitrogen concentration* – The frequency of purge cycles should be properly timed to maintain the N_2 concentration in the anode loop on acceptable values. Therefore, the time between two openings of the NP is regulated by a feed-forward controller.

- *Stack temperature* – The temperature of the fuel cells can be controlled by changing the coolant mass flow entering the stack. A feed-forward controller changes the rotational speed of the centrifugal pump N_{CP} to obtain the proper mass flow and match the stack temperature setpoint.

- *Coolant temperature* – Since the coolant mass flow is defined by a feed-forward controller, its temperature could affect the heat drawn from the stacks. To avoid this effect, the system includes a PID controller acting on the TV. Opening this valve, it is possible to mix part of the hot coolant with the cold refrigerant and to avoid temperature fluctuations at the stack inlet.

The control logics that regulate FCB and WSB are not considered at this stage, but will be designed and implemented in the future.

2.3 Commercial software for dynamic simulations: GT-Power

The software for this activity is the commercial software GT-Power by Gamma Technologies, it was chosen because it allows the simulation of energy systems of different types in both stationary and dynamic conditions. The software is mainly used in companies as a design tool to predict the performance of energy systems in order to reduce costs in terms of physical testing of components, optimization of geometries, identification of problems, development of a control strategy, etc. The software belongs to the category of multi-physics simulator, so it can evaluate several aspects simultaneously, from fluid dynamics to the electrical ones. GT-Power allows you to make quick simulations that include both simple 0D calculations up to the study of 1D and 2D phenomena with calculation times of the order of seconds or minutes, unlike CFD or 3D FEA calculations that can take even days or weeks.

GT-Power is an advanced simulation software mainly used in the automotive and engine engineering industries. It allows engineers to analyze the behavior of engine power systems, including internal combustion engines, turbochargers, fuel supply systems, cooling systems and more. Here a description of how GT-Power works from a practical point of view is given.

Template Definition: The first phase involves defining the model of the system that you want to simulate. This can be an internal combustion engine, a fuel supply system, a turbocharger or, as in this case, a PEMFC system. The size, parameters and initial conditions of the system must be specified.

Component selection: GT-Power offers a wide library of standard components, such as heat exchangers, valves, tubes, etc., that can be dragged and placed in the model display.

Component Configuration: Each component must be configured with its specific properties and parameters. This configuration is done through a series of dialog and drop-down menus within the software.

Component connection: This is done by dragging connections between the components. For example, it is possible to connect a compressor to a shaft mechanically and through the fluid piping dynamically. These connections will define the flow of fluid and the interaction between the components.

Initializing simulation conditions: Before performing the simulation, it is necessary to specify the initial conditions of the system. This could include the initial temperature, the initial pressure, the rotation speed, etc. These initial conditions are crucial to determining the behaviour of the system during the simulation.

Definition of simulation criteria: Simulation criteria must also be defined, such as the duration of the simulation, the data sampling interval, the variables to be monitored and the desired outputs.

Running the simulation: GT-Power solves mathematical equations that describe the behaviour of the system over time and generates output data that show how the system behaves under different conditions.

Results analysis: This may include analysis of performance, efficiency, emissions and other relevant parameters.

Optimization and iteration: usually the aim of the simulation is to optimize the system. In this case, you can make changes to the components, initial conditions or simulation criteria and repeat the process until reaching the desired results.

GT-Power is a powerful tool for engineering of engines and power systems but requires an in-depth knowledge of engineering in the field of fluid dynamics, thermodynamics, and mechanics to be used effectively. Its flexibility allows engineers to simulate a wide range of systems and conditions, making it a valuable tool for the development and optimization of engines and related systems.

Custom component creation

Some components of the GT-power library are not detailed enough to accurately simulate certain phenomena. The humidifier component in the commercial software couldn't simulate a crossflow configuration with the desired level of detail to show and correctly simulate the mass exchange inside the component. Therefore, our research group developed in MATLAB-Simulink a specific model of humidifier we described in [59]. In GT-Power is not possible to create a real custom component but is allowed to create a communication between MATLAB-Simulink and GT-power and integrate the two models in a co-simulation mode. One of the requirements for this co-simulation configuration to work properly is that the GT-Power model works on a computer on which MATLAB is not installed.
The process of integrating the MATLAB-Simulink code with a GT-Power model can be divided into stages:

- The Simulink model must be modified and integrated with a Simulink interface block created by Gamma Technologies. The block must be connected to all input and output of the component and the interface must

be correctly configured and linked to the "mux" and "demux" components in MATLAB-Simulink.

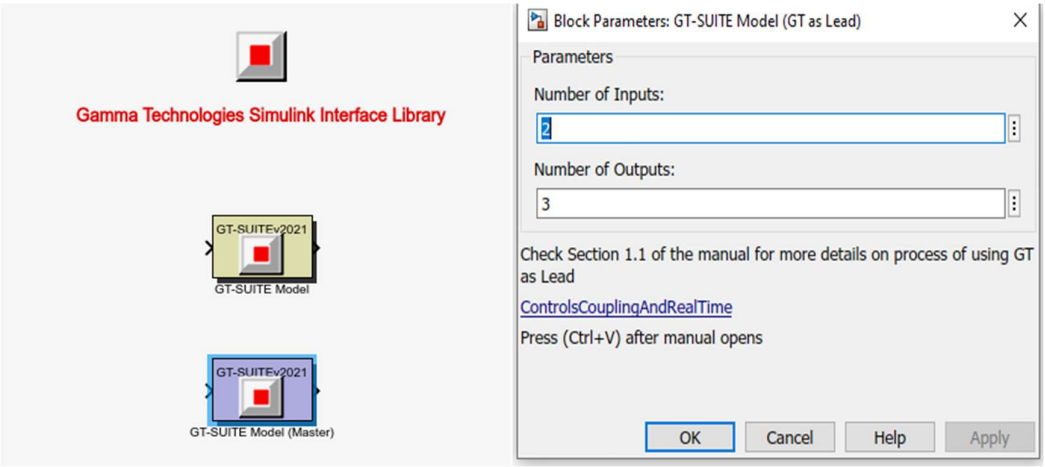

Figure 39. *MATLAB-Simulink interface of the component created by Gamma Technologies for co-simulation.*

- Thanks to the add-on package “coder”, the model in Simulink can be compiled generating a file.dll. In the GT-Power model, using the

"SimulinkHarness" block and choosing the *import simulink model* option, the previously generated .dll file is imported in GT.

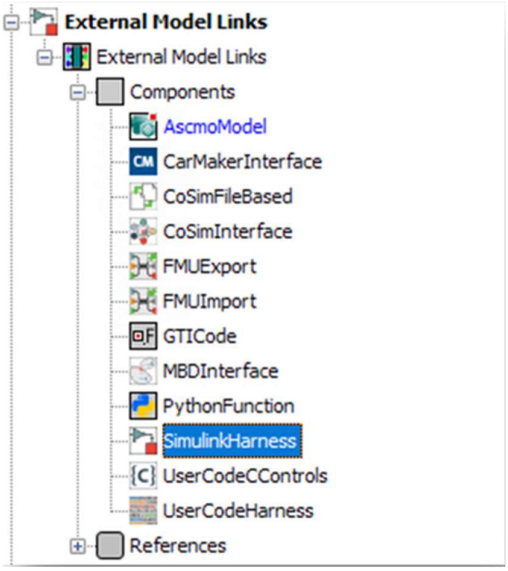

Figure 40. *List of co-simulation code from the GT-Power library.*

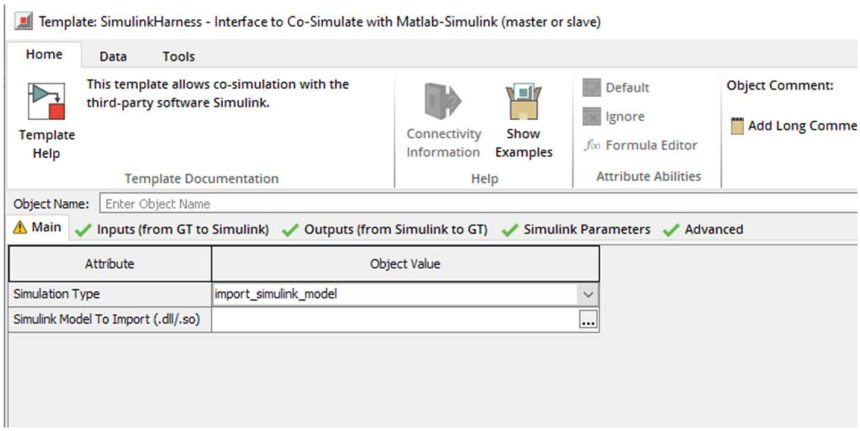

Figure 41. *Setup of the GT-Power simulink co-simulation block component.*

- Define all the initial conditions of the input and output variables from the component and the parameters in GT-Power.

Main | Inputs (from GT to Simulink) | Outputs (from Simulink to GT) | Simulink Parameters | Advanced | Plots

Attri...	Signal Description	Wireless Signal or RLT	'SendSignal' Named-Signal Name	Initial Input Value	Duration at Initial Input	Input Signal GT Map Labels	Input GT Signal Units
					s		
1	m_dot_wet_in	ign	ign	0.27	0.3	def	ign
2	p_wet_out	ign	ign	260000.0	0.3	def	ign
3	m_dot_dry_in	ign	ign	0.26	0.3	def	ign
4	x_h2o_wet_in	ign	ign	0.18	0.3		
5	x_co2_wet_in	ign	ign	0.0	0.3		

Main | Inputs (from GT to Simulink) | Outputs (from Simulink to GT) | Simulink Parameters | Advanced | Plots

Attri...	Signal Description	Signal Name (Transmitted Wirelessly)	Initial Output Value	Duration at Initial Output (Cosimulation Only)	Output Signal GT Map Labels	Output GT Signal Units
				s		
4	Out_Dryflow_m_dot	ign	0.2607	1.0	def	kg/s
5	Out_Wetflow_T	ign	338.0	1.0		
6	Out_Dryflow_T	ign	339.0	1.0		
7	Out_Wetflow_Xh2o	ign	0.1042	1.0		

Main | Inputs (from GT to Simulink) | Outputs (from Simulink to GT) | Simulink Parameters | Advanced | Plots

Attri...	Parameter Descriptions	Parameter Names	Parameter Values
1	Wet Flow on-design_m	WFmin	0.276
2	Wet Flow on-design_p	WFpin	265300.0
3	Wet Flow on-design_T	WFtav	359.75
4	Wet Flow on-design_R	WFr	323.4

Figure 42. *Setting of parameters and input and output variables.*

The final plot of how the integrated block looks is shown in *Figure 43* and *Figure 44*(all components can be included in a subsystem for a more ordered result).

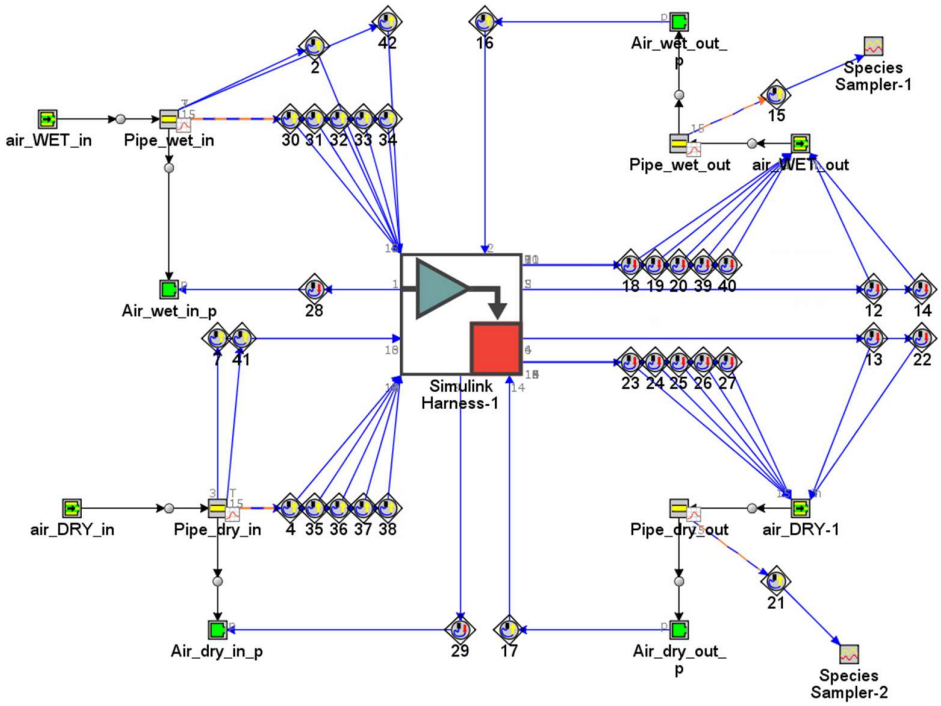

Figure 43. *Simulink model connected to 4 pipes for the calibration of the new component.*

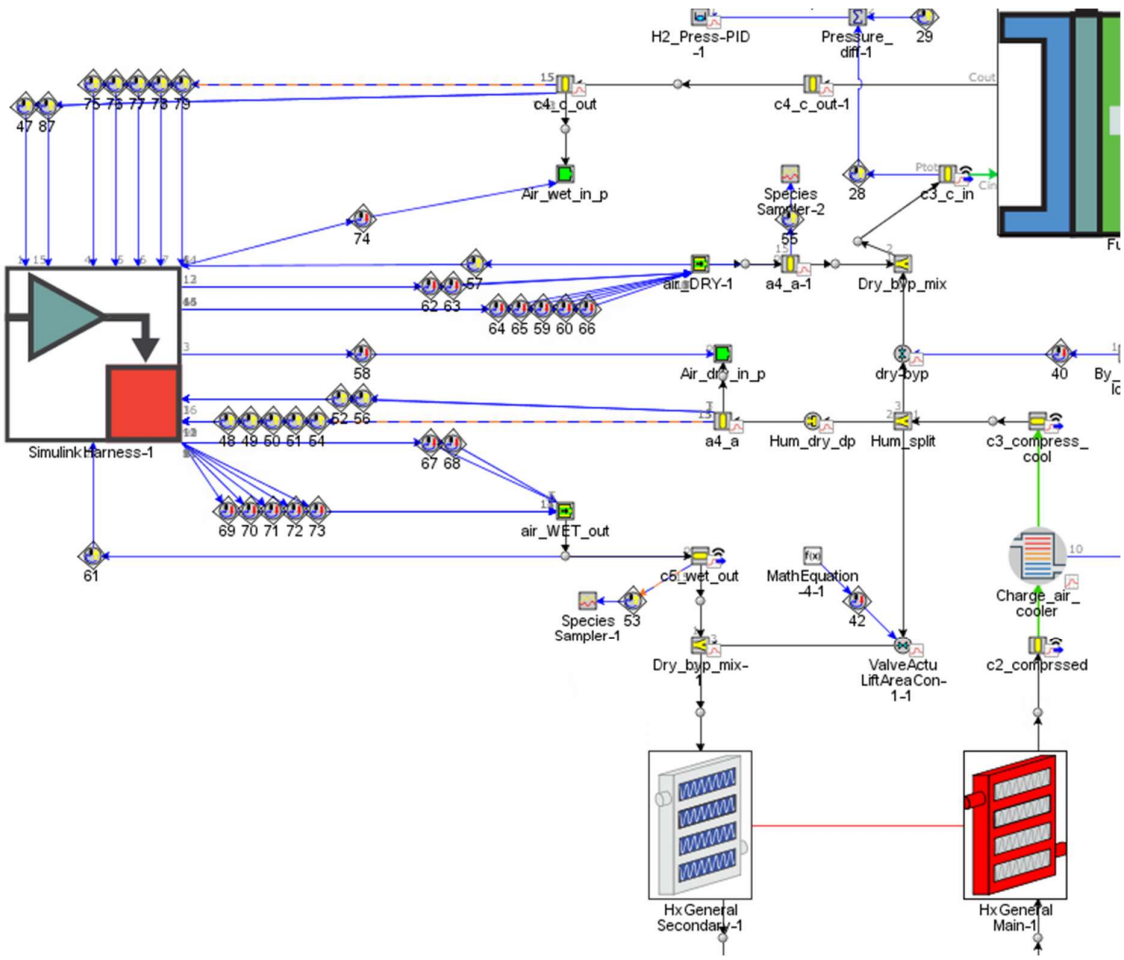

Figure 44. *Integration of the custom model within a PEMFC model in GT-Power.*

2.4 Model description

A simulation model was developed to analyse the performance of the TC-PEMFC plant described in *Figure 37*. Even if each component includes a specific set of equations to simulate their physics (e.g., heat transfer or mass transfer), most of them compute the pressure losses relying on the standard equations of a pipe.

The TC-PEMFC system was modelled considering the following main assumptions:

- The PEMFC is made by two stack that are always working in the same conditions. Thus, it was possible to group the two stacks into a single PEMFC model, significantly reducing the simulation time. This modification is acceptable because the power generated by a fuel cell stack grows linearly with the number of cells in it, with a negligible effect on its overall performance. Consequently, the mass flows entering the fuel cell model must be doubled and the components in the anode loop must be scaled up accordingly. The cathode and cooling circuits, instead, do not require any modification because they serve both stacks in the real system.
- The pure H_2 flow entering the anode loop is provided at the required pressure and temperature. Therefore, it was not necessary to include in the model the components between H_2 tank and HPR.

The model includes the simulation of the anode and cathode circuits, the refrigeration and the electrical system.

PEMFC

Regarding the PEMFC model, the fuel and coolant flows go through the stack in counter-flow configuration with regards to the air flow. The PEMFC component interface includes all the data needed for its performance evaluation. The equations used in this work for the evaluation of the polarization of the cell are described inTable ***15***. In addition, the model takes into account the crossover of nitrogen and water through the membrane The second one is broken into two mechanisms, electro-osmotic drag and back diffusion. All the correlations used to model these phenomena have been calibrated on the PEMFC specifications.

The cell receives as inputs the anode and cathode flows, which react generating a direct electric current and forming water. The current is conveyed on an electric circuit modelled operating with two loads in parallel.

Cathode circuit

The cathode circuit is interfaced with the ambient both at the compressor intake and at the turbine outlet. This configuration is defined in the model by two pressure boundary conditions. The air mass flow rate is determined by the rotational speed of the TC and by the pressure losses in the circuit. Both the compressor and the turbine were modelled using pre-existing maps and were mechanically linked by a shaft component that imposes the same rotational speed N_{TC}. The value of N_{TC} is directly set by a feed-forward controller, without modelling the physics of the EM. To compute the net power output of the system, the efficiency of the EM is always assumed to be constant. The power demand required by the electric motor is evaluated through the use of the electric and mechanical conversion efficiencies (11) fixed for all operating condition.

$$P_{EM} = \frac{P_C - P_T}{\eta_{Mec} \cdot \eta_{El}} \tag{11}$$

After going through the compressor, the flow is pre-heated by the GTG, which is modelled as a plate gas-to-gas heat exchanger. The heat transfer equation Eq. (12) evaluates the energy balance between the two fluids, Main (compressor side) and Secondary (turbine side), and the solid wall of the heat exchanger. The GTG performance is evaluated with liner interpolation starting from a map of experimental points. For each of these point the software requires pressure and temperature boundary conditions to evaluate the heat transfer and the pressure losses of the component.

$$\frac{dT_{wall}}{dt} = \frac{Q_m - Q_s}{\rho V C_p} = \frac{\left[\left(\frac{h}{1+hR_f}\right) A\Delta T\right]_m + \left[\left(\frac{h}{1+hR_f}\right) A\Delta T\right]_s}{\rho V C_p} \quad (12)$$

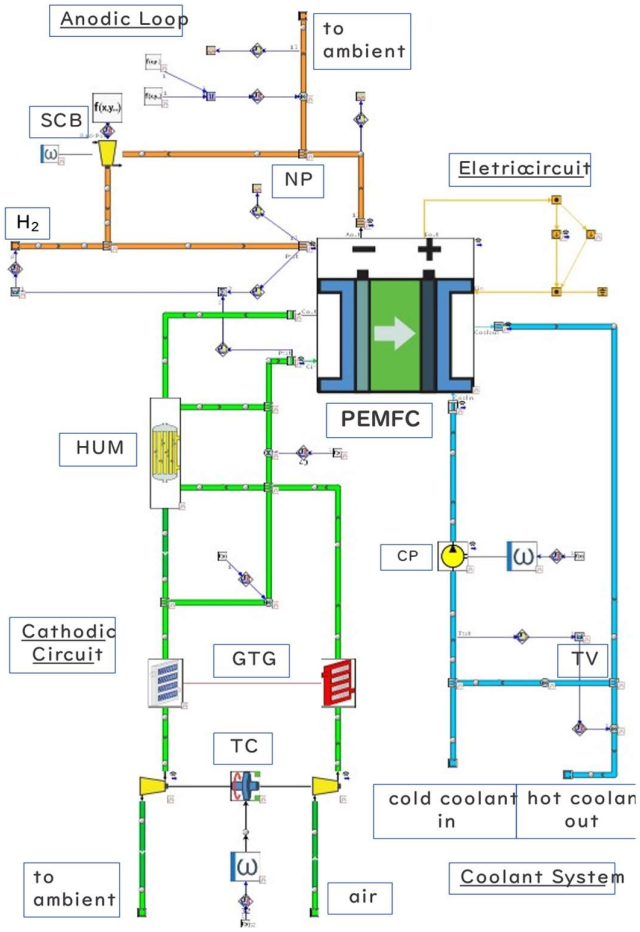

Figure 45. *GT-Power model view (in green the cathode loop, in orange the anode loop, in blue the cooling circuit).*

The last auxiliary component on the air circuit is the HUM, which is modelled adopting a shell-tube configuration. Water transfer from wet to dry side is driven by vapour pressure difference across the membrane and it is function of

the water content and the temperature. Among the different models to describe the water diffusivity thought the membrane in this work we consider Springer's [60]. Furthermore, there is also a simple heat transfer correlation applied between the wet and the dry gases. The humidifier component is a static and passive object that does not allow the regulation of wet and dry flows. Therefore, the regulation of the humidity entering the cell is carried out by the DSB. This bypass valve is modelled with an almost linear behaviour and it is controlled by a feed-forward that determines its opening.

Anode circuit

The anode circuit is interfaced with the hydrogen tank at the HPR, and with the ambient at the NP outlet. Also in this case, this configuration is represented by two pressure boundary conditions, the first one set by the PID controller and the other one fixed at ambient pressure. The SCB installed on the anode circuit is used to recirculate the unused fuel to the stack inlet. It is characterized by low mass flow rates and a pressure ratio that does not exceed 1.4.

Table 15. *PEMFC polarization losses equations.*

Fuel cell operating voltage	$V_{cell} = V_{Nernst} - V_{act} - V_{mt} - V_{ohm} - V_{delOC}$	(13)
Nernst potential	$V_{Nernst} = \frac{-\Delta \bar{g}_f}{2F} = \frac{\left(\bar{g}_f\right)_{H_2O} - \left(\bar{g}_f\right)_{H_2} - 0.5 \cdot \left(\bar{g}_f\right)_{O_2}}{2\mathrm{F}}$	(14)
Activation losses (Tafel equation)	$V_{act} = \begin{cases} \frac{R_{gas} \cdot T}{2F} \cdot \left(\frac{i}{i_0}\right) & i \leq \frac{i_0}{(1-\alpha)} \\ \frac{R_{gas} \cdot T}{2\alpha F} \cdot ln\left(\frac{i}{i_0}\right) & i > \frac{i_0}{(1-\alpha)} \end{cases}$	(15)

Exchange current density [60][11]	$i_0 = i_0^{ref} a_c L_c \left(\frac{P_{O_2}}{P_{ref}}\right)^{\gamma} exp\left(\frac{E}{R}\left(\frac{1}{T_{ref}} - \frac{1}{T_{cell}}\right)\right)$	(16)
Mass transport losses (concentration)	$V_{mt} = -C \cdot ln\left(\frac{i}{i_L}\right)$	(17)
Ohmic losses	$V_{ohm} = i \cdot R_{ohm}$	(18)
Ohmic resistance	$R_{ohm} = t_m/\sigma_m$	(19)
Membrane conductivity [61][12]	$\sigma_m = (b_{11}\lambda_m - b_{12})exp\left(b_2\left(\frac{1}{303} - \frac{1}{T_{cell}}\right)\right)$	(20)

The peculiarity of this component is that the density of the fluid strongly influences its behaviour. For this reason, the performance of the SCB is defined by multiple maps, one for each different fluid. The N_2 crossover within the PEMFC leads to a variation of the anode flow composition and density. Consequently, the operating point of the SCB changes over time. The SCB model is not included in the GT-Power library. To simulate its performance, the standard compressor model was adopted and modified to linearly interpolate the maps as a function of the intake density. Furthermore, the original maps were scaled up to take into account the simplifying assumptions described at the beginning of this section. In fact, each stack is served by a SCB in the real layout.

[11] P_{ref} is 1 atm, T_{ref} is 298.15 K and E is 66 kJ/mol. The $i_0^{ref} a_c L_c$ is evaluated in the pre-processing using i_0 as input and P_{O2} and T_{cell} from the reference condition. During the simulation it is held constant to evaluate i_0 function of P_{O2} and T_{cell}.

[12] b_{12} is 0.00326, b_2 is 1268. b_{11} is evaluated in the pre-processing using R_{ohm} as input and $lambda_m$ and T_{cell} from the reference condition. During the simulation it is held constant to evaluate R_{ohm} function of $lambda_m$ and T_{cell}.

Grouping the two PEMFCs in a single stack model, it was necessary to double the mass flow rate recirculated by the SCB.

Fresh hydrogen is taken from a pressurized tank, preheated by the FPH and expanded to the desired pressure through the HP valve. In the model the temperature is fixed, and neither the heat exchanger nor the pressure reducing valve are simulated. The pressure boundary condition is imposed by a PID controller to maintain a pressure difference of 200 mbar with the cathode.

The N_2 crossover from cathode to anode was defined in the PEMFC model in terms of molar flow rate per N_2 partial pressure difference, and it was set equal to $1.15 \cdot 10^{-5}$ mol/s m^2 bar. The cross section area of the NP was set equal to $2.24 \cdot 10^{-6}$ m^2 and its purging cycle was set up in order to keep the average volume fraction of H_2 in the anode loop at 70%. The NP is regulated by a square wave function. The opening time of the valve is always 1 s, but the time between two purging cycles depends on the operating condition of the plant, i.e., on the electrical current value.

Cooling circuit

The fluid processed in the cooling circuit is a water-ethylene glycol mixture (50-50% by volume). The fluid circulating in the loop is moved by a centrifugal pump controlled by a feed-forward drive. The simulation of this component is based on the GT-Power liquid pump model. The operating conditions of the pump are determined through the linear interpolation of performance maps of pump rotational speed, volumetric flow rate, pressure rise, and efficiency. The calculation of the power requirement of the pump is based on (21) where $\eta_{s,CP}$ is the isentropic efficiency of the coolant pump.

$$P_{CP} = \dot{m}_{CP} \cdot \frac{p_{out,CP} - p_{in,CP}}{\rho_{in,CP} \cdot \eta_{s,CP}} \tag{21}$$

Modelling assumption for atmospheric PEMFC

The standard PEMFC system must respect some conditions for the comparison between the two models to be meaningful. In fact, the system could be designed to have the same size, nominal power or efficiency of the TC-PEMFC plant. The methodology adopted in this paper is to simulate a PEMFC system that generates the same maximum power of the TC-PEMFC system, with the same net efficiency. Operating the stack closer to the ambient pressure, its efficiency is lower. Consequently, to generate the same power, it is necessary to enlarge the stack. To increase the size of the stack, the active area of the PEMFC was scaled up. Consequently, all the auxiliary systems already considered in the pressurized model had to be resized accordingly, and all the controllers had to be properly tuned. This section briefly describes the layout of the PEMFC system and the main differences with the turbocharged solution.

In the standard PEMFC system, the GTG is not present anymore on the cathode loop. In fact, since the system works at a much lower pressure than the TC-PEMFC, the temperature increase through the compressor is reduced, and the benefits of the GTG would be negligible. Moreover, removing this component lowers the pressure losses on the air path.

The HUM is always installed before the PEMFC and, regulating the DSB valve opening, it can be used to adjust the relative humidity at the cell inlet. Since the humidifier processes a different mass flow rate, it had to be resized.

The compressor works with a smaller pressure ratio in this system (1.5-1.7), but there is no turbine to recover energy and generate back pressure at the end of the air line. For this purpose, an orifice was designed and installed at the air discharge to obtain a PEMFC cathode inlet pressure of approximately 1.5 bar in nominal condition.

Similarly to the turbocharged system, the mass flow rate processed by the compressor must be enough to guarantee a constant air excess ratio at the

PEMFC inlet equal to 1.8. Cell inlet temperatures are considered to be the same of the turbocharged case.

A new component that was added in this standard PEMFC system is the charge air cooler (CAC), a heat exchanger connected to the refrigerant circuit that cools down the air flow before entering the HUM. The addition of this component is necessary due to the absence of the GTG. This component was not available in the GT-Power library and so it was modelled as a pipe with a certain heat exchange that is proportional to the heat taken by the coolant circuit.

Since this system should be characterized by a reduced BoP power consumption, the SCB was replaced with an ejector for the anode recirculation. The nitrogen purge system is designed in the same way, but the timing of the purge cycles had to be adjusted to obtain an average molar fraction of H_2 equal to 70% in the anode loop.

2.5 Result and comparison

This section describes the results obtained from the model simulations. At each time step, the model saves the thermo-physical properties of the flows and the characteristic operational parameters of the components, such as TC rotational speed and PEMFC voltage. The system was simulated for 300 s in three different operating conditions. At first, it was simulated in nominal conditions, corresponding to a PEMFC electrical current I of 100% of its nominal value.

It is necessary to point out that all the results that refer to a specific operating point are averaged over the simulation time. This is necessary because the purge valve NP is periodically opened to lower the nitrogen concentration in the anode loop. Therefore, the system never reaches a proper stationary condition, as shown by Figure 46.

This picture shows how the composition of the anode flow changes during normal operation at I=100%. It is possible to verify that the target 70% average concentration of H_2 in volume fraction, equivalent to about 25% in mass fraction (orange dashed line), is met, and thus that the purge cycles have been properly timed.

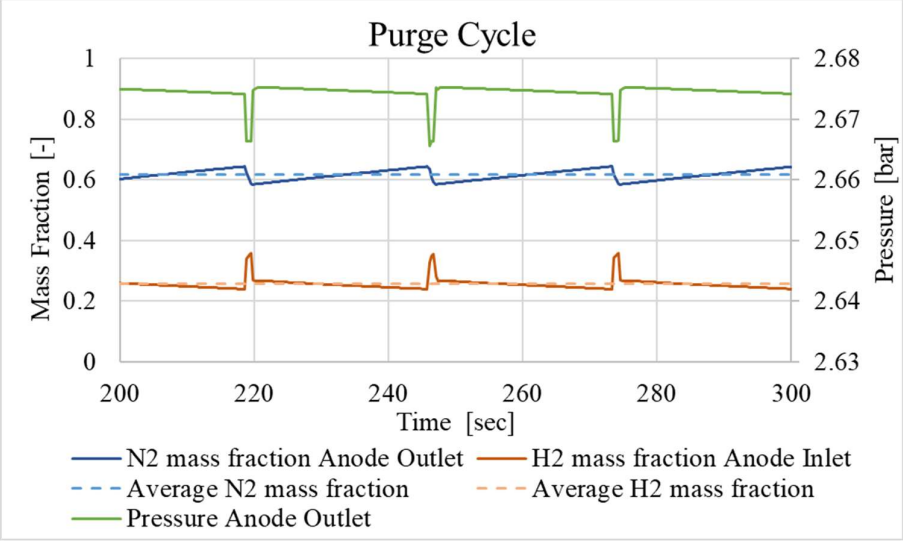

Figure 46: *Nitrogen and hydrogen volume fraction at the PEMFC anode outlet and inlet, respectively (left axis) and anode inlet pressure (right axis).*

From the simulation of the system in nominal conditions, it possible to obtain its main operational parameters, which are reported in *Table 16*.

Table 16: *TC-PEMFC system design point operation.*

TC - PEMFC performance		
Net Power System / Nominal Power	100%	-
Electric Current / Nominal Current	100%	-
Net Efficiency	0.57	-
Average Single Cell Voltage	0.769	V
Air Excess Ratio	1.8	-
Fuel Stoichiometry	2	-
Compressor Electric Motor Power	13.2	kW

After defining the nominal conditions of the system, the study continued with the investigation of its off-design performance, imposing electrical currents equal to 31.3% and 140.6% of the nominal value (minimum and maximum, respectively).

Due to the current variations, there is a change in the mass flow rates and pressures of the plant. This leads to variations of the PEMFC Nernst potential and to modifications of the polarization curve. The temperature has a slight influence on the polarization curve, but the range in which it varies for this application is not significant.

Figure ***47*** highlights the advantages of the stack pressurization. The green curve represents a typical polarization curve at constant pressure of a PEMFC like the one considered for this study. At higher currents, an atmospheric system can only follow the green curve, with a significant reduction of voltage and efficiency. On the contrary, with the compressor, the TC-PEMFC system can increase the stack pressure at higher loads, raising the operational points over the green curve. In this way, the system limits the reduction of efficiency and guarantees a more uniform performance.

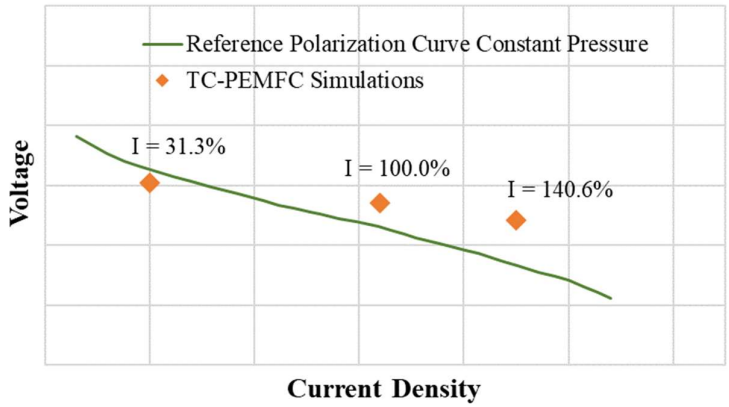

Figure 47: *Comparison between the operational points of the system (in terms of voltage and current density) and a typical PEMFC polarization curve at constant pressure.*

The result of the off-design analysis of the pressurized system is shown in the Table 17, with the net power and the efficiency values of the system corresponding to the maximum, the minimum of the operating range and design point. As will be shown below, the behaviour of the efficiency is monotonic decreasing with a trend similar to that of atmospheric systems.

Table 17: *Power and efficiency of the TC-PEMFC system for different load conditions.*

Load	***Net System Power/Nominal Power***	***Net Efficiency***
Min	33 %	59.7 %
Design	100 %	57.0 %
Max	132 %	53.3 %

Another interesting information that can be derived from the simulations regards the pressure drops along all the components and the pressure distribution of the whole system. The pressure decrease is more significant on

the cathode side, due to a higher number of components and a greater mass flow rate. The analysis of pressure losses gives a particularly useful information, which can be used to size the compressor of the TC and optimize the design of the system.

A0	Module intake
A1	**Compressor intake**
A2	**Compressor discharge**
A3	**Gas-to-gas hot outlet**
A4	**CAC outlet**
A4A	**Humidifier dry inlet**
A4B	**Dry side bypass valve inlet**
A4C	Fuel cell bypass valve inlet
A5	**Stack inlet**
A5A	**Humidifier dry outlet**
A5B	**Dry side bypass valve outlet**
A6	**Stack outlet**
A6A	**Humidifier wet inlet**
A6B	Wet side bypass valve inlet
A7	**Gas-to-gas cold inlet**
A7A	**Humidifier wet outlet**
A7B	Wet side bypass valve outlet
A7C	Fuel cell bypass valve outlet
A8	**Turbine inlet**
A9	**Turbine outlet**

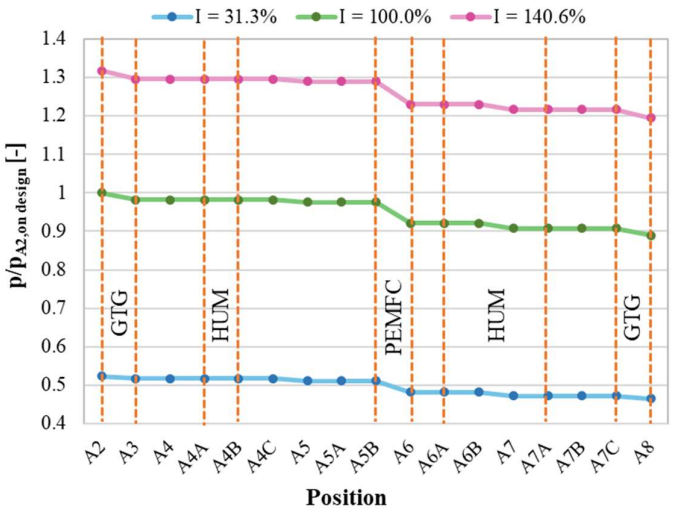

Figure 48: *Pressure distributions between the compressor outlet and the turbine inlet, for minimum, nominal and maximum load.*

Figure 48 shows the pressure trend along different sections of the circuit. As explained on the left of the figure, each section is identified by a different tag. The pressures are reported from the compressor discharge section (A2) to the turbine inlet (A8). The pressures are not explicitly displayed but normalized on the nominal compressor outlet pressure because of confidentiality requirements. From *Figure 48*, it can be seen how all the pressures in the system increase at higher currents, in agreement with *Figure 47*. Since the compressor is the only component that pressurizes the air flow, the pressure trend is always constant or decreasing between A2 and A8. The most significant pressure loss is caused

by the fuel cell stack, which accounts for almost the 49% of the total circuit losses in all the operative conditions.

To assess the advantages of the TC-PEMFC solution, the system should be compared with a standard PEMFC system of similar size. To do so, another dynamic model was developed in GT-Power. The PEMFC system was simulated in various conditions, and its operational parameters were compared to the ones of the TC-PEMFC plant.

The results of the simulations confirms that the net power output for the maximum point is very close to the one of the TC-PEMFC system, as initially established for this comparison. However, it was necessary to increase the size of the atmospheric stack by 30% to produce the same net power (i.e., considering the auxiliaries) of the pressurized cell. The difference between the net powers evaluated in the nominal point is approximately 2.5%, but as the current decreases this difference becomes more pronounced. At minimum load, the power of the TC-PEMFC system exceeds the one of the standard PEMFC by more than 10%.

The compressor should work with a lower pressure ratio and provide a similar mass flow rate. To increase the compressor N_C in design condition, the component was scaled up using a geometrical similitude with a 0.75 factor. The design point of the compressor is defined to reach the right mass flow rate, resulting in a higher rotational speed (125000 rpm compared to 81400 rpm for the pressurized case). Even if the pressure ratio is lower, the power required by the electrical motor is higher than the turbocharged case, because of the absence of the turbine. Further information is reported in the Table 18.

It was not necessary to re-design the coolant circuit to properly manage the standard PEMFC system. The centrifugal pump has the same dimension, but

its rotational speed was set slightly higher because of the larger size of the fuel cell stack and the presence of the CAC.

Table 18: *Traditional atmospheric PEMFC system design point operation.*

Atmospheric PEMFC performance		
Net Power System/ Nominal Power	100%	-
Electric Current/ Nominal Current	100%	-
Net Efficiency	0.56	-
Average Voltage	0.794	V
Air Excess Ratio	1.80	-
Fuel Stoichiometry	1.91	-
Compressor Electric Motor Power	30.24	kW

Also in this case, the power and efficiency values of the system are collected at the design point and at the maximum and minimum load points in Table 19.

Table 19: *Power and Efficiency of the atmospheric PEMFC system for different load conditions.*

Load	***Net System Power/Nominal Power***	***Net Efficiency***
Min	31 %	57.8%
Design	100 %	56.2%
Max	132.3 %	53.0%

The results of Table 17 and Table 19 have been reported in Figure 49 to graphically show the trend of the two Power-Efficiency curves. The comparison shows how the two trends are similar and that the greatest differences are obtained for low loads, while at maximum load the two systems have almost the same efficiency value. This can be explained by the fact that the atmospheric

cell for high loads works with a higher pressure due to the BPO which, having a fixed geometry, pressurizes the air circuit, approaching almost 2,5 bar and getting closer to the behaviour of the TC-PEMFC system.

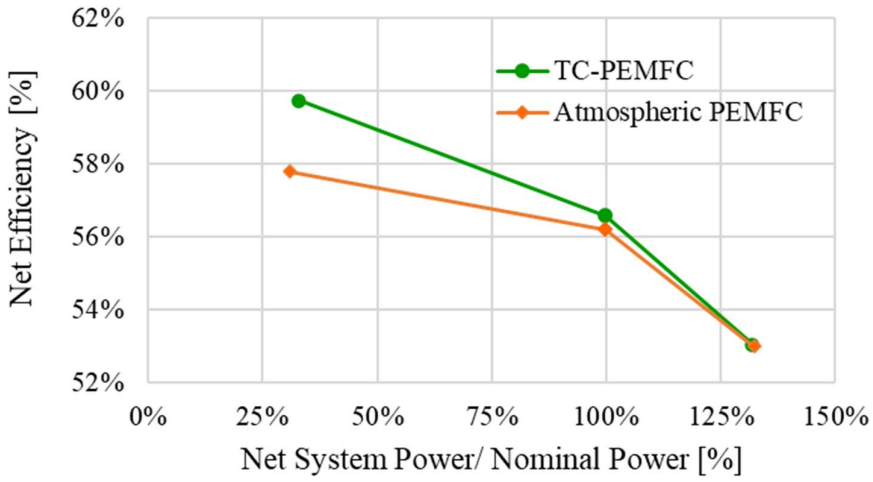

Figure 49: *Efficiency – Power curve for the two different configurations.*

Afterwards, the BoP power consumption of the two PEMFC systems was compared. Two characteristic features of the turbocharged system are that:

- Part of the compressor power demand is covered by the turbine.
- The anode loop flow is recirculated by the SCB, which requires an additional power supply, even if small.

The powers absorbed by the auxiliaries in different operative conditions are represented in ***Figure 50***. It is important to specify that, for the TC-PEMFC system, the power generated by the turbine was already subtracted from the compressor power shown in the picture, according to Eq. (11). The power produced by the fuel cell increases for higher currents, and so does the one required by the auxiliary systems.

As expected, the power absorbed by the compressor accounts for the greatest contribution, and for this reason the analysis of pressure losses in the cathode circuit is very important. However, the percentage of power absorbed by the compressor is mitigated by the turbine in the TC-PEMFC configuration. On the other hand, the rotational speed of the SCB is fixed, and the pressure in the anode loop is regulated by the HPR. These features, together with the low mass flow rate of the anode loop, lead to a very low and almost constant blower power consumption. In fact, the power absorbed by the SCB is only 2% of the BoP total at maximum load, as shown in ***Figure 50***.

These results, combined with the off-design analysis of Figure 49, highlight all

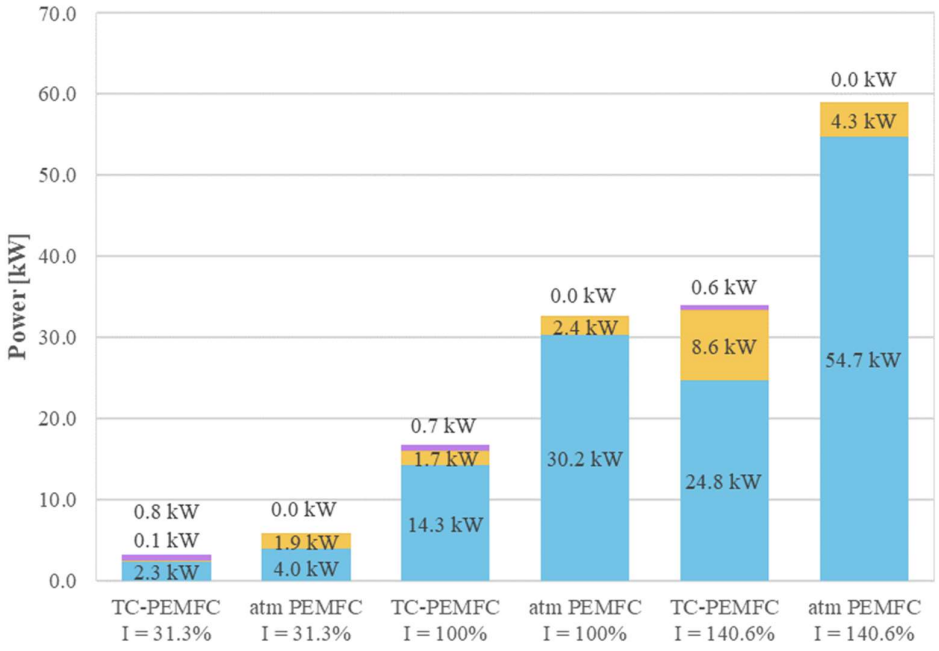

Figure 50: *Powers adsorbed by auxiliary systems in the three operating conditions for pressurized and atmospheric configuration.*

the advantages of the turbocharged solution. In fact, even if the operating pressure is higher, the power required by the BoP is always lower, due to the

power recovery of the turbine. More in details, the BoP power of the turbocharged system is lower than the atmospheric one by 4% at minimum load, 6% at nominal load and 7% at maximum load. This aspect leads the TC-PEMFC system always to operate with higher net efficiencies than the atmospheric PEMFC, while having also a significantly higher power density.

2.6 Concluding remarks

This work presented a model of a turbocharged PEMFC system including all the auxiliary systems and control logics needed for its correct operation. The model was used to simulate the operation of this innovative system in various operative conditions and to assess its performance.

The system was designed to be fuelled with pure hydrogen and generate more than 200 kW in nominal conditions. The simulations show very promising results, with a nominal net efficiency of 57%. Moreover, the pressurization of the stack by the compressor limits the decrease of efficiency at high power load. In fact, even at maximum load the system operates with a very high net efficiency, equal to 53%. The best performance was achieved at minimum load, because of the reduction of ohmic losses in the cell. In this condition, the net efficiency was equal to 60%.

To highlight the advantages of this solution, another model was developed to simulate a standard PEMFC system. This plant, which relies on a compressor to provide the air flow, was designed to work with the same electric current and provide the same net electric power.

Comparing the two plants, it was possible to see that the turbocharged solution can bring an improvement in efficiency of almost 1% percentage points for the nominal condition and even higher in off-design, reaching an increase of almost 3% at minimum load. This result can only be achieved through the power

recovery of the turbine, which significantly reduces the power drawn by the compressor, and consequently the whole BoP power consumption. The power absorbed by the auxiliaries of the TC-PEMFC showed a reduction of 4% at minimum load, 6% at nominal load and 7% at maximum load.

However, the greatest advantage is the higher power density of the turbocharged system. In fact, the PEMFC stack of the standard system requires a 30% increase of cell area to generate the same net maximum power. Such a considerable reduction of the stack size makes the TC-PEMFC configuration extremely interesting for all those applications where low volume, weight and emissions are a priority, above all the transportation field.

This technology requires additional efforts to be commercialized but the results are promising and the pressurization through the use of a turbocharger seems to be an appealing solution. Furthermore, the fact that the anodic loop requires a dynamic model for the on/off purging valve, allowed us to further investigate the model performance also in transient conditions like step response and ramps, reported in a paper that will be published in the next ASME – Turbo Expo. Future activities will include a more complex load following and start up and shut down phases.

3 Pressurization of SOFC

In this paragraph another type of cell is described, Solid Oxide Fuel Cell (SOFC), which is part of the high temperature fuel cells, in fact usually working in the range between 600-1000 °C. Unlike PEMFCs, due to their operating condition, they suggest the possibility of cogeneration since the exhaust gases of the cell can be used as thermal power [62], [63] or, alternatively as incoming flow into a turbine to use the high enthalpy difference and produce mechanical power [64], [65]. As observed in the case of pressurized PEMFC, also in case of SOFC, pressurization has advantages since increases performance in terms of power density and efficiency [66]. For this reason, it may be convenient to use the power produced by the turbine to move a compressor. While in the case of low temperature cells the balance between turbine power and compressor power was mostly negative in every condition, requiring additional power by an electric motor, in this case given the great energy of exhaust gases the use of an electric engine may not be required and even using micro gas turbines (mGT) to produce an additional amount of electric power.

Solid oxide cells are currently mostly powered by methane or Natural gas, however the high temperatures and constituting materials do not present complexity from the point of view of carbon monoxide poisoning, allowing the use of different hydrocarbons or hydrogen carriers.

The SOFCs can be pressurized using a micro gas turbine or a turbocharger. For the first solution, mGTs typically generate a power ranging from 25 to 250 kW. They are based on single cycle or recovered layout reaching efficiencies of 15% up to 30% regenerated [67]. In Figure 51 is presented the simplified plant scheme of coupling a solid oxide fuel cell with a micro gas turbine with the addition of a preheater for the air before entering the cell and an alternator to

recover the excess electric power created by the turbine also giving the possibility of regulating the rotational speed of the machine [68]. There are SOFC-mGT studies conducted by Siemens Westinghouse in collaboration with the University of California Irvine (UCI) that involve the study of a system that produces 180 kW through tubular cells and 40 kW produced by mGT with overall efficiency of 53% [69], [70]. Siemens-Westinghouse also developed a hybrid system of 1 MW of power that unfortunately never started its operations [69].

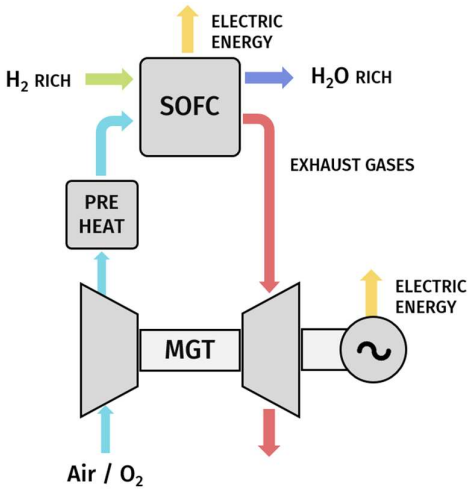

Figure 51. *Simplified layout of a SOFC-MGT hybrid system.*

Rolls-Royce Fuel Cell Systems, that later became LG Fuel Cell Systems (LGFCS), started their activities on SOFC-MGT systems in 1992, with the goal of developing a 1 MW hybrid system [70]. A prototype of their system, which was composed by 250 kW modules (240 kW fuel stack + 10 kW MGT), was tested and performed an efficiency of 55% [71].Mitsubishi Heavy Industries was one of the first companies involved into the development of SOFC-MGT systems, since the 1980s. They started designing and manufacturing a 200 kW system in 2004,

which was successfully tested in 2007 for more than 1500 hours reaching an efficiency of 52.1% in nominal conditions [70].

The most recent advancements on the development of a fully operational SOFC-mGT system were achieved in industry by Mitsubishi-Hitachi Power Systems (MHPS), a company jointly established by Mitsubishi Heavy Industries and Hitachi. A 250kW SOFC-MGT demonstration plant was designed by MHPS and installed at the Ito Campus of Kyushu University (Japan), where it was able to operate for more than 10,000 hours between 2015 and 2017. Today the company website lists the SOFC-MGT system among its products [72].

The primary challenges to the integration of Solid Oxide Fuel Cells (SOFC) and mGT, mostly come from the disparities in operational parameters compared to conventional gas turbine operations [73]. Hence, the design of control systems is of primary relevance, as emphasized in references [74], [75], primarily because of the numerous operational constraints of the SOFC that must be controlled to prevent its deterioration. The inclusion of both the MGT and the SOFC in the system incurs significant expenses, hence constraining the economic viability of the system [76].

These systems with the interaction between two complex machines make the control especially in transitional phases not easily predictable compared to the configuration of an atmospheric fuel cell. During unsteady working conditions in fact all the parameters of pressure and temperature and mass flow vary and can lead tothe entry into dangerous operating zones like fluid dynamic instability due to the surge phenomenon. This is easily inducted also by the large volume of the stack interposed between the compressor and the turbine [77]. The complexity and cost of these systems means that tests are carried out mainly by a model and not by experimental facilities. In fact, these systems in addition of being very expensive are also delicate and can be damaged both mechanically and by thermal stress [78]. Pressurization can also degrade the

cell and decrease its performance [66]. At high pressures it is easier for nickel oxidation to occur which increases the carbon deposition. Our research group, TPG group [79], as other research centres [80] [81], have built an emulator of this type of plant that simulates the fluid dynamic behaviour of a solid oxide fuel cell with big volumes and tests the micro turbine response. The opposite approach is to simulate the operation of the gas turbine and realize an experimental test bench of an SOFC [82].

Due to these numerous difficulties, in recent years also the possibility of using a turbocharger instead of the micro turbine has been studied [83], [84]. Currently turbochargers are widely diffused coupled with the internal combustion engine. The concept is the same, pressurizing the air before entering the system to increase the performance using a certain compressor power that is partially recovered by the exhaust gases that go in the turbine (*Figure 52*). This solution leads to a considerable cost reduction that can accelerate the development of hybrid pressure systems (a couple hundreds of euros for a turbocharger [85] compared to more than 1000 €/kW for an MGT [86], [87]).

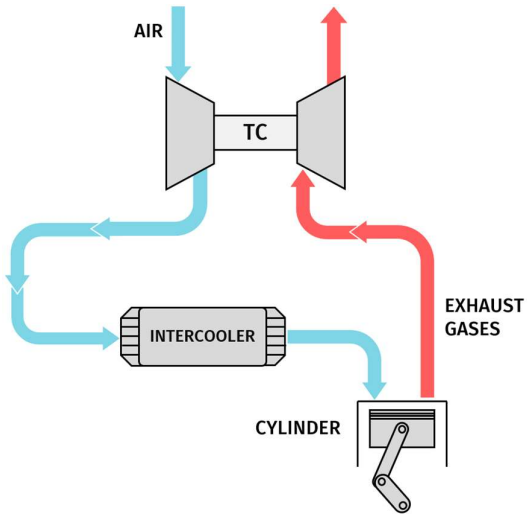

Figure 52. *Scheme of a turbocharged internal combustion engine.*

The drawbacks of this solution are the reduction of generated power (around 10-15% in comparison with a SOFC-MGT system), and the loss of control on the turbomachinery rotational speed. When the SOFC is pressurised by an MGT, the alternator plays an important role in the system control during the off-design and part load operations. Specifically, the air flow rate is controlled by the shaft rotational speed acting on the electrical generator. This leads to the possibility of keeping the fuel cell operating parameters acceptable for a wide range of operating conditions, because the air mass flow is used to cool down the SOFC.

3.1 Commercialized models of SOFC

This paragraph describes the data collected for high-temperature SOFC fuel cell plants, which do not have very good performance for small-scale mobile applications but are more promising for stationary power generation. As the size of the application increases, solid oxide cells start to be more affordable than the low-temperature alternative, because the energy production system takes up more space in equal size (more number and size of auxiliary components), but the fuel used, typically methane, has a better energy density than that of hydrogen.

As in the case of PEMFCs, the SOFCs also have a modular composition, so to obtain more substantial powers it is sufficient to put together stacks and modules of the same type. A particular feature of fuel cells, in general, is the possibility of changing size without affecting the efficiency of the system. The volume and weight variation is almost linear with little variation in the performance of the auxiliary systems.

Currently a number of SOFC systems are already available on the market that can be purchased, the data of some of which have been listed in ***Table 20***,

reporting some useful features at the design stage. A reference is associated with each business model to find further information about the operating performance, data sheets or the manufacturer's website.

Table 20: *SOFC commercialized solutions*

	Power	*Dimensions*	*Weight*	*Configuration*
Sunfire	**Remote 400**: 350 [W] **Remote 900**: 750 [W] **Home:** 750 [W]	660 x 540 x 400 [mm] 600 x 680 x 1120 [mm] 600 x 680 x 1150 [mm]	65 [kg] 185 [kg] 150 [kg]	Atmospheric
SolidPower	**BlueGEN**: 1,5 [kW] **BG – 15:** 1,5 [kW]	1010 x 600 x 660 [mm] 1200 x 550 x 800 [mm]	195 [kg] 250 [kg]	Atmospheric
Convion	**C60:** 60 [kW]	2,33 x 2,78 x 2,09 [m]	-	Atmospheric
Bloom Energy	200 [kW] 250 [kW] 300 [kW]	7,85 x 1,35 x 2,26 [m] 7,85 x 1,35 x 2,26 [m] 9,83 x 1,32 x 2,18 [m]	12,6 [tons] 13,6 [tons] 15,8 [tons]	Atmospheric
H2E Power	**H2E MINI:** 250 [W]	4,88 x 0,427 x 3,81 [m]	25 [kg]	Atmospheric
SOFCMAN	**E-1200W Stack** **E-5kW Stack**	175 x 140 x 212 [mm] 364 x 284 x 240 [mm]	23,5 [kg] 120 [kg]	Atmospheric
Mitsubishi	250 [kW]	12 x 3,2 x 3,2 [m]	33 [tons]	Pressurized

At the moment, among high-temperature fuel cell systems, the widely most marketed solution is that of atmospheric SOFC cell which has reached a degree of technology readiness high enough to allow this type of system to begin to take

a small piece of the market. They are still expensive and difficult to maintain but the advantage of reducing emissions with the use of low-carbon fuels (since SOFC cells can use CO as fuel) has led many companies to consider this cell as an option to produce energy. With regard to the pressure configuration, usually between about 2.5-5 bar absolute, it is currently the subject of numerous studies due to the advantages related to increased efficiency and compactness, but the only solution available are prototypes by Mitsubishi systems [88].

All the solutions presented in the table refer to systems not designed for marine applications. These cells, at present, are used for small-scale domestic applications such as high-efficiency cogeneration plants or for medium-sized and large stationary applications (>200kW) to produce low-emission electricity.

3.2 Plant layout

In order to prove the advantages of pressurized SOFC systems compared to atmospheric one we conducted simulations with two different layouts described in this section.

The pressurized system has the same layout of the bio-Hypp project, a TC-SOFC fed with biogas. For our study the fuel was conferred in methane, and this comported a different mass flow rate since the molar mass changes. The mass difference required a new calibration of the ejector whose geometry was previously fixed to reach the right speed in the throat area. In *Figure 53* presents the plant layout of the innovative turbocharged SOFC system.

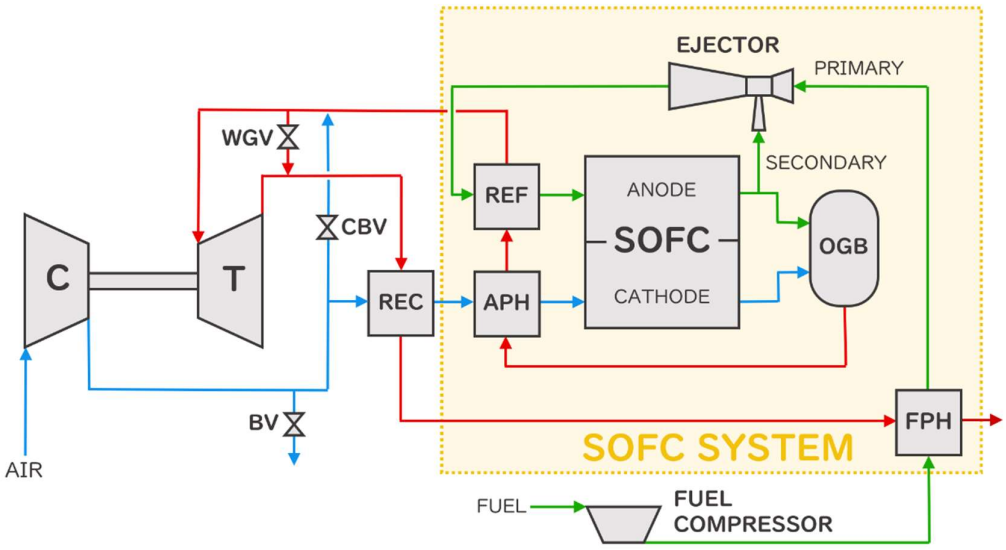

Figure 53. *Turbocharged SOFC plant layout; in blue the cathode side air flow, in green the anode side fuel flow and in red the exhaust flow.*

On the cathode side, the air flow is pressurized by the compressor and pre-heated by the turbine exhausts while flowing through a standard stainless-steel recuperator (REC). Some additional heat is provided by an SOFC system internal heat transfer, represented in by the air pre-heater (APH). On the anode side, the fuel is compressed, and heated through the fuel pre-heater (FPH) before entering the ejector primary duct. Similarly to the APH, the FPH is not an actual heat exchanger, but it represents an internal heat transfer between nearby ducts. The fuel flow drives the partial recirculation of the stack anode outlet flow to the secondary nozzle of the ejector. Primary and secondary flows are then mixed within the ejector before entering the external reformer (REF). The anode recirculation guarantees the minimum steam amount necessary to drive the chemical reactions occurring in the REF and to avert carbon deposition inside the SOFC [89]. The reformer produces hydrogen through the steam methane reforming (SMR) Eq. (22) and the water gas shift (WGS) Eq. (23) reactions [90], feeding the SOFC anode with the reformed fuel flow.

$$CH_4 + H_2O \rightarrow CO + 3H_2 \quad (22)$$

$$CO + H_2O \leftrightarrow CO_2 + H_2 \quad (23)$$

Inside the SOFC, oxygen and hydrogen participate in the electrochemical reaction Eq. (24) to generate electric power. For this reaction to take place, O^{2-} ions have to migrate through the electrolyte from the cathode to the anode, where water is produced and electrons (e^-) are released from the electrochemical oxidation of H_2. Since the two sides of the SOFC are linked by an electrical connection, the electrons are able to flow to the cathode, generating the electric power.

$$H_2 + O^{2-} \rightarrow H_2O + 2e^- \quad (24)$$

The portion of anodic outlet flow which is not recirculated into the secondary duct of the ejector, is mixed with the cathodic outlet air flow and oxidized inside the off-gas burner (OGB). Therefore, the unused fuel in the SOFC produces the surplus heat useful to pre-heat the cathodic air and to drive the endothermic chemical reactions inside the REF. The combustion of the SOFC exhausts is also necessary to prevent the emission of pollutants into the atmosphere. The exhaust flow reaches the turbine inlet generating, through its expansion, the mechanical power necessary for the turbocharger operation. The turbine exhaust gases are then used to pre-heat the compressed air in the REC and the biogas in the FPH, before being released into the atmosphere.

The system must run under many constraints, which will be described in more detail in the next paragraphs. For this reason, it was equipped with a set of valves, whose openings are determined to guarantee correct operation of the system, both in nominal and off-design conditions. Cold bypass (CBV), bleed (BV) and wastegate (WGV) control valves are visible with their pipelines. The CBV diverts part of the compressed air flow to upstream of the turbine, lowering

the turbine inlet temperature and reducing the air mass flow entering the REC. The BV discharges part of the compressed air into the atmosphere, reducing the cathode inlet mass flow. The WGV is used to direct part of the SOFC system exhaust flow directly to the REC entrance, bypassing the turbine.

The second layout is reported in *Figure 54*. The system shows almost the same components but the pressure in all the system is slightly higher that the atmospheric one. Instead of a compressor the is a blower that is used to supply the air to the system. The main effort in this case was to reach the 650 °C at the REC, in this way the performance related to the operating temperature were maximised and at the same time the cost of this component is the one of a stainless one. For higher temperature the material would be not suitable requiring additional costs.

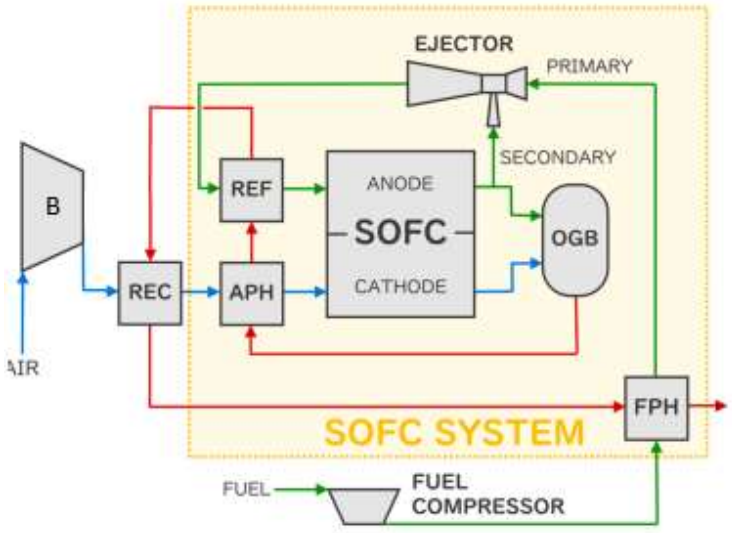

Figure 54. *Atmospheric SOFC plant layout; in blue the cathode side air flow, in green the anode side fuel flow and in red the exhaust flow.*

3.3 TRANSEO tool for dynamic simulation

To model the dynamic behavior of energy power systems as the SOFC one previously described, analyze its transient characteristics, and evaluate control mechanisms, we developed a dynamic model using TRANSEO, a specialized computational tool created by the Thermochemical Power Group (TPG) for assessing the dynamic performance of energy systems [91]. While Matlab®-Simulink® platform is adopted for time management and visualization, TRANSEO relies on Fortran and C codes to determine chemical compositions, thermodynamic properties, and component performance. These codes are integrated with Matlab®-Simulink® via C MEX functions.

Initially designed for microturbine-based systems, TRANSEO's modularity and flexibility enables its adaptation to advanced energy systems, including pressurized fuel cell systems. Although primarily focused on mass and energy balances, TRANSEO can simulate dynamic effects but with some exception like pressure wave propagation, neglected because not inherent to the type of study we want to conduct. While some components within TRANSEO can mimic complete dynamics, this approach is resource-intensive and not utilized in our model, which adopts a lumped-volume approach to simulate component transient behavior. It's important to note that individual components within TRANSEO have been validated against experimental or literature data in prior studies conducted by TPG researchers.

The process involved configuring each component (i.e., active, inactive-forward, or inactive-backward states, as explained in a following section) to accurately determine the physical properties of the working fluid throughout the system. Additionally, a calibration of characteristic parameters was necessary to align the dynamic model with the steady-state model and meet the SOFC system specifications.

The lumped-volume model relies on two main elements: an actuator disk to replicate off-design component performance and a duct with equivalent length and cross-sectional area to account for fluid dynamic delays. The actuator disk evaluates the outlet conditions using the inlet and duct conditions, while the duct introduces a time delay based on its geometrical properties. The transient behaviour in the duct is governed by equations (25)-(27).

$$\frac{d\dot{m}}{d\tau} = \frac{A_{duct}}{L_{duct}} \left(C - \left(p_3 - p_{1,tot}\right) - \dot{m}\,(w_3 - w_1)\right) \tag{25}$$

$$\frac{d(c_v\,\rho_{avg}\,\Lambda\,T_{tot})}{d\tau} = \dot{m}\left(H_{2,tot} - H_{3,tot}\right) - \dot{q}_s \tag{26}$$

$$\frac{d(c_{p,s}\,M_s\,T_s)}{d\tau} = \dot{q}_s - \dot{q}_{loss} \tag{27}$$

Subscripts "avg" denote average values, "tot" refers to total physical quantities, and "s" to the material constituting the pipe. Subscripts 1, 2, and 3 denote different sections of the component, as illustrated in

Figure *55*: 1 represents the component inlet, 2 corresponds to the actuator disk outlet and duct inlet, and 3 signifies the component outlet.

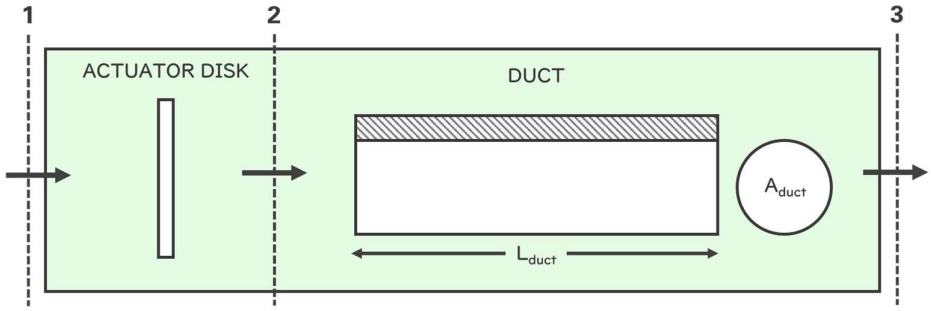

Figure 55. Structure of a standard TRANSEO component based on the lumped volume.

The duct equations are not spatially discretized, implying that they are integrated over time rather than along the duct length. Mass flow is assumed to be uniform across the duct and subject to the overall momentum equation.

3.4 Model description

The mathematical models used for this study are those implemented in the components of the TRANSEO library, a simulation tool by the research group Thermochemical Power Group (TPG) of the University of Genoa. This software is used to perform simulations of energy power systems and to evaluate their performance in off-desing and dynamic conditions. TRANSEO was developed in the MATLAB-Simulink environment, this makes the model intuitive thanks to its graphical interface, which gives the possibility to modify various parameters without entering into the programming language. TRANSEO models require Fortran and C functions to perform calculations of thermodynamic and physical properties, the chemical compositions of flows and the performance of certain components.

Fuel supply system

The fuel supply system includes a series of components that are used to prepare the fuel and send it to the inlet of the anode in the thermo-physical conditions required for the proper operation of the cell. This subsystem includes a fuel compressor, a heat exchanger and a reformer.

The compressor model has the only purpose of evaluating the power required for the compression of the flow of methane and the increase in temperature of the fluid as a result of this process. This first operation, since is not much energy consuming (due to the low mass flow rate of the fuel), is assumed to happen at constant isentropic adiabatic efficiency equal to 0.80. The required inputs are

the vector characterizing the input flow and the desired pressure to be achieved, which in the case of a pressurized system was fixed at 4.5 bar and in the atmospheric case slightly more than 1 bar to overcome the circuit losses.

From the input pressure and the desired output pressure, the mathematical model calculates the compression ratio and then the output temperature (28) with an iterative cycle that takes into account the fact that the specific heat of the gas varies with its properties.

$$T_{out} = T_{in}(1 + \frac{\beta^{(k-1/k)}}{\eta_c} - \frac{1}{\eta_c}) \tag{28}$$

The power absorbed by the machine is calculated as:

$$P_c = \dot{m}_{in}(c_{p,out}T_{out} - c_{p,in}T_{in}) \tag{29}$$

For the heat exchanger (all those used in the two plant schemes have the same structure), it has been simulated with a 1D model of a counter-flow plate heat exchanger. The heat exchanger is discretized in the direction of the fluid and the exchanged heat (Δq) at each point is calculated using the equation (30).

$$\Delta q = \frac{T_{hot} - T_{cold}}{\frac{1}{h_{hot}\, A_{HE,el}} + \frac{1}{h_{cold}\, A_{HE,el}} + \frac{\lambda_{pl}\, A_{HE,el}}{t_{pl}}} \tag{30}$$

The formula contains the areas of the discretization elements ($A_{HE,el}$), the convection coefficients ($h_{ho}\ and\ h_{cold}$) calculated from a Nusselt number dependent on the flow regime, the thickness of the plate (t_{pl}) and its thermal conductivity (λ_{pl}).

Finally, the reformer that was modelled as in the previous case of heat exchanger with a 1D model, but in this case co-flow type. The component is discretized and in each section the model solves the methane steam reforming and water-gas shift reactions that occur in the fuel flow. To do this, two sides of equilibrium are calculated using the formula (33) to then solve the two reactions (31) (30) and find the partial pressures of the different chemical species.

$$K_{SMR}^{eq} = \frac{p_{CO}\, p_{H_2}^3}{p_{CH_4}\, p_{H_2O}} \tag{31}$$

$$K_{WGS}^{eq} = \frac{p_{H_2}\, p_{CO_2}}{p_{CO}\, p_{H_2O}} \tag{32}$$

$$K_R^{eq} = A_R\, T^4 + B_R\, T^3 + C_R\, T^2 + D_R\, T + E_R \qquad with \quad R = SMR, WGS \tag{33}$$

The coefficients used to find the equilibrium constants are derived from considerations made in the literature. The same equations present in the component heat exchanger are also modelled to define the temperatures of fuel and air.

SOFC stack

The fuel cell is simulated with a 1D model discretized in N_{discr} different sections. All the equations implemented within the model are presented in

Table 21 and take into account aspects of the operation of a SOFC. The table is divided into two groups of equations, at first the equations useful for calculating the electrochemical aspects are shown, then the conservation equations are presented.

With regard to the kinetics of the electrochemical part of the cell, the Nernst potential is calculated using the formula (36) from which the activation, ohmic and concentration losses in the formula are deduced. (37),(38). In the following formulas these losses are specifically assessed (39)-(44) using coefficients and variables of the geometry of the cell and the thermo-physical properties of the flows that pass through it.

The conversion reaction of methane into hydrogen is completed inside the cell. The equations (45),(46) define the two balance coefficients of the MSR and WGS reactions that are evaluated in the same way as the reformer component.

The last lines of the table are used to define the thermo-fluid dynamics of the component: equations of mass balance, energy and momentum.

Finally, the power produced by the cell is calculated using the formula (34) from which you can obtain the efficiency of the system (35) measured as the ratio between the net power obtained and the power of the fuel used, therefore the power for lower heating power (LHV).

$$P_{net} = P_{cell} - P_{C,fuel} \tag{34}$$

$$\eta_{net} = \frac{P_{net}}{\dot{m}_{fuel} LHV_{fuel}} \tag{35}$$

Table 21: *Equations implemented in the SOFC component.*

Local Electrochemical Kinetics	**Nernst Voltage**	$V_{Nernst} = -\frac{\Delta G}{n_e F} = -\frac{\Delta G^0}{n_e F} - \frac{R_g T_s}{n_e F} \cdot \ln\left(\prod_i p_i^{v_i}\right)$	(36)
	Cell Voltage	$V_{real} = V_{Nernst} - \Delta V^{tot}$	(37)
		$\Delta V^{tot} = \Delta V^{ohm} + \Delta V^{act} + \Delta V^{conc}$	(38)
	Ohmic Losses	$\Delta V^{ohm} = R^{ohm} \cdot j_{cell}$	(39)
	Activation Losses	$j_{cell} = j_0 \left[\exp\left(\theta_a \cdot \frac{F}{R_g T} \cdot \Delta V^{act}\right) - \exp\left(\theta_c \cdot \frac{F}{R_g T} \cdot \Delta V^{act}\right)\right]$	(40)
		$j_{0,an} = \gamma_{AN} \cdot \frac{p_{H_2}}{p_{ref}} \cdot \frac{p_{H_2O}}{p_{ref}} \cdot \exp\left(-\frac{E_{an}^{act}}{R_g T_s}\right)$	(41)
		$j_{0,ca} = \gamma_{ca} \cdot \left(\frac{p_{O_2}}{p_{ref}}\right)^{0.25} \cdot \exp\left(-\frac{E_{ca}^{act}}{R_g T_s}\right)$	(42)
	Concentration	$\Delta V_{an}^{conc} = -\frac{R_g T}{n_e F} \cdot \ln\left(\frac{1 - \frac{j_{cell} R_g T t_{an}}{n_e F D_{an}^{eff} p X_{H_2}^{fg}}}{1 + \frac{j_{cell} R_g T t_{an}}{n_e F D_{an}^{eff} p X_{H_2O}^{fg}}}\right)$	(43)

			$$\Delta V_{ca}^{conc} = -\frac{R_g\, T}{n_e\, F} \cdot \ln\left(\frac{1}{X_{O_2}^{fg}} - \left(\frac{1}{X_{O_2}^{fg}} - 1\right) \cdot exp\left(\frac{j_{cell}\, R_g\, T\, t_{ca}}{2\, n_e\, F\, D_{ca}^{eff}\, p}\right)\right) \quad (44)$$
Equilibrium Chemical			$$K_{WGS}^{eq} = \frac{p_{CO_2}\, p_{H_2}}{p_{CO}\, p_{H_2O}} \quad (45)$$ $$K_{SMR}^{eq} = \frac{p_{CO}\, p_{H_2}^3}{p_{CH_4}\, p_{H_2O}} \quad (46)$$
Local Balances	**Mass**	Gases	$$\frac{\partial n_i^*}{\partial x} = r_i \quad (47)$$
	Energy	Gases	$$\sum_i n_i^*\, c_{p,mol,i} \cdot \frac{\partial T_g}{\partial x} + \sum_i c_{p,mol,i} \cdot \frac{\partial n_i^*}{\partial x} \cdot \left(T_g - T_s\right) + h\, B \cdot \frac{1}{t_{ch}} \cdot \left(T_g - T_s\right) = 0 \quad (48)$$
		Solid	$$\frac{1}{t_{cell}} \cdot \sum_g h\, B\, \left(T_g - T_s\right) - \frac{1}{t_{cell}} \cdot \left(\frac{\Delta H}{n_e\, F} + V\right) \cdot j_{cell} + \lambda_s \cdot \frac{\partial^2 T_s}{\partial x^2} = \rho_s\, c_s \cdot \frac{\partial T_s}{\partial \tau} \quad (49)$$

	Momentum	Gases	$\Delta p_{distr} = \frac{4f}{D_h} \cdot L_{cell}$	(50)
			$f = \frac{14.2}{Re}$	(51)
			$\Delta p_{conc} = \kappa \cdot \frac{\rho\, V^2}{2}$	(52)
			$\kappa = \Psi \cdot \left(1 - \frac{A_{sd}}{A_{ld}}\right)$ $\begin{cases}\Psi = 1.0 & \text{for the inlet} \\ \Psi = 0.5 & \text{for the outlet}\end{cases}$	(53)

Ejector

The ejector has been modelled with a 0D model that works with the information of three flows: primary, secondary and output. Inside it the conservation equations of the current (54), the momentum equation (55) and the energy conservation (56) are solved.

$$\dot{m}_{prim} + \dot{m}_{sec} = \rho_{out}\, c_{out}\, \Omega_{out} \tag{54}$$

$$p_{out}\Omega_{out} - p_{prim}\Omega_{prim} - p_{sec}\Omega_{sec} - \int_{prim-sec}^{out} p\, d\Omega = \dot{m}_{prim} C_{dis} c_{prim} + \dot{m}_{sec}\, c_{sec} - \dot{m}_{out}\, c_{out} \tag{55}$$

$$\dot{m}_{prim}\left(H_{prim} + \frac{1}{2}\, c_{prim}^2\right) + \dot{m}_{sec}\left(H_{sec} + \frac{1}{2}\, c_{sec}^2\right) = \dot{m}_{out}\left(H_{out} + \frac{1}{2}\, c_{out}^2\right) \tag{56}$$

In the ejector model, two different geometries were evaluated in the two plant schemes due to different operating characteristics. The geometry of the ejector is fixed so it must ensure a proper recirculation in all operating conditions to have the right amount of steam to feed the reforming and WGS reactions and avoid carbon deposits inside the cell. To verify that this is done accurately, the Steam to Carbon ratio (STCR) is calculated (57).

$$STCR = \frac{n_{H2O}}{n_{CH4}.n_{CO}} \tag{57}$$

Air supply system

The cathode side is fed with air taken from the environment that is prepared before entering the cell. For the atmospheric layout, the air goes through a blower which attributes a slight increase on pressure to the fluid and then a heat exchanger that raises its temperature. For the pressurized system, the modelling is more complex because the compressor must rotate at the same speed of the turbine that is moved by the outlet flow from the off-gas burner (OGB). The pressure of the system is defined by the effect of the pressurization of the compressor and the back pressure of the turbine. The model uses both compressor and turbine performance maps from which the values of rotation speed, reduced mass flow, pressure ratio and efficiency are extracted. The formula (58) is used to evaluate the power in both cases. The two powers must be the same with less than a 1% waste attributable to mechanical losses.

$$P = \dot{m}_{out}(H_{out} - H_{in}) \tag{58}$$

An important parameter for adjusting and defining the operating point of the compressor is the surge limit, a condition of strong instability that generates flow fluctuations in the ducts of the air circuit and is obviously a not desired phenomenon. Therefore, a coefficient that identifies this condition is defined

(59), when it reaches the unit value you reach the surge condition, for safety reason it is a good habit avoiding to go below a $K_p = 1.10$.

$$K_p = \frac{\dot{m}/\beta}{\dot{m}_{surge}/\beta_{surge}} \quad \textbf{(59)}$$

Control system

Solid oxide fuel cells require to work within defined constraints, for example the cells considered in our case study have limitations that must be met at any time of their operation. The limits required by the manufacturer are shown in

Table 22 below. There are limits concerning the temperature which must not exceed 860 °C to comply with the limits imposed by the materials and limits on the temperature gradient to avoid mechanical stress of the cell due to the different dilation coefficients of the different materials in the cell. For the same reason, a limit is also specified on the temperature difference between anodic and cathodic inlet.

There are limits regarding the difference between the pressures, the limit on the minimum voltage of the individual cell, on the slope of the current ramp (strictly linked to the temperature ramp) and finally limits on the two utilization factors that represent the percentage of reagent that actually reacts inside the cell.

Table 22: *Operating constrains defined by the producer (*Staxera GmbH SOFC module).

Item	Limit	Comment
Gas inlet temperature	≤ 860°C	Air (Cathode) and Fuel (Anode) side
Stack core temperature	≤ 860°C	
Cathode inlet temperature gradient	≤ 10 K/min ≤ 5 K/min	Heating up to operating temperature Cooling down from operating temperature
Max. temperature difference anode inlet – cathode inlet	250 K	
Pressure difference Anode-Cathode	≤ 30 mbar	Pressure measurement should be enabled by the test environment
Operating pressure	≤ 30 mbar gauge	Gauge pressure inside stack related to ambient pressure
Minimum cell operation voltage	0.6 V	Average cell voltage (total voltage divided by number of cells)
Current ramp	2 A/min 30 A/min	Increasing current Decreasing current
Air utilization	≤ 30%	Operating altitude ≤ 1000 m
Fuel utilization	≤ 85%	

Power control system

In both plant layouts described above, the regulation of the power is accomplished with the control of the fuel supply system. The power of a cell depends on the amount of fuel consumed (60), depending on a certain current i_{cell}, and the efficiency of the operating point determined by the voltage (61). Real voltage (V_{real}) considers the potential of Nernst deducted from its loss contributions. In general, efficiency decreases as the current increases. Factors

such as pressure and temperature positively influence the performance of the cell, which is why the system is adjusted to keep the temperature of the fixed cell at the maximum acceptable limit for the functional limits of the system.

$$P_{cell} = V_{real} \cdot i_{cell} \cdot N_{cell} \tag{60}$$

$$\dot{n}_{fuel} = \frac{i_{cell}\, N_{cells}}{U_f\ 2\ F} \cdot \frac{1}{4\ X_{CH_4}} \tag{61}$$

Then, for the adjustment of the power, the current to the desired load is established and the corresponding fuel flow rate is calculated.

Temperature control system

Temperature adjustment is essential to avoid exceeding the limits imposed by the characteristics of the cell. Unlike PEMFCs, solid oxide fuel cells do not have a dedicated cooling circuit that takes care of absorbing heat, but they use air flow in the cathode side to keep the temperature in the cell constant, in fact, from

Table 22, the maximum limit on the air usage factor is 30% that means working with strong excess of air.

In the pressurized SOFC system the temperature adjustment occurs using the WGV and CBV valves that bypass a certain amount of air. The first bypasses a portion of hot air from the input of the turbine to its exit, sending it directly to the REC, the second takes a certain amount of compressed air going out of the

compressor without letting it to pass into the cell and sends it directly into the turbine by decreasing the flow of the REC and reducing the temperature in the inlet of the turbine, in this way it is possible to control the temperature of the air in the cell (about 860 °C) while the temperature at the input at the REC <650 °C, therefore, without excessive thermal stresses.

On the other hand, in pressurized systems, attention must also be paid to the system pressure variation, resulting from the change in the speed of rotation of the turbocharger. For this reason, the regulation of air flow needs to be assessed very carefully, and it represents one of the current challenges of research, to maximize the flexibility of the system to the requirements of electric charge variation. In this regard, the use of the CBV valve is preferable to the WGV as it allows to mitigate pressure variations during partial loads.

Storage system

The fuel storage system that feeds the SOFC is filled with methane which is stored in liquid form. Using the SOFC systems, you can therefore think of using large LNG tanks that also provide for the power supply of internal combustion engines. The modelling used in this case, however, provides the definition of a dedicated volume ($V_{dedicated}$) requested to the user as an input from which the number of tanks used with the formula is calculated (62).

The volume of fuel contained in the tanks is calculated using the formula (63), while the amount of fuel used in each simulation time interval and the corresponding filling level (SoC) are expressed in (64) and (65).

$$N_{tank} = \frac{V_{dedicated}}{V_{tank}} \ (to\ be\ approximated\ to\ the\ bigger\ whole\ number) \qquad (62)$$

$$M_{LNG,tot} = \rho_{LNG} \cdot V_{tank} \cdot N_{tank} \qquad (63)$$

$$M_{LNG}(t+1) = M_{LNG}(t) - \dot{m}_{LNG\ consumed}\, dt \tag{64}$$

$$SoC = \frac{M_{LNG}(t+1)}{\mathrm{M_{LNG,tot}}} \tag{65}$$

The required mass output is calculated according to the desired power using the model described in the previous paragraph. The fuel must evaporate and then heated up to the required temperature by the SOFC stack (66) and(67). Depending on the system chosen for the simulation, it may be necessary to preheat the fuel by a certain amount of heat (for pressure systems the calculations were performed assuming a T of fuel input of 250 °C, which could be the result of its adiabatic compression):

$$Q_{prerisc} = m_{NG} \cdot c_{p,NG} \cdot (T_{req} - T_{comb}) \tag{66}$$

$$Q_{evap} = m_{LNG} \cdot \lambda_{evap,LNG} \tag{67}$$

Validation

The SOFC systems modelling described above have been already validated through the years. All the components that are included in the system layout are the result of thorough past studies by the TPG research group whose results have already been published in several papers available in the literature [92], [93], [94], [95], [96], [97]. The articles present validations of the various components with the detailed description of the plant setup used to carry out the experimental campaigns and subsequently the validation process.

The reformer and the SOFC cell were mainly validated in articles [94] and [93], where the results from the models were compared with experimental data obtained through tests carried out on a Staxera GmbH SOFC system. Among the data that have been collected there are measurements of temperature, flow, pressure variations and electrical power. Initially, the modelling of the system

was based on behaviour in design conditions. Values of voltage, current density and temperature were compared for 5 different values of electrical power produced.

The recuperator was validated in [97], the ejector in [96] and the turbocharger in [95].

3.5 Results

The comparison between the two configurations results in a higher efficiency of the system pressurized as can be observed in *Figure 56*. Both the systems increase the efficiency reducing the operating load due to the polarizations effects. Even if the pressurized technology seems to be appealing, as already sad, introduces some limitations and complexities. The volume and the weight are much more important for the pressurized layout and the TRL is lower. This aspect means that the pressurized system can be a valuable option. In the case of atmospheric SOFCs, there are models that are used in order to optimize the operation in "combined heat and power" (CHP) and therefore are characterized by a higher heat production. The curves shown here instead optimize the electrical efficiency at the expense of the thermal power.

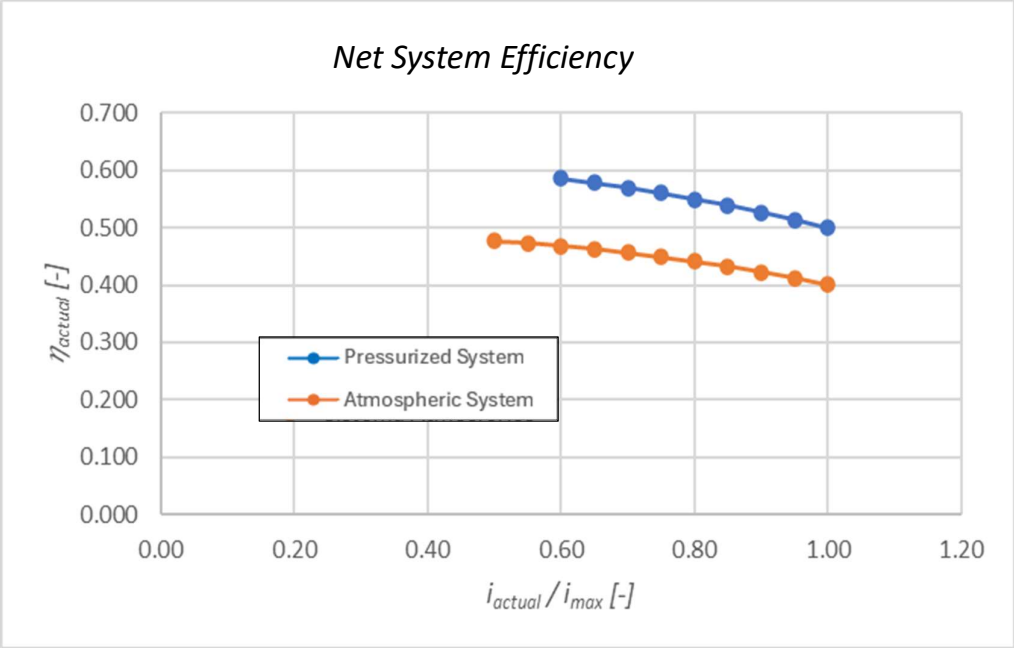

Figure 56. System efficiency as a function of the dimensionless operating current of the two types of system.

The possibility of using this kind of system for maritime application seems interesting since the fuel flexibility can lead to use the LNG already on board (for a LNG tanker for instance) feeding the boil off into the SOFC. The only issue related to the use of high temperature fuel cell is the transient that can't follow the load profile of a ship. For this reason, could be used to satisfy the base load for lower emissions and the additional power requirement could be accomplished by traditional internal combustion engine maybe fed with natural gas, in order to bring only one fuel onboard.

From a load profile of a ship, we build a tool in collaboration with FINCANTIERI, CETENA and other research groups of the University of Genoa, that can quickly simulate the power distribution among different technologies in a mix that includes diesel generator, fuel cell and batteries [98].

The model in TRANSEO results complex and computationally demanding and usually for shipping application the simulation time are in the order of days. To

make simulation faster we adopted a family of curves obtained from the static results of detailed models.

The dynamic response of the SOFCs is slower than that of the other energy systems considered in this work; therefore, with the detailed model simulations of load variations were performed to verify that the dynamics of the system was negligible in the required simulation time interval (15 min). The results of the calculations show that the static model can also be used in this case, with limitations on the slopes of the loading ramps. The information relating to the load variation limits is defined by the manufacturers and is expressed as limits to the current variation in A/min.

If the current variation of the system is greater than permitted, the system responds with a lower current and therefore power (ramp up case) or a higher current (ramp down case). Usually, the strictest limits concern increasing power ramps.

Each output variable (current, electric and thermal power, fuel mass flow rate, emissions, etc) can be expressed in function of the operating current through an adimensionalized curve with the nominal current as shown in Figure 63 and Figure 64. Depending on the type of system (pressurized or atmospheric) one of the two families of curves is adopted, using the correlations (68)-(71) interpolating with a linear method. To simulate properly the dynamic, we fitted a first order delay (*Figure 57*) in order to simulate the dynamic of each parameter.

$$i_{actual} = f\left({}^{P_{el,\,actual}}\!/_{P_{el,max}}\right) i_{max} \tag{68}$$

$$\eta_{actual} = f\left({}^{i_{actual}}\!/_{i_{max}}\right) \tag{69}$$

$$P_{th,\,actual} = f\left({}^{i_{actual}}\!/_{i_{max}}\right) P_{el,max} \tag{70}$$

$$\dot{m}_{fuel,\,actual} = f\left({}^{i_{actual}}/_{i_{max}}\right) P_{el,max} \tag{71}$$

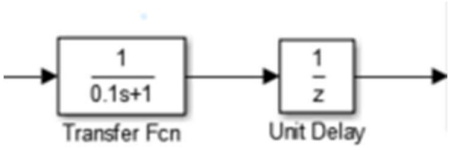

Figure 57. *Matlab-Simulink blocks to simulate a delay.*

SOFCs work at high temperatures and mostly at costly temperatures. Therefore, start up and shut down are phases that involve significant thermal variations and involve strong thermal stress on the components of the cell causing their progressive deterioration. For this reason, SOFCs must be keept at a temperature as constant as possible, and possibly not at maximum load. Alternatively, it can be envisaged to use a certain amount of heat to be supplied to the cell to maintain the temperature during the phases of inactivity.

For the reason above mentioned in *Figure 58* a result of simulation of a SOFC atmospheric is shown that follows a load profile as could be seen from the moment the FC is turned on and it keep working. The load transient is compensated by batteries that have a faster response and for high load requirement the diesel generator immediately starts and provides the missing portion of power.

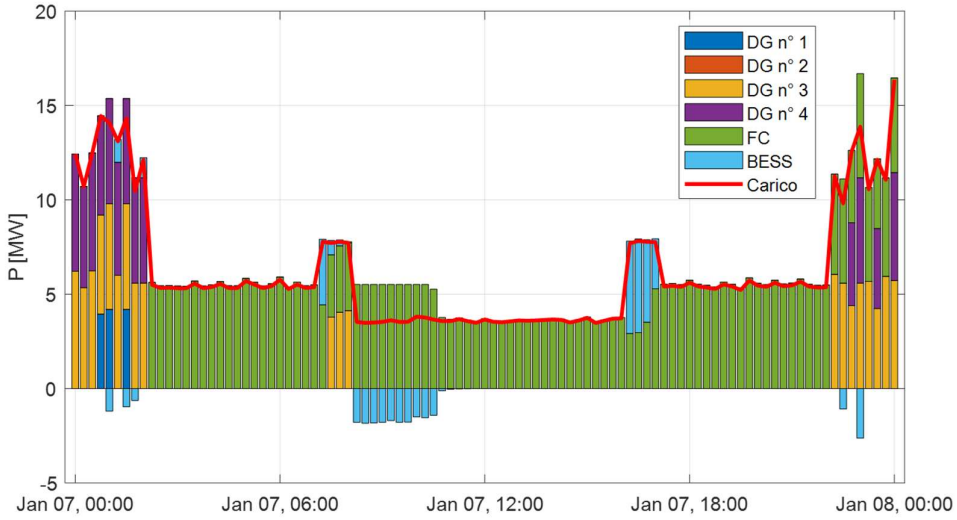

Figure 58. *Load profile filled with the power produced by different technologies.*

GT-Power results for pressurized SOFC model

This section provides a brief description of the work done during a period abroad spent at Accelleron-Industries in Baden, Switzerland. For confidential reasons, the information provided is not complete but will be partly published in an article that will be presented at the European Fuel Cell Forum conference: 2024. The activity regards the simulation of a hybrid SOFC system using the commercial GT-Power software also used for comparison in Section 2.

In this work has been developed the entire plant layout of a hybrid SOFC.

The components were calibrated on literature data and validated by the company that produces the software. The SOFC data are calibrated via the work done by Becker et al. [99] (*Figure 59*) due to the size of 1MW that was of interest given the large size of the turbocharger produced by Accelleron-Industries. The specifications of the system are reported in *Table 23*.

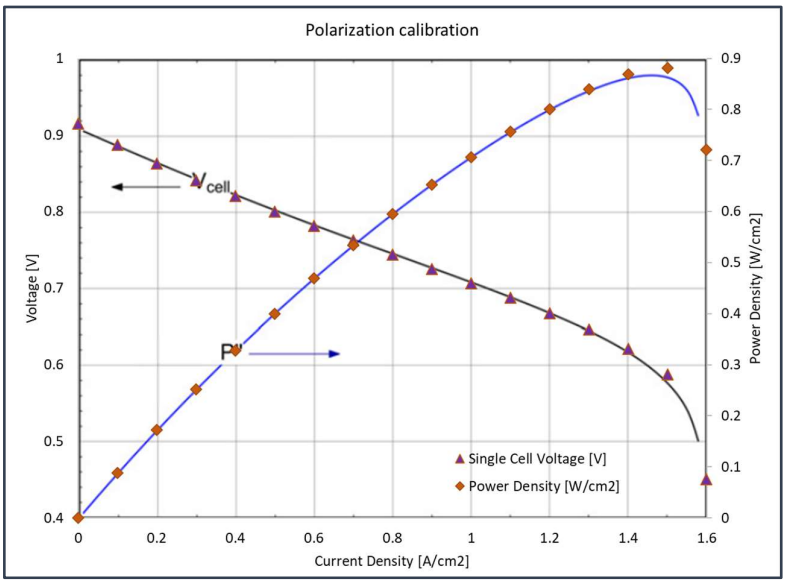

Figure 59. *Calibration of the cell on literature data* [99].

Table 23: *Target specification for the model implementation.*

Output Target		
Total net Power	1	[MW]
SOFC electrical Power	950	[kW]
eTurbo Power Take Out (PTO)	50	[kW]
Number of cells	3200	[-]
Global Fuel Utilization	0.8	[-]

The cell was preliminarily characterized under various loads and thermophysical conditions to study its behaviour and analyse its possible optimal range of work. For this reason, performance was verified by changing the properties in the cell input as temperature, composition, pressure and utilization factor. The temperature at the inlet can be modified by changing the thermal management of the system, as the pressure and flow can be set by the turbine and compressor operation fitting, so this investigation is useful for the

design of the system. The inlet composition in the normal operation of the system is the result of several variables such as the behaviour of the pre-reformer, the recirculation factor and the flow rate of fresh charge of fuel.

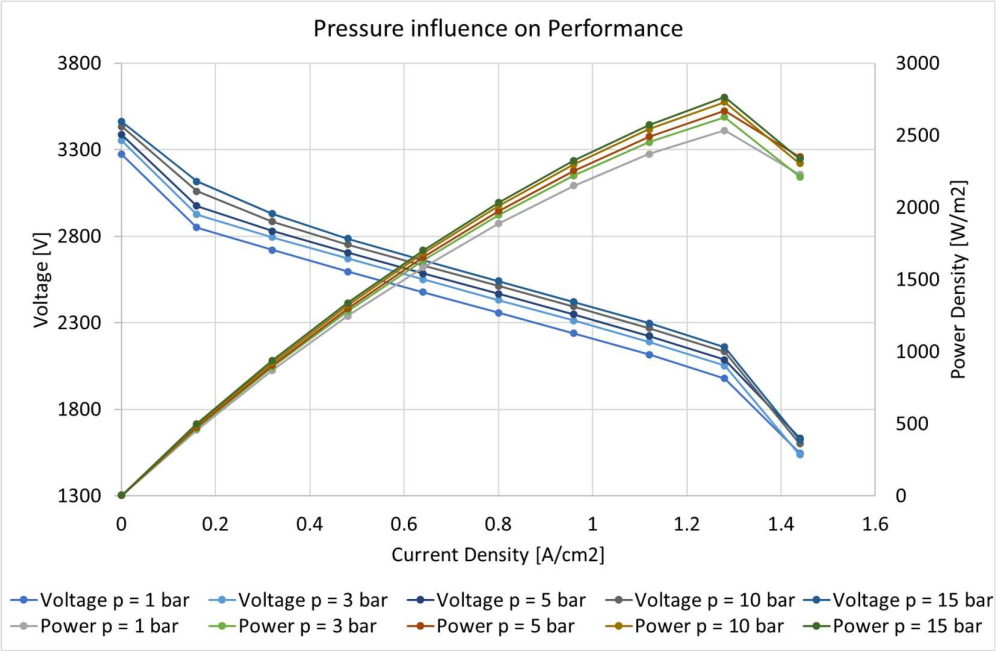

Figure 60. *Partial pressure of reactants influence on the performance of a cell.*

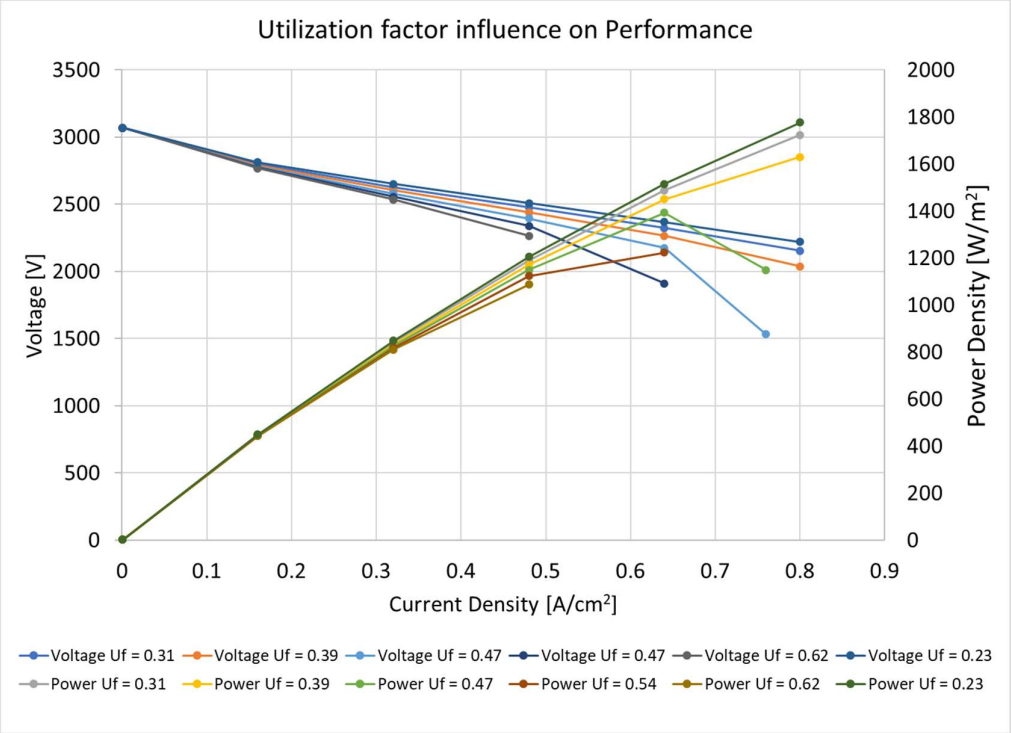

Figure 61. *Utilization factor influence on cell performance.*

As for the reformer it has also been calibrated on literature data [100]. The reformer component currently does not exist in the GT-Power library and for this reason it was necessary to use a catalytic reactor component (the model in GT-Power is shown in *Figure 62* and *Figure 63*) and the equilibrium equations of the chemical species participating in the MSR and WGS reactions have been implemented (*Figure 64*).

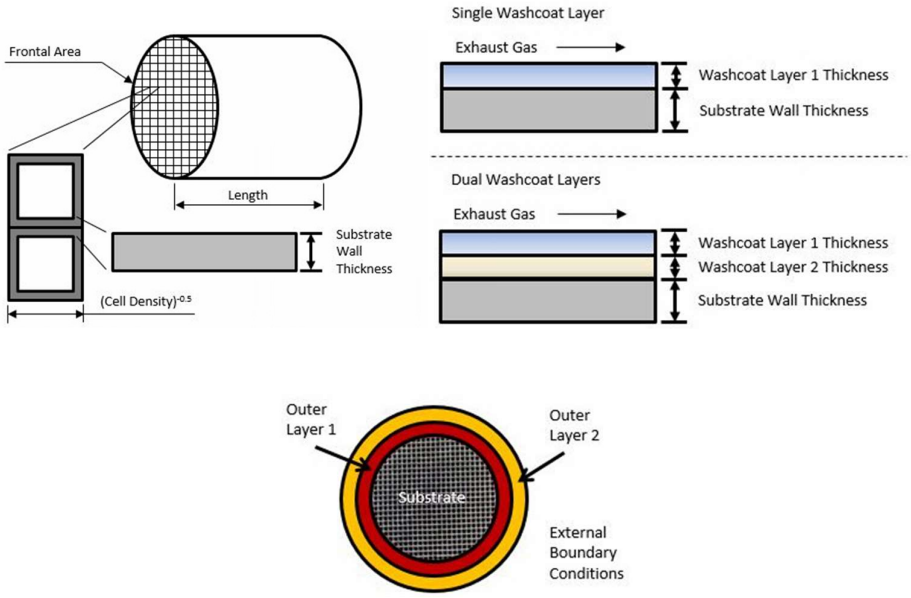

Figure 62. *Graphical representation of the geometry of a reformer.*

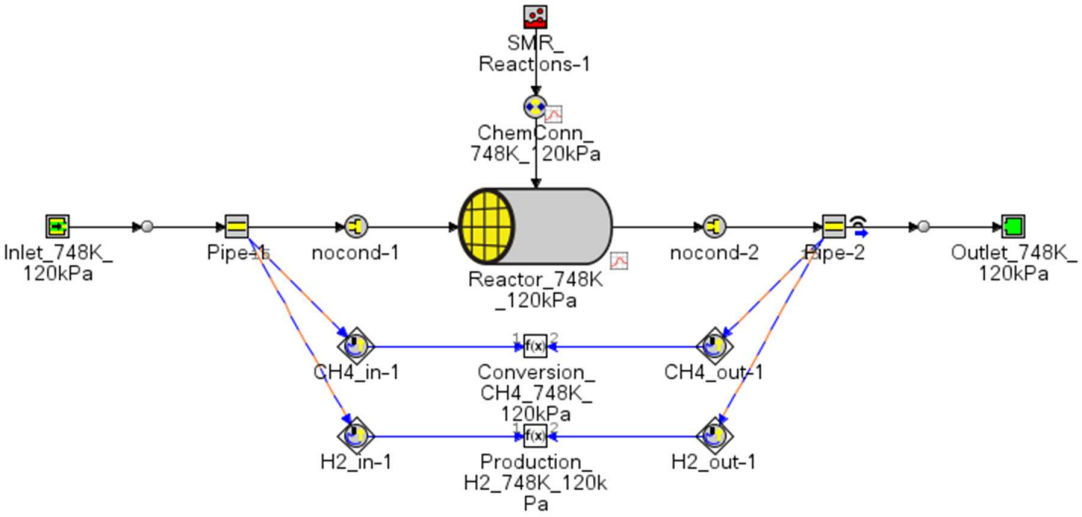

Figure 63. *Reformer model in GT-Power.*

Associated Site Element	Reactants	Products	Pre-exponent Multiplier	Activation Temperature or Energy	Concentration Expressions
				kJ/mol	
Ni	CH4 + H2O	CO + 3H2	5.922E8	209.2	G(1)*(G(PCH4)*G(PH2O)^0.5/G(PH2)^1.25...
Ni	CO + H2O	CO2 + H2	6.028E-4	15.4	G(1)*(G(PCO)*G(PH2O)^0.5/G(PH2)^0.5)*...
Ni	CH4 + 2H2O	CO2 + 4H2	1093.0	109.4	G(1)*(G(PCH4)*G(PH2O)/G(PH2)^1.75)*(1-...

General and Inhibition Functions Index	Description of General and Inhibition Functions	General and Inhibition Functions G(i)
1	(Catalyst Mass (kg)/Bed Volume (cm...	([Cat_Mass]/[Reactor_Volume])*1000
PCH4	Partial Pressure CH4 (kPa)	max({CH4}*1E-3,1E-6)
PH2O	Partial Pressure H2O (kPa)	max({H2O}*1E-3,1E-6)
PH2	Partial Pressure H2 (kPa)	max({H2}*1E-3,1E-6)
PCO	Partial Pressure CO (kPa)	max({CO}*1E-3,1E-6)
PCO2	Partial Pressure CO2 (kPa)	max({CO2}*1E-3,1E-6)
KP1	Equilibrium Constant 1 (kPa^2)	1.198E17*exp(-26830/T)
KP2	Equilibrium Constant 2 (kPa^0)	1.767E-2*exp(4400/T)
KP3	Equilibrium Constant 3 (kPa^2)	2.117E15*exp(-22430/T)
den	Inhibition	1+5.127E-13*exp(-(-140000)/8.314/T)*{CO}*1E-3+9.251*exp(-(15900)/8.314/T)*({H2O}/max({H2},1E-8))

Figure 64. *User interface of the reactor component with an example of values for methane reforming in GT-Power.*

The implementation of the reformer gave the following results testing the component in the same condition as the reference data [100].

Table 24: *Reference condition for the reforming calibration.*

Input parameters:

Operating pressure	1	[Bar]
Operating Temperature	1073	[K]
X molar H2	0	[-]
X molar CH4	33	[-]
X molar CO	0	[-]
X molar CO2	0	[-]
X molar H2O	67	[-]

From the results obtained in the simulation it could be observed that the conversion of the CH_4 is in agreement with the literature reference and the complete conversion occurs above 1000 K but the STCR=2 limits the conversion of CO in CO_2. Moving the equilibrium of the WGS to the product side is required to reduce the CO at the SOFC outlet to avoid dangerous leakage and to produce more hydrogen. For this reason, the influence of STCR on the reformer conversion performance is reported in *Figure 66*. Increasing the STCR the CO is decreasing but at the same time the vapour in the mixture decreases the partial pressure of the H_2 and consequently also the Nernst potential.

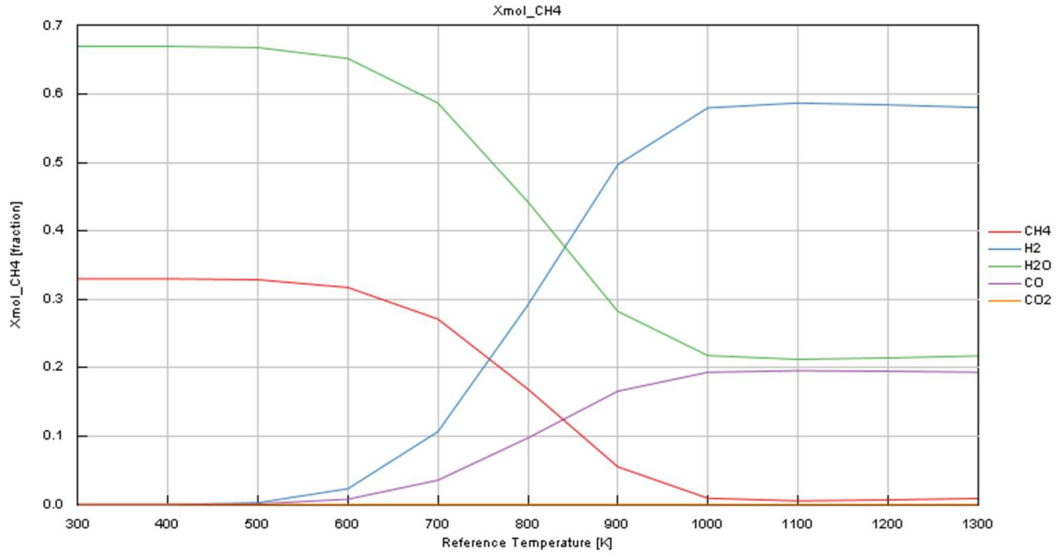

Figure 65. *Influence of the Temperature on the equilibrium of MSR and WGS reactions.*

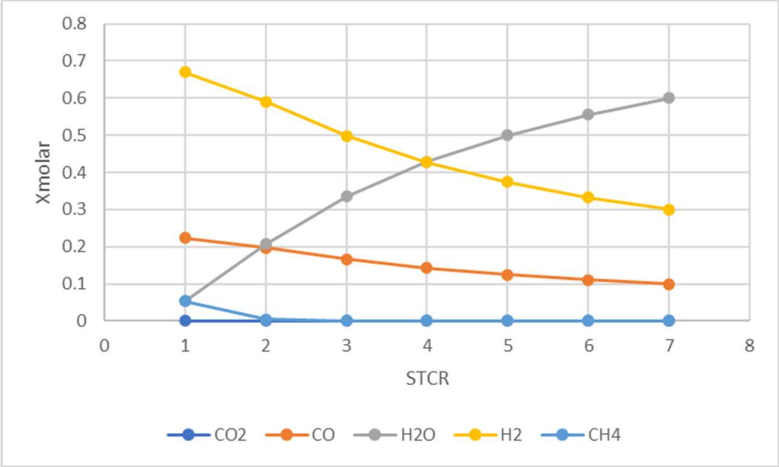

Figure 66. *Influence of the STCR on the equilibrium of MSR and WGS reactions.*

The system with the reformer and the cell and all the other components used to make work the system in correct operating conditions were defined and the result is the layout presented in *Figure 67*. The compression of the air entering the cell brings an important advantage from a performance point of view; in fact, the Nernst potential is increased since it depends on the partial pressures of reactants and products. To increase the flexibility of the system an eTurbo machine was considered. Furthermore, the thermal management of the system is the most challenging aspect of the design process and for this reason different layouts were tested.

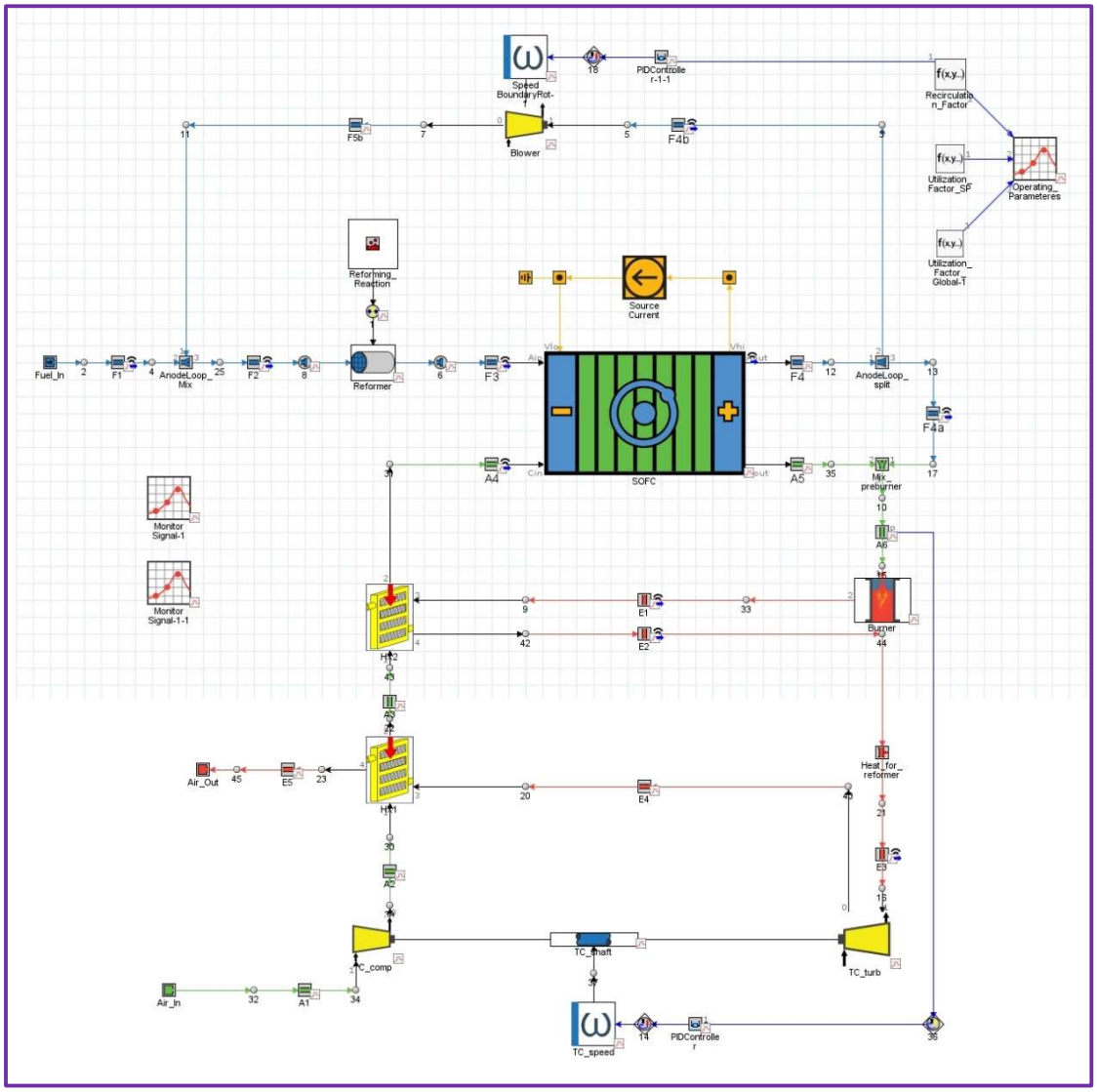

Figure 67. *SOFC-eTurbo plant configuration developed in GT-Power.*

4 Ammonia SOFC

This section presents a brief analysis on the technological solutions that are currently under investigation for ammonia fed SOFC systems and the feasibility of using ammonia for high temperature fuel cells [101]. This analysis will be the foundation for additional simulation activities that will be carried out by the TPG research group during the next years. An ammonia fed SOFC model is presented in this chapter with its validation against literature and a first plan layout design is presented. The model is developed in MATLAB-Simulink and is mainly used to find the most efficient configuration.

The design of ammonia SOFCs is derived from the current state of art of methane SOFCs, which have reached a quite advanced TRL, especially for atmospheric systems. In fact, these two systems share some similarities:

- Both the fuels could react inside the cell directly**,** producing the hydrogen for the electrochemical reaction.
- Both reactions are endothermic, even if the ammonia cracking reaction requires a smaller heat amount. For this reason, the external reformer or cracker could have a not complete conversion rate and use the fuel for the thermal management of the cell.

However, there are significant differences related to the use of ammonia, that must be taken into account during the design process of the plant layout and of the auxiliary systems.

- The ammonia cracking reaction does not require vapour to occur. Usually, in the reforming case, the anodic recirculation prevents the use of an additional component to produce vapour and, instead, the vapour produced inside the cell is taken from the cell outlet and mixed before the

reformer. This could mean that in ammonia case recirculation can be avoided from this point of view.

- The recirculation decreases the partial pressure of the hydrogen saturating the loop with nitrogen and vapour produced inside the SOFC, but at the same time increases the global utilization factor increasing also the efficiency of the system.
- The ammonia decomposition through eq. (5) increases the volumetric mass flow rate because the number of moles is doubled (from 1 mole of NH_3 we obtain a sum of 1/2 moles of N_2 and 3/2 of H2). This limits the possibility of recirculation, which is a normal practice with methane SOFC to provide steam to the MSR and WGS reactions, pre-heat the stack inlet and increase the fuel utilization. In fact, the amount of N_2 produced both in the cracker and in the SOFC is a high percentage of the flow and recirculating it could drastically reduce the concentration of hydrogen inside the cell.
- Unlike methane, ammonia is very toxic. Inhaling ammonia, even in small ppm and for short expositions times, could be very dangerous [102]. Furthermore, since the application could be marine, the ammonia release in the environment could also cause damage to the sea flora and fauna [103]. Therefore, leakages must be strictly monitored, and it is mandatory to include an auxiliary system to eliminate any possible content of ammonia left in the exhaust gasses.

4.1 Literature review

After a first investigation on the possibility of using ammonia as a hydrogen carrier inside SOFC, the available studies, both experimental and modelling,

are reported. The NH_3 SOFCs could be divided into categories according to different parameters:

- **Geometry**: planar, cone-shape, micro-tubular or honeycomb.
- **Supporting layer**: electrolyte, anode or cathode.
- **Direction of the flows**: co-flow, counter-flow or crossflow.
- **Fuel preparation**: direct ammonia or pre-cracked.
- **Heat supply to cracker**: external or internal decomposition.
- **Mass transfer direction through the electrolyte**: oxide-ion-conducing (O-SOFC) and (H-SOFC) proton-conducing.
- **Operating pressure**: atmospheric or pressurized.

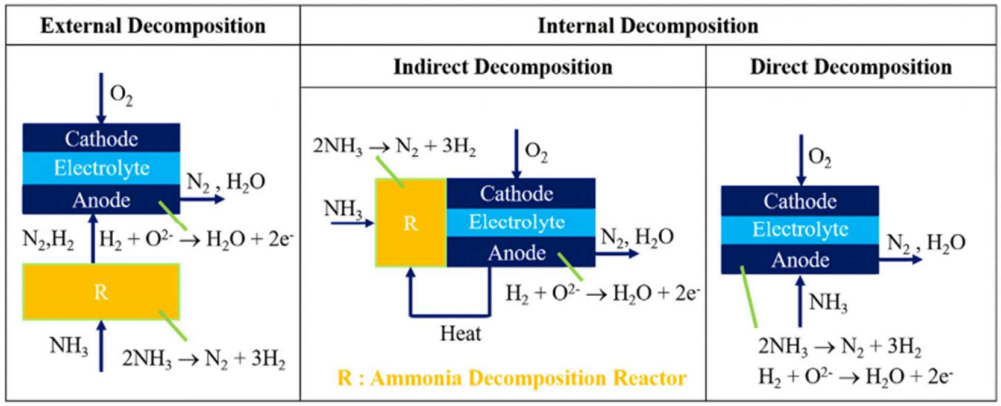

Figure 68. *Possible configuration for ammonia decomposition* [104].

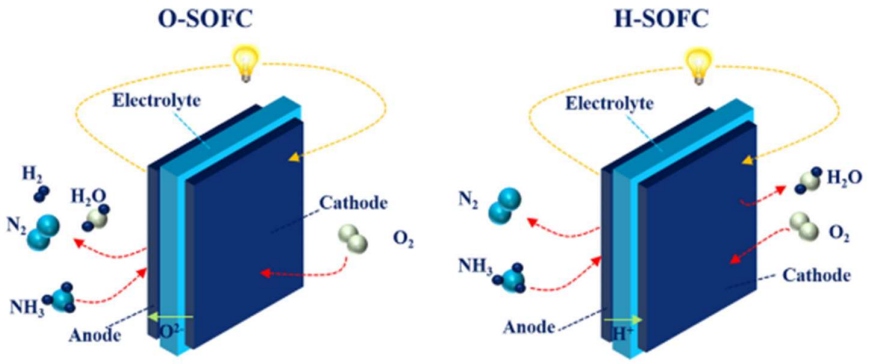

Figure 69. *Possible configuration for ammonia decomposition* [104].

In the last years, more and more study on ammonia SOFC are conducted and published, at the moment there isn't a configuration that is affirmed to be the most promising, the investigation of different possibilities is under investigation [101], [104], [105], [106], [107], [108], [109], [110], [111], [112], [113], [114], [115], [116].

Most of the studies are trying to understand if feeding ammonia directly in the cell is possible and the performance is reliable. The possibility of a DA-SOFC is motivated by the fact that the cracker component could be neglected in a BoP reducing volumes, costs and complexity. In the work of Rathore et al. [104] a comparison among the studies on direct ammonia according to the different materials is proposed, dividing the result in electrolyte supported cells and anode supported one (*Figure 70* and *Figure 71*). Results show that anode supported SOFC reaches the highest performance in terms of power density, using Ni–$Ce_{0.8}Sm_{0.2}O_{1.9}$ (SDC) for the anode, an SDC (50 μm) electrolyte, and an $Sm_{0.5}Sr_{0.5}CoO_{3-\delta}$ (SSC)–SDC cathode.

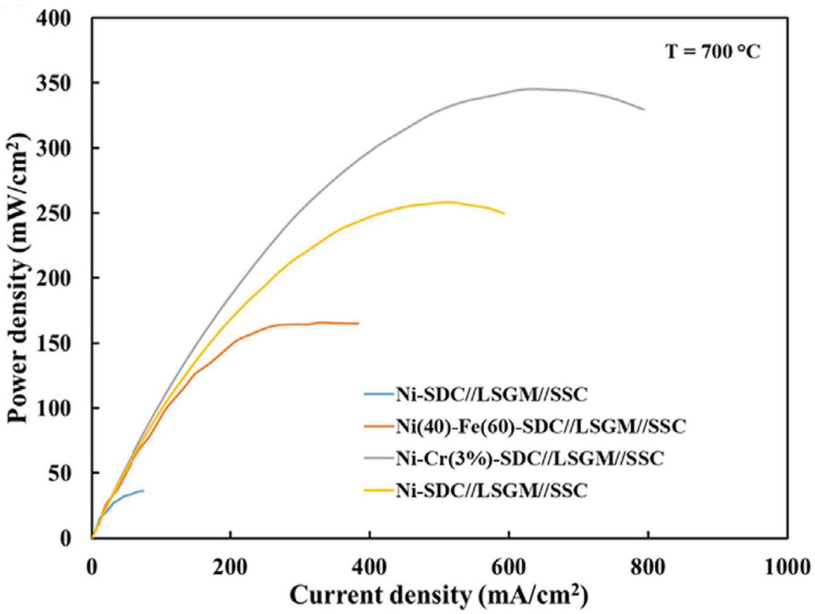

Figure 70. *Cell performance curves for electrolyte supported cells at 700 °C* [104].

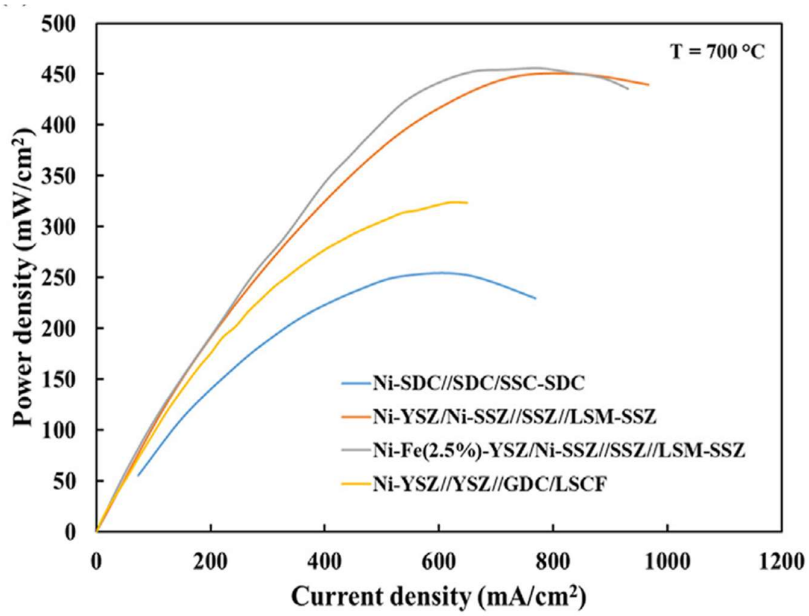

Figure 71. *Cell performance curves for anode supported cells at 700 °C* [104].

4.2 Layout analysis

In the last few years, multiple system configurations were proposed. The starting point is the actual state of art with methane, but of course a lot of design choices adopted for natural gas are for specific purpose. The main difference consists in the methane reforming process. To find the optimal layout, some relevant solutions from the literature are here presented, highlighting their advantages and disadvantages.

- The WGS and MSR require H_2O vapor to proceed that is a product of the reaction of electrochemical conversion of the hydrogen, to be sure to have the right amount of hydrogen in cell the traditional methane SOFC work with an anodic recirculation.
- This component also increases the utilization factor of the hydrogen but at the same time reduces the partial pressure of the H_2 and reduces the Nernst potential and so the efficiency of the cell.
- As in methane case we can use an after burner to burn the last part of fuel that didn't react for heat generation to be sent to a bottoming cycle or for cogeneration purpose. In this case, the reached temperature must be lower that the temperature of formation of NO_x.

A first solution is the system studied in the SOC4NH3 Project [117],in which the authors designed a 1.5 kW SOFC layout to be fed with ammonia. Figure 72 shows the layout of this system. Ammonia is evaporated by waste heat from the catalytic burner and expanded through a turbo expander. The evaporated ammonia is preheated to the anode inlet temperature in a heat exchanger. A once-through fuel utilization of almost 85% can be achieved at a high cell voltage due to the absence of water at the anode inlet. This is possible because of the absence of a recirculation loop. The stack is cooled by excess cathode air, as for

the methane state of art. The combined anode and cathode exhaust gases are combusted in a catalytic burner with a maximum exit temperature under 900 °C, ensuring negligible NOx emissions (< 0.1 ppm).

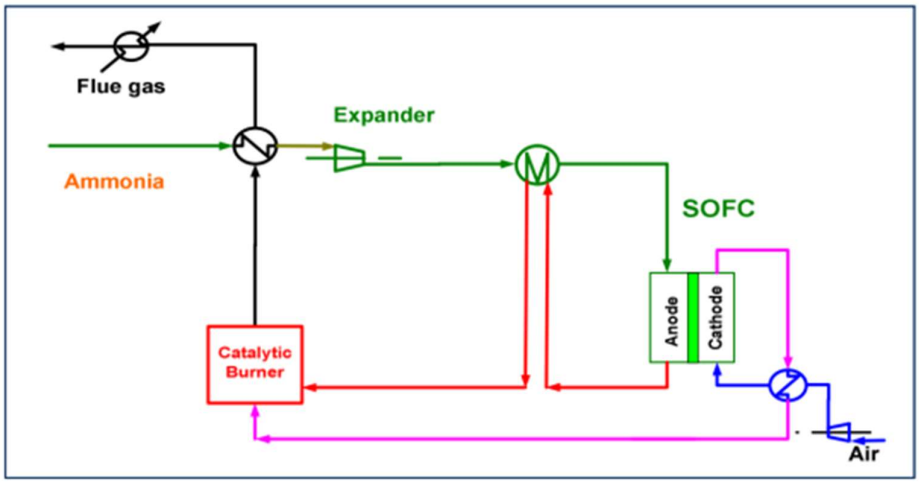

Figure 72 - *Ammonia SOFC layout proposed in the SOC4NH3 project* [117].

Ammonia SOFCs, if operated at low temperature, may present some issues with nitridation of the Ni, which can lead to failure [114](see chapter 4.5). This has to be taken into account when choosing the conditions of operation. Operating at 750 °C or above prevents these problems. During this project they also carried out durability test on the cell and a performance evaluation.

Another interesting application that gives lots of hints on how these systems behave and must be structured is the one presented in the study by K.H. Al-Hamed et al. [118], where the authors present an innovative combined system for train field applications. The plant layout is displayed in Figure 73.
The SOFC is just a part of this system, but it is directly fed with ammonia, making it a relevant application for this review. However, the main subsystem that provides electric power for the propulsion of the locomotive is the Solid

Oxide Fuel Cell (SOFC) and Gas Turbine (GT) subsystem. The other bottoming subsystems recover the waste heat to produce more electric power, space cooling or heating, and hot water. Ammonia is preheated in the fuel regenerator before it is directly injected to the anode side of the solid oxide fuel cell and redirected to the combustor. This is necessary to reach the operating temperature of the SOFC, which is assumed to be in the 500-800 °C range. In parallel, air is pressurized by the air compressor and then preheated as it goes through the air regenerator. Then, it enters the cathode side of the fuel cell providing the oxygen for the electrochemical reaction.

Not all the ammonia is consumed by the fuel cell. The remaining amount is mixed with air and fresh fuel before being burnt in the combustor. The result of this combustion are high-temperature high-pressure exhaust gases that can enter the gas turbine at its appropriate temperature range (around 1030 °C). This would not be possible without mixing the exhausts with a fresh charge of fuel. The expanded exhaust gases from the turbine are then used to supply heat to both the air and fuel regenerators. From the results, the authors affirm to have reached a utilization factor of 80% and a SOFC efficiency of 65% in nominal conditions, corresponding to an electric power output of 2158 kW (about 70% of the total electric power demand).

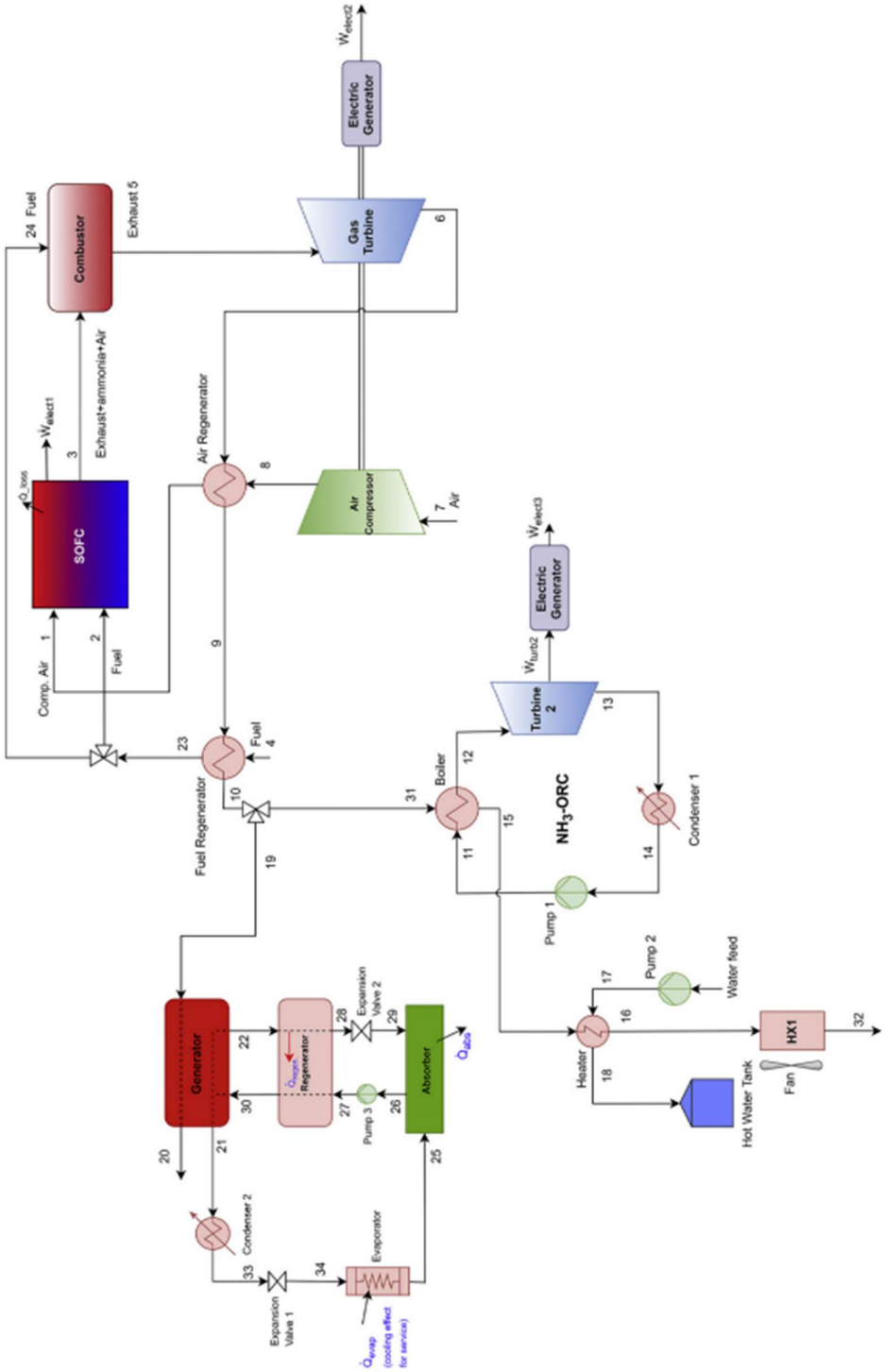

Figure 73 *- Combined plant layout with an Ammonia SOFC*[118].

In a modelling activity done by Di Micco et al. [119] the performance of a SOFC modelled in Aspen Plus™ for a maritime application is shown. In the study a typical load profile is defined and the SOFC is compared to traditional ICE fed with FO. The fuel cell module in this work produces 118.3 kW scaled to reach the corresponding power of the ICE equal to 8.3 MW. The fuel cell module works with 750 °C and a utilization factor of 0.8, achieving a 0.714 V at nominal power condition. The study focuses on the total weight and volume of the innovative system. The schematic plant layout is reported in *Figure 74*.

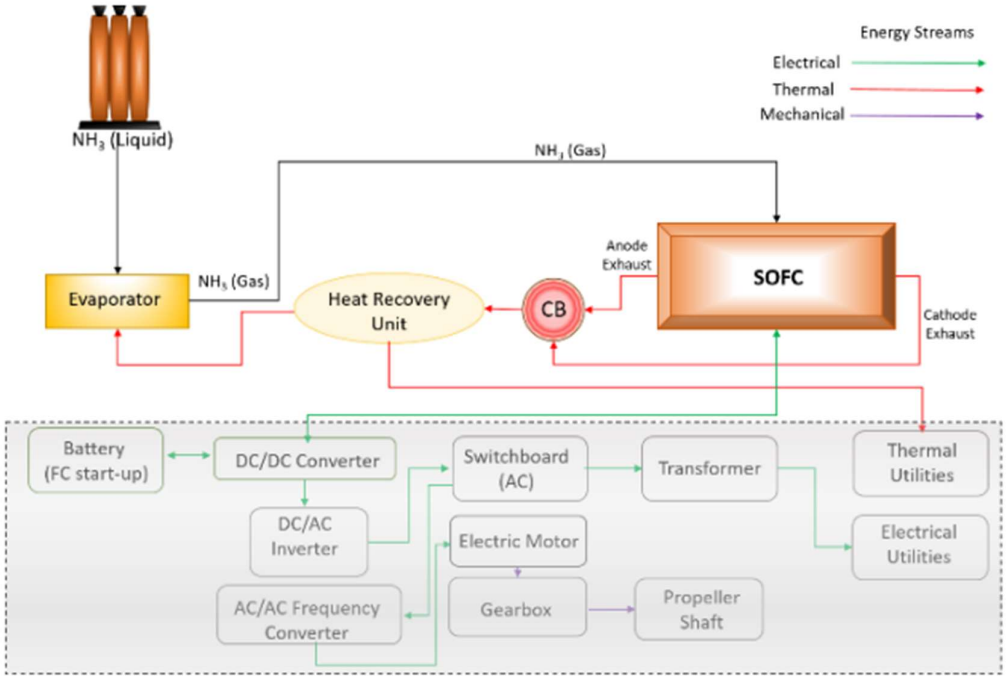

***Figure 74** – NH_3-SOFC model for maritime application* [119].

One last example of application is the one presented by A. Perna et al. [109]. The plant proposed in this study is represented in Figure 75. This system was designed to also produce hydrogen. The SOFC in this case is still fed directly with ammonia, but since hydrogen production is the main goal of this system,

the utilization factor is much lower than in the previous application. This plant has a different purpose from the ones presented above, therefore it is not possible to compare their performance. However, this layout provides some interesting ideas on the use of a separation membrane system that could be used to increase the partial pressure of hydrogen and contrast the effect of the ammonia cracking reaction generating large amounts of inert gas.

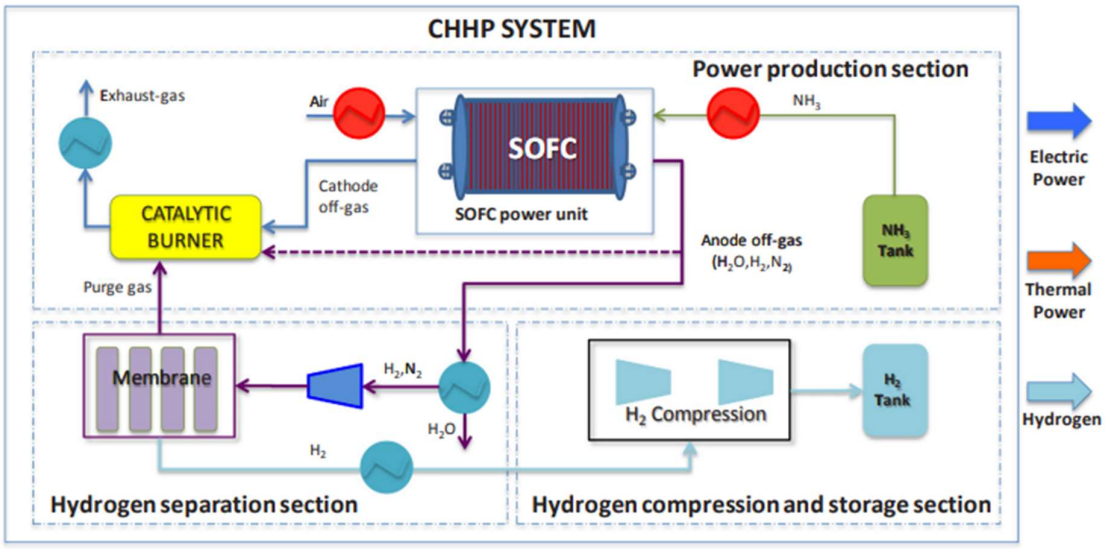

***Figure 75** - Combined plant layout for hydrogen, heat and power production with an ammonia SOFC* [109].

As in the previous cases, many different design choices have been presented in literature. These choices are motivated by specific application requirements or by results of preliminary calculations. Similarly, the marine focus of this project introduces some specific requirements and constraints that will influence the design choices of the ammonia SOFC system. The modelling and simulation activities carried out will be devoted at determining the best solutions among the many available:

- Many different types of systems can be developed: pressurized/atmospheric, planar/tubular cells, internally/ externally cracked, directly/indirectly fed.
- The ammonia cracking process could be done internally inside the cell or outside in a cracker. If an external cracker is used, the right amount of ammonia to pre-crack must be determined as well.
- The ammonia at the stack outlet can be recirculated or not. Recirculation increases the overall fuel utilization but introduces various issues, as previously explained. Including a recirculation loop also requires the installation of a compressor (blower) or an ejector. Recirculating part of the outlet flow can also be used to increase the temperature of the fresh fuel, optimizing the thermal management of the system.
- If recirculation is adopted, the exhaust flow can be reintroduced in the loop before or after the cracking. The first solution could lead to a better ammonia conversion, thanks to higher temperatures inside the cracker, but at the same time a lower partial pressure of ammonia may negatively affect the equilibrium of the reaction.
- If recirculation is adopted, hydrogen membrane separators can be used to limit its partial pressure decrease.
- The position of all heat exchangers must be determined in order to maximize the waste heat recovery.
- Using ammonia, a high concentration of N_2 in the exhausts is expected. The combustor operative temperature must be properly controlled to have not unwanted emissions (NO_x mainly).

4.3 Model description

To understand the behaviour of ammonia fed SOFC we implemented a model of the cell that considers the possibility of using this fuel. The first step was to

decide which kind of configuration to use. To begin the modelled cell was considered at atmospheric pressure, planar and the fuel and the air are fed in co-flow setup. In literature there are some examples of experimental activities on cells fed with direct ammonia. We tried to replicate the results to validate our model. The trend in the most recent work is to feed the cell with 100% NH_3 fuel and make it crack inside the anode. The result is usually compared to hydrogen case or ammonia/hydrogen blends or equivalent hydrogen (N_2/H_2 blends to simulate the ammonia pre-cracking).

The model of the cell is a 1D model implemented in MATLAB-Simulink. The cell is discretized in n parts along the direction of the flow (Fig. 1). The thermochemical properties are evaluated at the centre of the discretization following the flow chart in Fig. 3 and at the boundary. Each discretization takes the information from the interface upstream and after the evaluation it sends the information downstream.

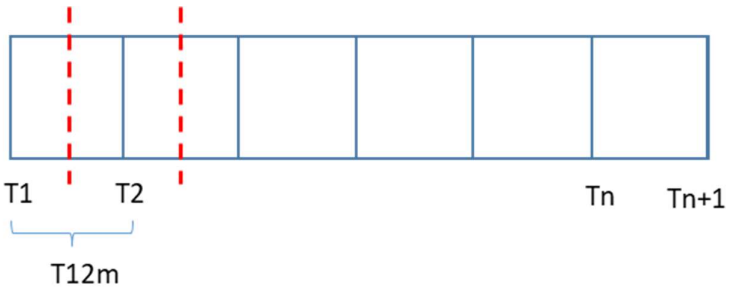

Figure 76 *– Schematic representation of the discretized fuel cell.*

The model uses **two iterative cycles**, one on the voltage error along the cell and the other on the error on the thermal balance. The voltage must be almost constant in the cell while the current varies, so even if the discretization divides the cell in sections, the difference in voltage between the end of the electric circuit must be the same for each part. The thermal loop is required since after

the first evaluation of ammonia reacted the thermal balance is evaluated defining a new temperature. With the new temperature the ammonia equilibrium could be changed and so the thermal balance.

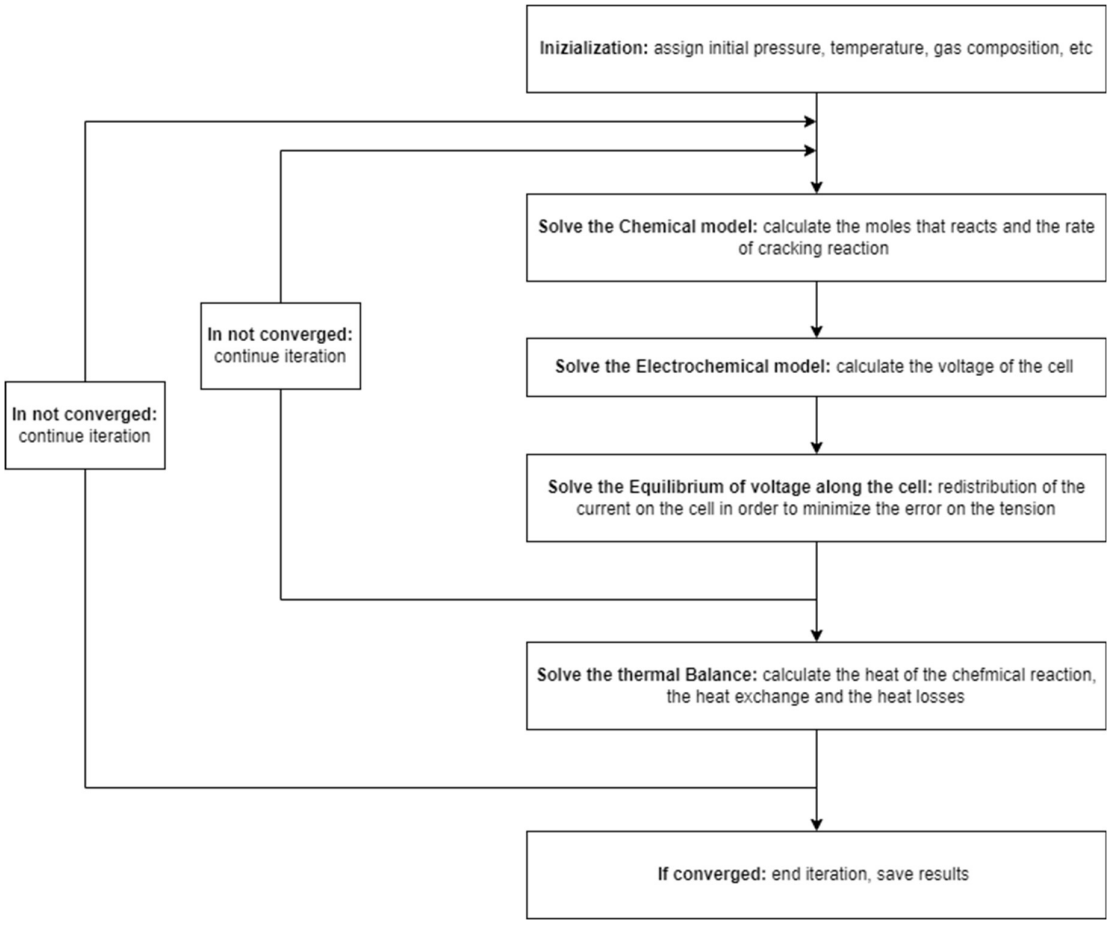

Figure 77 *– Logical process map implemented inside the model.*

As showed above in the flowchart the model considers different aspects of the physics of the cell:

- **Chemical equilibrium**: The current delivered is an input of the cell and is used to evaluate how much hydrogen and oxygen reacts and the ammonia cracked is evaluated.

- **Electrochemistry**: When the composition is set, the real electrochemistry takes place with the Nernst and the polarizations evaluation. To close this loop the voltage of the cell is checked, all the discretization must have the same tension and the current changes.

- **Thermal evaluation**: in this last part the production and absorption of heat is evaluated making a thermal balance considering the endothermic reactions, the electrochemical conversion of hydrogen, the temperature of the flows and of the solid part and the thermal losses.

- **Pressure losses**: Are evaluated at each temporal step outside of the cell.

- **Performance**: the output of the cell includes the evaluation of parameters to evaluate the performance of the cell, as current, tension, fuel and oxygen utilization factor, efficiency…

The actual state of art of SOFC is given by the use of natural gas that must be converted into hydrogen to produce electricity from its electrochemical conversion. The conversion of methane into hydrogen needs two reactions: the MSR (Methane Steam Reforming) and the WGS (Water Gas Shifting). The reaction is endothermic and is used inside the cell as a tool for thermal management to mitigate the temperature increase due to the electrochemical conversion of the hydrogen. The ammonia conversion could be used in the same way as it is endothermic too.

As for the study of ammonia cracking, it has been modelled in part following previous work. In the model, the equilibrium point of the reaction is calculated

by minimizing the Gibbs function which considers various parameters such as temperature, pressure and the quantity of products and reactants.
The reaction of ammonia decomposition is the (72) and includes only 3 chemical species. From the first and the second law of thermodynamics, we can use the combination of energy and entropy balance with the Gibbs function that could be written as (73).

$$NH_3 \rightarrow \frac{1}{2}N_2 + \frac{3}{2}H_2 \tag{72}$$

$$G \cong H - TS \tag{73}$$

The MATLAB function "fmincon" compute the minimization of the Gibb's free energy equation, that in the end results like (74), where μ_i represent the chemical potential of species I and n_i is the number of moles of specie i.

$$F = min\frac{G}{RT} = \sum_{i=1}^{k} n_i \left(\frac{\mu_i^0(T)}{RT} + ln\left(\frac{P}{P_0}\right) + ln\left(\frac{\dot{n}_\iota}{\sum n_i}\right)\right) \tag{74}$$

It could be observed that in the equation the influence of the temperature, of the pressure and of the number of moles of species are included. The final equation is described in literature [120].
The results were validated with data modifying the inputs of the formulation, in *Figure 78* an example evaluated with this procedure is reported. The simulation shows the decomposition of 1 mole of NH_3 with 0 moles of N_2 and H_2 at different temperatures at 1, 5, 10, 15 bar (from the lighter to the darker). As could be observed the temperature helps the cracking reaction and the pressure has the opposite effect moving the equilibrium in the opposite direction.

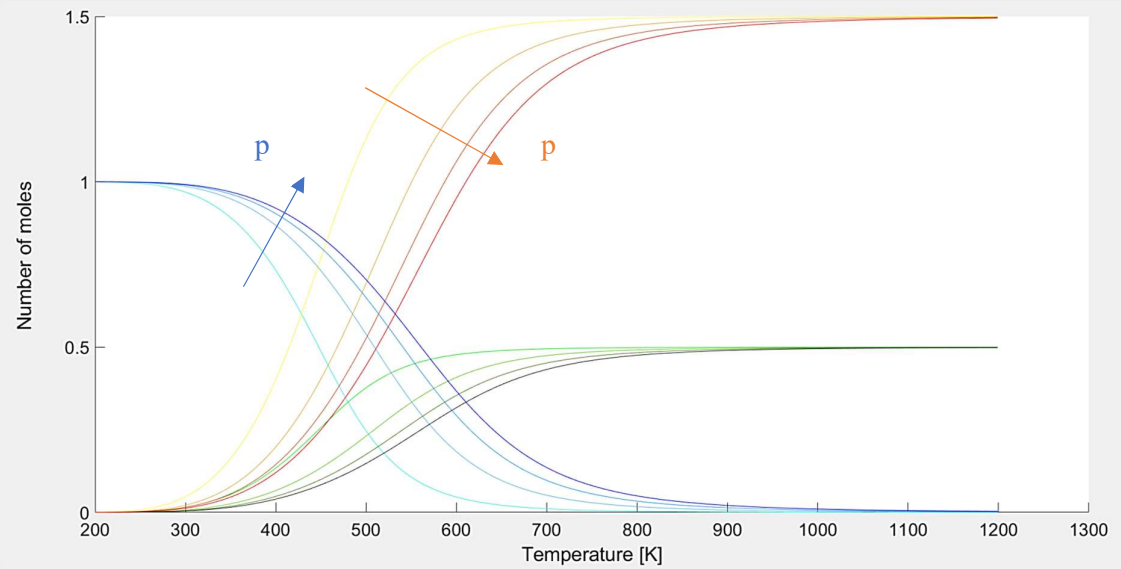

Figure 78 *– Ammonia decomposition equilibrium at different temperatures and pressures (NH3 in blue, H2 in red and N2 in green going from low to high pressure with darker colours, 1, 5, 10 and 15 bar).*

After the evaluation of the equilibrium, to take into account the kinetic of the phenomenon, we used a percentage approach, so the conversion reaches a certain percentage of the equilibrium in order to simulate the catalytic effect of the Nickel. This is a first approximation that should be checked with a comparison, for instance, with a literature study.

In this study we didn't consider the possibility of having the electrochemical conversion of the ammonia that occurs according to the reaction of equation (75) and (76) because from recent works it seems difficult that this kind of reaction happens [104], [121], [122].

$$NH_3 + 5O^{2-} \rightarrow 2NO + 3H_2O + 10e^- \quad (75)$$

$$2NH_3 + 3NO \rightarrow \frac{5}{2}N_2 + 3H_2O \quad (76)$$

For anode made of Ni-YSZ the reaction rate could be expressed by the eq. (77):

$$r^{Ni-pore} = 98.4exp\left(\frac{-1.20 \times 10^5}{RT}\right) p_{NH_3}^{0.69}\left(p_{H_2} + 750\right)^{-0.39} \quad (77)$$

4.4 Results

In this chapter some result on the performance of SOFC fed with ammonia are presented with regards to the methane case as comparison. The simulations are conducted on the SOFC module with different condition of pressure, temperature, load, composition to characterise the fuel cell. The geometric constants are reported in *Table 25*. The module fed with methane produces 33 kW electric power in direct current with nominal current equal to 30.3 A. The reference data are those from Staxera GmbH SOFC system.

Table 25: *SOFC geometry specification assumptions for modelling activities.*

Variable	*Value*	*Unit*
Number of cells	1500	*[-]*
Length of the cell	0.09	*[m]*
Anode thickness	40	*[μm]*
Cathode thickness	40	*[μm]*
Electrolyte thickness	95	*[μm]*
Anode current collector thickness	0.25	*[mm]*
Cathode current collector thickness	0.25	*[mm]*
Width of the cell	0.11	*[m]*
Anodic channel height	2.5	*[mm]*
Cathodic channel thickness height	2.5	*[mm]*
Anodic porosity	0.4	*[-]*
Cathodic porosity	0.4	*[-]*

Anodic current collector porosity	0.3	*[-]*
Cathodic current collector porosity	0.3	*[-]*
Mean diameter of pores	1	*[μm]*
Anodic tortuosity	3	*[-]*
Cathodic tortuosity	3	*[-]*
Anodic current collector tortuosity	3	*[-]*
Cathodic current collector tortuosity	3	*[-]*
Solid density (FeCr Alloy)	7700	*[kg/m^3]*
Solid specific heat (FeCr Alloy)	660	*[J/kg K]*
Cell thermal conductivity	24	*[W/m K]*

The hypothesis done for the simulation are the following:

- The air mass flow rate that is fed into the cell is evaluated by a controller on the stack temperature. Since the cooling is accomplished with the cathodic flow the controller regulates the pressure since the max temperature reaches 860 °C, temperature constrain of the cell.
- The fuel supplied is controlled too. The comparison between different composition or fuel can be done using the same single pass utilization factor.
- The load condition is determined by the current information given as input for the fuel cell model.
- The cell is discretized to better understand the behaviour inside the component.
- The methane reference case has the composition reported in *Table 26* that is the composition at the anode inlet already processed by the reformer constant for all the load conditions.

Table 26: *Reference pre-reformed flow mass composition for methane case.*

X_{H2}	***0.423***
X_{H2O}	*0.230*
X_{CH4}	*0.021*
X_{CO2}	*0.140*
X_{CO}	*0.186*

The methane case is the reference we use for all the simulation. The pressure and temperature are taken from the reference case and the comparisons are done with the same utilization factor changing the mass flow rate.

The methane case simulates a pre-reformer but the conversion of the reactants from the reaction of MSR and WGS is not complete and they are partially processed inside the cell as could be evinced from *Figure 79* and *Figure 80* where the hydrogen fraction firstly increase because the conversion of methane occurs and then decreases because it is used in the electrochemical reactions. With lower load this change is more accented.

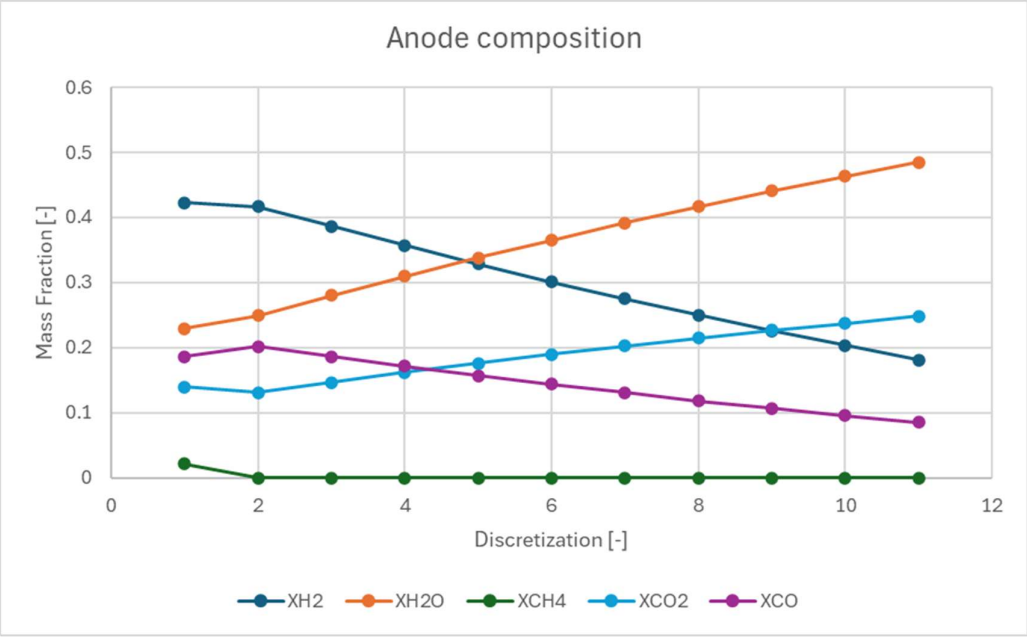

Figure 79 *– Anode composition along the cell for 1.3 bar at 100% load.*

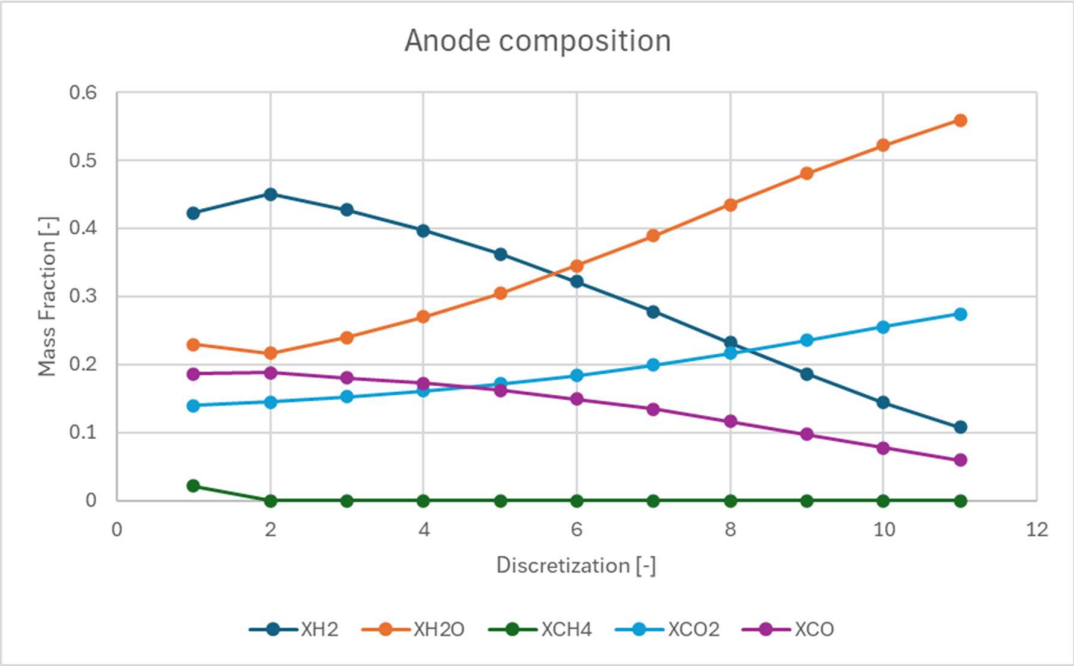

Figure 80 *– Anode composition along the cell for 1.3 bar at 80% load.*

The temperature as previously specified is controlled by the air mass flow rate so for all the cases the maximum temperature is 860 °C (1133 K) but the slope of the temperature varies. The endothermic reaction of reforming absorbs more heat, and the resulting temperature is lower at the inlet. This results in higher temperature difference and so thermal stress for the cell, still having less than 160 °C difference. *Figure 81* shows the difference in temperature profile for different fuel compositions at different pressures for full load condition. From this picture, the pressure seems not to influence so much the temperature variation with exception in moving the equilibrium of the decomposition reactions.

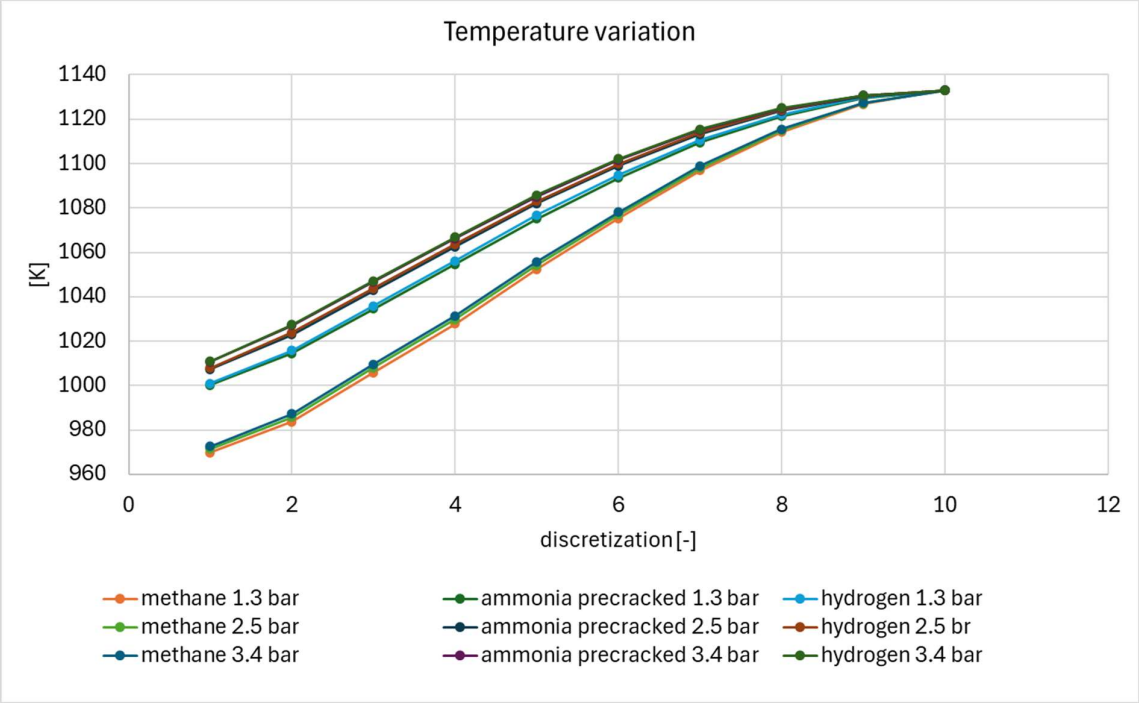

Figure 81 *– Temperature along the cell for different pressure level at 100% load.*

Analyzing the temperature changes, varying the load the differences are even lower from case to case (*Figure 82*). Changing the load should change the heat production inside the cell, however this phenomenon is not appreciable due to the type of control adopted. The air mass flow rate is the variable that changes in function to the load in order to keep the temperature constant (*Figure 83*).

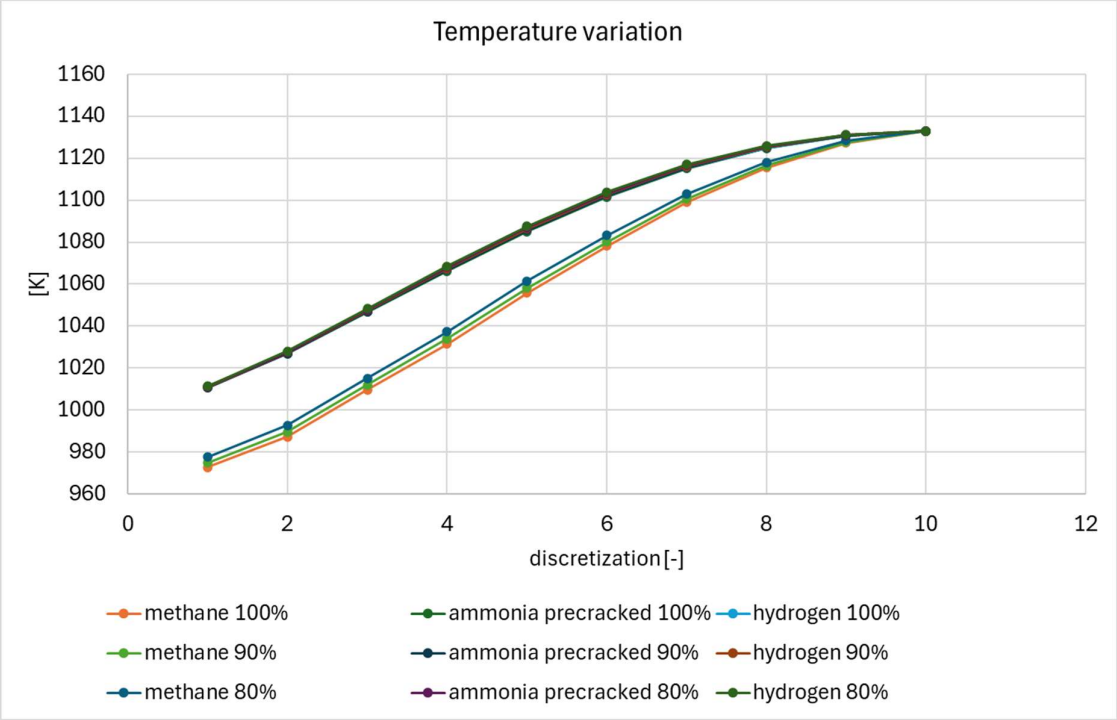

Figure 82 *– Temperature along the cell for different loads level at 3.4 bar.*

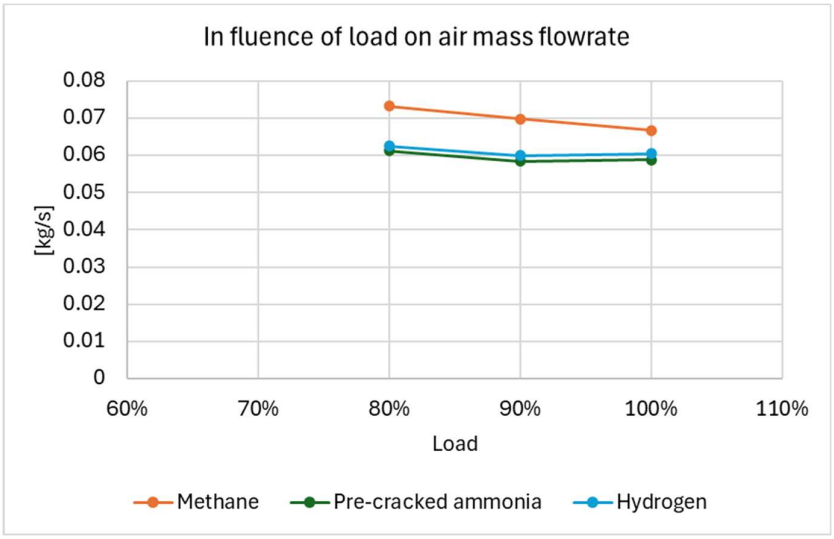

Figure 83 *– Air mass flow rate at different load for different fuels.*

For the efficiency of the cell in *Figure 84* shows the increase in efficiency due to the pressurization and also the higher efficiency of pre-cracked ammonia in comparison to methane case using the same utilization factor. A further consideration could be done looking at the efficiency changing according to the load percentage (*Figure 85*). The reduction of load and thus of current increases the efficiency because the polarization losses are reduced for low current values.

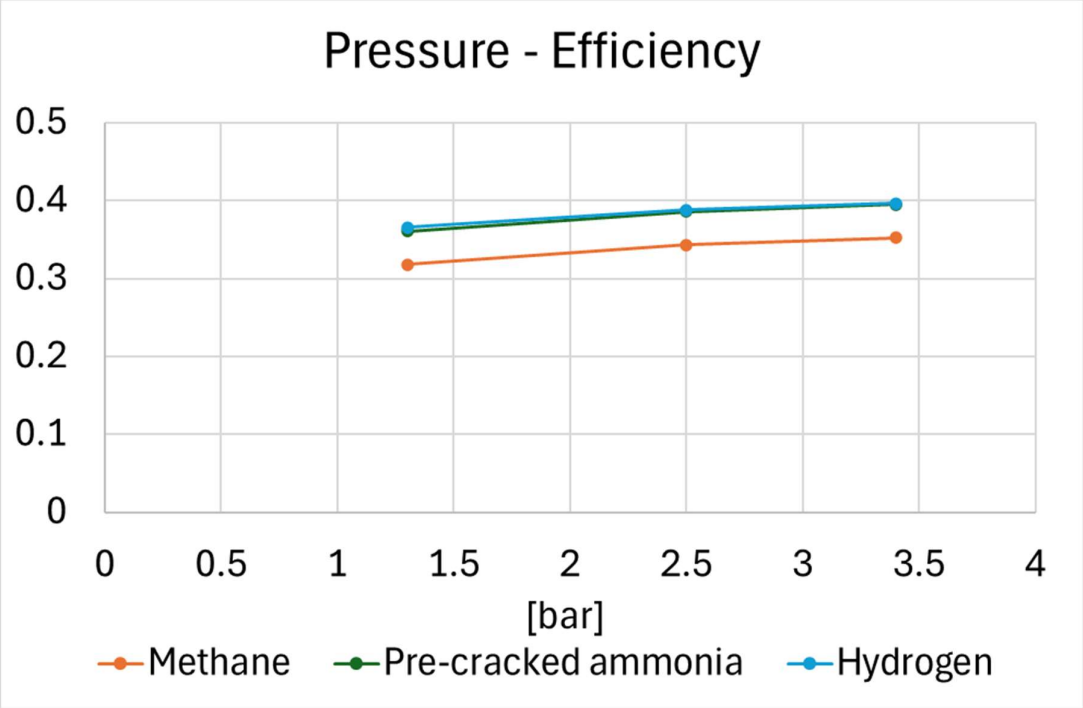

Figure 84 *– Efficiency changes in function of the pressure.*

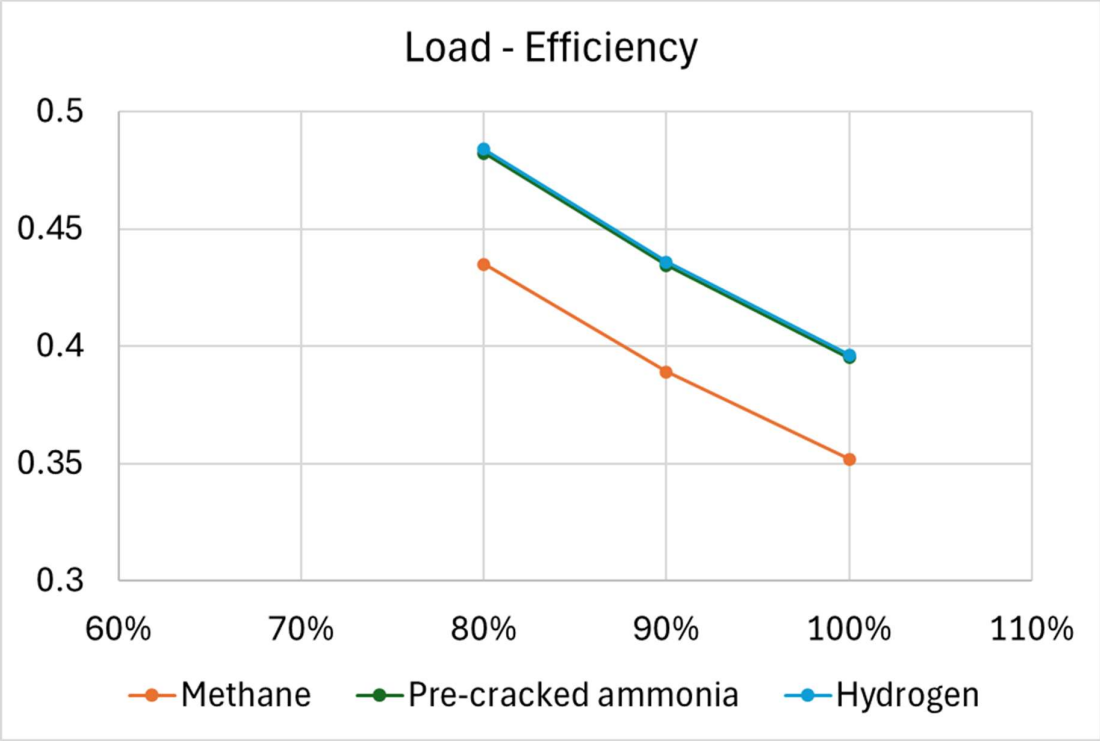

Figure 85 *– Efficiency changes in function of the load percentage.*

4.5 Ammonia compatibility with materials

The possibility of using ammonia as fuel for SOFC is under investigation and was shown in this chapter. The advantages and disadvantages were discussed from a systemistic and thermal point of view but it's important also to mention the fact that ammonia is a very aggressive and corrosive substance and could have some compatibility issues with the material of the components especially in the presence of contaminants such as water vapour and air [123]. Corrosion-resistant materials such as stainless steel are therefore required for efficient fuel cell design and performance. Furthermore, In the case of SOFC-O, steam is

generated at the anode and can mix with unreacted ammonia; this may lead to corrosion of metal pipes.

When ammonia is fed to the SOFC system for power generation and if the ammonia is not fully cracked, there is a strong possibility that the nickel surface of the anode (Ni-YSZ) converts into nitride (Ni_3N), resulting in volumetric changes in the anode microstructure of the cell, an increase in ohmic overpotential, and electrode delamination. Additionally, materials widely used in the Ni-YSZ anode must resist redox reactions to crack the ammonia fuel; otherwise, nickel particles in the Ni-YSZ anode can form Ni_3N. This redox reaction can cause cell degradation or even electrolyte cracking by increasing the interfacial polarization between the electrolyte and anode [124].

Most paper in review that study the performance of ammonia fed fuel cell doesn't show a lower performance of the SOFC but the above issue could affect the degradation rate and make the cell decrease their efficiency quicklier.

4.6 Concluding remarks

In this chapter, a first analysis was shown on the possibility of using ammonia in SOFC since the high temperature in the cell allow the use of hydrogen carriers and the temperature is high enough to make the ammonia decomposition happening.

The substance has some issues from safety point of view, but it is already widely produced in the chemical industry and more and more companies are thinking of using it in naval internal combustion engines.

Some plant layouts were investigated and finding an optimal configuration is one future work that is now on going, evaluating for instance is using recirculation or not. Recirculation can increase fuel utilization but may

introduce issues. Hydrogen membrane separators can limit partial pressure decrease. Heat exchanger positions must be determined for waste heat recovery. Once the system is ready the final result will be the performance in terms of efficiency but also in terms of emissions since ammonia can lead to NO_x production.

5 Conclusions

In conclusion, the analysis of the maritime field has demonstrated the reliability of simulations conduced using HELM in aligning with real cases, indicating the potential for further investigation into additional case studies. The competitiveness of fuel oil engines versus alternative engine fuels, particularly LNG, has been highlighted across various power and operating hour ranges. Alternative technologies such as fuel cells have shown significant competitiveness, particularly in high emission relevance scenarios, despite cost and volume limitations due to their low Technology Readiness Level (TRL).

Further exploration into fuel cell solutions, particularly turbocharged PEMFC systems, revealed promising performance outcomes. Simulation results showcased a nominal net efficiency of 57%, with efficiencies remaining high even at maximum load conditions due to stack pressurization by the compressor. The turbocharged system demonstrated efficiency improvements of up to 3% at minimum load compared to standard PEMFC systems, attributed to power recovery from the turbine reducing overall Balance of Plant (BoP) power consumption. Additionally, the turbocharged system exhibited higher power density, making it particularly attractive for applications prioritizing low volume, weight, and emissions, such as transportation.

The use of pressurization gave important results in terms of efficiency of the system and the feasibility of these systems as power systems for propulsion was tested and they resulted too slow for normal operation but still they could be adopted for base load condition in order to reduce a big quantity of emissions.

Additionally, initial analysis on the feasibility of using ammonia in SOFC systems has shown promise, given the high temperature fuel flexibility. While safety concerns exist, the substance is already widely used in the chemical industry, with increasing interest in its application in naval internal combustion

engines. The possibility of using ammonia in fuel cell is arousing interest in the research and industrial field.

Overall, the findings underscore the potential of fuel cell technologies, both in maritime propulsion and as part of broader energy transition efforts, though further research and development efforts are necessary to address technical and operational challenges and realize their full potential in the maritime sector.

Bibliography

[1] European Commission, "The European Green Deal," 2019.

[2] K. Hainsch, L. Göke, C. Kemfert, P.-Y. Oei, and C. Von Hirschhausen, "European Green Deal: Using Ambitious Climate Targets and Renewable Energy to Climb Out of the Economic Crisis," *DIW Weekly Report*, vol. 28+29, no. 28/29, pp. 303–310, 2020.

[3] "Maritime Forecast to 2050 - DNV - DNV." Accessed: Mar. 02, 2024. [Online]. Available: https://www.dnv.com/maritime/publications/maritime-forecast-2023/index.html

[4] S. S. V. Subbarao and R. Kadali, "Impact of COVID-19 pandemic lockdown on the public transportation system and strategic plans to improve PT ridership: a review," *Innovative Infrastructure Solutions*, vol. 7, no. 1, Feb. 2022, doi: 10.1007/S41062-021-00693-9.

[5] "Energy system - IEA." Accessed: Mar. 02, 2024. [Online]. Available: https://www.iea.org/energy-system

[6] "ABS, 'Pathways to sustainable shipping', 2020."

[7] "MARPOL Annex VI-Prevention of Air Pollution from Ships National Workshop (virtual) on Ratification and Effective Implementation of MARPOL Annex VI for Algeria."

[8] "International Maritime Organization." Accessed: Mar. 02, 2024. [Online]. Available: https://www.imo.org/

[9] L. van Biert, M. Godjevac, K. Visser, and P. V. Aravind, "A review of fuel cell systems for maritime applications," *Journal of Power Sources*, vol. 327. Elsevier B.V., pp. 345–364, Sep. 30, 2016. doi: 10.1016/j.jpowsour.2016.07.007.

[10] Q. Wang, H. Zhang, J. Huang, and P. Zhang, "The use of alternative fuels for maritime decarbonization: Special marine environmental risks and solutions from an international law perspective," *Front Mar Sci*, vol. 9, Jan. 2023, doi: 10.3389/fmars.2022.1082453.

[11] S. Verhelst, J. W. Turner, L. Sileghem, and J. Vancoillie, "Methanol as a fuel for internal combustion engines," *Progress in Energy and Combustion Science*, vol. 70. Elsevier Ltd, pp. 43–88, Jan. 01, 2019. doi: 10.1016/j.pecs.2018.10.001.

[12] D. Bellotti, M. Rivarolo, L. Magistri, and A. F. Massardo, "Feasibility study of methanol production plant from hydrogen and captured carbon dioxide," *Journal of CO2 Utilization*, vol. 21, 2017, doi: 10.1016/j.jcou.2017.07.001.

[13] M. Pérez-Fortes, J. C. Schöneberger, A. Boulamanti, and E. Tzimas, "Methanol synthesis using captured CO2 as raw material: Techno-economic and environmental assessment," *Appl Energy*, vol. 161, 2016, doi: 10.1016/j.apenergy.2015.07.067.

[14] S. M. Shovon *et al.*, "Advancements in hydrogen generation, storage, and utilizations: A comprehensive review of current trends in Bangladesh," 2024, doi: 10.1016/j.energy.2024.130477.

[15] H. A. Marshall, *Advanced transmission systems for new propulsion technologies*. Elsevier, 2022. doi: 10.1016/B978-0-323-90979-2.00016-0.

[16] A. Brisse, J. Schefold, and A. Léon, *High-temperature steam electrolysis*. Elsevier, 2021. doi: 10.1016/B978-0-12-819424-9.00009-4.
[17] J. Hansson, S. Brynolf, E. Fridell, and M. Lehtveer, "The potential role of ammonia as marine fuel-based on energy systems modeling and multi-criteria decision analysis," *Sustainability (Switzerland)*, vol. 12, no. 8, Apr. 2020, doi: 10.3390/SU12083265.
[18] F. Y. Al-Aboosi, M. M. El-Halwagi, M. Moore, and R. B. Nielsen, "Renewable ammonia as an alternative fuel for the shipping industry," *Current Opinion in Chemical Engineering*, vol. 31. Elsevier Ltd, Mar. 01, 2021. doi: 10.1016/j.coche.2021.100670.
[19] Y. Haseli, "Maximum conversion efficiency of hydrogen fuel cells," *Int J Hydrogen Energy*, vol. 43, no. 18, pp. 9015–9021, May 2018, doi: 10.1016/j.ijhydene.2018.03.076.
[20] M. Turco, A. Ausiello, and L. Micoli, "Fuel cells operating and structural features of MCFCs and SOFCs," in *Green Energy and Technology*, Springer Verlag, 2016, pp. 31–76. doi: 10.1007/978-3-319-03215-3_2.
[21] E. Weidner, R. Ortiz Cebolla, and J. Davies, "Global deployment of large capacity stationary fuel cells," 2019. doi: 10.2760/372263.
[22] E. R. Nielsen *et al.*, "Status on Demonstration of Fuel Cell Based Micro-CHP Units in Europe," *Fuel Cells*, vol. 19, no. 4, p. fuce.201800189, Jul. 2019, doi: 10.1002/fuce.201800189.
[23] Grand View Research, "Fuel Cell Market Size & Share | Industry Growth Report, 2027," 2020.
[24] National Fuel Cell Research Center, "Stationary Fuel Cell Cost Trends," 2018.
[25] X. Zhang *et al.*, "Towards a smart energy network: The roles of fuel/electrolysis cells and technological perspectives," *International Journal of Hydrogen Energy*, vol. 40, no. 21. Elsevier Ltd, pp. 6866–6919, Jun. 08, 2015. doi: 10.1016/j.ijhydene.2015.03.133.
[26] A. G. Olabi, T. Wilberforce, and M. A. Abdelkareem, "Fuel cell application in the automotive industry and future perspective," *Energy*, vol. 214, p. 118955, Jan. 2021, doi: 10.1016/j.energy.2020.118955.
[27] L. van Biert, M. Godjevac, K. Visser, and P. V. Aravind, "A review of fuel cell systems for maritime applications," *Journal of Power Sources*, vol. 327. Elsevier B.V., pp. 345–364, Sep. 30, 2016. doi: 10.1016/j.jpowsour.2016.07.007.
[28] A. Baroutaji, T. Wilberforce, M. Ramadan, and A. G. Olabi, "Comprehensive investigation on hydrogen and fuel cell technology in the aviation and aerospace sectors," *Renewable and Sustainable Energy Reviews*, vol. 106, pp. 31–40, May 2019, doi: 10.1016/j.rser.2019.02.022.
[29] A. G. Olabi, T. Wilberforce, and M. A. Abdelkareem, "Fuel cell application in the automotive industry and future perspective," *Energy*, vol. 214, p. 118955, Jan. 2021, doi: 10.1016/j.energy.2020.118955.
[30] H. S. Das, C. W. Tan, and A. H. M. Yatim, "Fuel cell hybrid electric vehicles: A review on power conditioning units and topologies," *Renewable and Sustainable*

Energy Reviews, vol. 76. Elsevier Ltd, pp. 268–291, Sep. 01, 2017. doi: 10.1016/j.rser.2017.03.056.
[31] A. Papagianni, A. Kalfas, I. Aslanidou, M. D. Kavvalos, and K. Kyprianidis, "Conceptual Design of a Hybrid Gas Turbine-Solid Oxide Fuel Cell System for Civil Aviation."
[32] "First flight of DLR's HY4 fuel cell light aircraft," *Fuel Cells Bulletin*, vol. 2016, no. 10, p. 1, Oct. 2016, doi: 10.1016/s1464-2859(16)30261-9.
[33] R. O'Hayre, S. Cha, W. Colella, and F. B. Prinz, "Fuel Cell Fundamentals," *Fuel Cell Fundamentals*, May 2016, doi: 10.1002/9781119191766.
[34] A. Kirubakaran, S. Jain, and R. K. Nema, "A review on fuel cell technologies and power electronic interface", doi: 10.1016/j.rser.2009.04.004.
[35] "Global deployment of large capacity stationary fuel cells - Publications Office of the EU." Accessed: Mar. 13, 2024. [Online]. Available: https://op.europa.eu/en/publication-detail/-/publication/d5b49b34-6a28-11e9-9f05-01aa75ed71a1/language-en
[36] D. Rattazzi, M. Rivarolo, and A. F. Massardo, "An innovative tool for the evaluation and comparison of different fuels and technologies onboard ships," *E3S Web of Conferences*, vol. 238, p. 08001, Feb. 2021, doi: 10.1051/E3SCONF/202123808001.
[37] M. Rivarolo, D. Rattazzi, T. Lamberti, and L. Magistri, "Clean energy production by PEM fuel cells on tourist ships: A time-dependent analysis," *Int J Hydrogen Energy*, vol. 45, no. 47, pp. 25747–25757, Sep. 2020, doi: 10.1016/j.ijhydene.2019.12.086.
[38] M. Rivarolo, F. Iester, and A. F. Massardo, "An algorithm for comparative analysis of power and storage systems for maritime applications," *E3S Web of Conferences*, vol. 334, p. 06001, Jan. 2022, doi: 10.1051/E3SCONF/202233406001.
[39] "Think Hydrogen. Think Linde. | Linde Engineering." Accessed: Mar. 13, 2024. [Online]. Available: https://www.linde-engineering.com/en/index.html
[40] "Cryogenic Equipment Solutions | Cryogenic Dewars | Cryogenic Tanks | Cryogenic Hose." Accessed: Mar. 13, 2024. [Online]. Available: https://www.cryofab.com/
[41] "Cryogenics at its finest. Cryogenic engineering meets full service." Accessed: Mar. 13, 2024. [Online]. Available: https://www.cryotherminc.com/
[42] "Tracciatura gratuita del Traffico Marittimo - VesselFinder." Accessed: Mar. 13, 2024. [Online]. Available: https://www.vesselfinder.com/it
[43] S. Jafarzadeh and I. Schjølberg, "Operational profiles of ships in Norwegian waters: An activity-based approach to assess the benefits of hybrid and electric propulsion," 2018, doi: 10.1016/j.trd.2018.09.021.
[44] A. B. Stambouli and E. Traversa, "Fuel cells, an alternative to standard sources of energy," 2002. [Online]. Available: www.elsevier.com/locate/rser
[45] O. Z. Sharaf and M. F. Orhan, "An overview of fuel cell technology: Fundamentals and applications," *Renewable and Sustainable Energy Reviews*, vol. 32. pp. 810–853, Apr. 2014. doi: 10.1016/j.rser.2014.01.012.
[46] "Study on the use of fuel cells in shipping DNV GL 1 MARITIME STUDY ON THE USE OF FUEL CELLS IN SHIPPING."
[47] E. Gadducci, T. Lamberti, D. Bellotti, L. Magistri, and A. F. Massardo, "BoP incidence on a 240 kW PEMFC system in a ship-like environment, employing a

dedicated fuel cell stack model," *Int J Hydrogen Energy*, vol. 46, no. 47, pp. 24305–24317, Jul. 2021, doi: 10.1016/j.ijhydene.2021.04.192.
[48] O. B. Inal and C. Deniz, "Assessment of fuel cell types for ships: Based on multi-criteria decision analysis," *J Clean Prod*, vol. 265, Aug. 2020, doi: 10.1016/j.jclepro.2020.121734.
[49] E. Gadducci, T. Lamberti, M. Rivarolo, and L. Magistri, "Experimental campaign and assessment of a complete 240-kW Proton Exchange Membrane Fuel Cell power system for maritime applications," *Int J Hydrogen Energy*, vol. 47, no. 53, pp. 22545–22558, Jun. 2022, doi: 10.1016/j.ijhydene.2022.05.061.
[50] Wolf. Vielstich, Arnold. Lamm, H. A. (Hubert A. Gasteiger, and Harumi. Yokokawa, *Handbook of fuel cells : fundamentals, technology, and applications*. Wiley, 2003.
[51] M. Tekin, D. Hissel, M. C. Pera, and J. M. Kauffmann, "Energy consumption reduction of a PEM fuel cell motor-compressor group thanks to efficient control laws," *J Power Sources*, vol. 156, no. 1 SPEC. ISS., pp. 57–63, May 2006, doi: 10.1016/j.jpowsour.2005.08.037.
[52] S. Kang, K. Min, and S. Yu, "Dynamic modeling of a proton exchange membrane fuel cell system with a shell-and-tube gas-to-gas membrane humidifier," *Int J Hydrogen Energy*, vol. 37, no. 7, pp. 5866–5875, Apr. 2012, doi: 10.1016/j.ijhydene.2011.12.063.
[53] D. K. Kim *et al.*, "Efficiency improvement of a PEMFC system by applying a turbocharger," *Int J Hydrogen Energy*, vol. 39, no. 35, pp. 20139–20150, Dec. 2014, doi: 10.1016/j.ijhydene.2014.09.152.
[54] M. Cavo, E. Gadducci, D. Rattazzi, M. Rivarolo, and L. Magistri, "Dynamic analysis of PEM fuel cells and metal hydrides on a zero-emission ship: A model-based approach," *Int J Hydrogen Energy*, vol. 46, no. 64, pp. 32630–32644, Sep. 2021, doi: 10.1016/j.ijhydene.2021.07.104.
[55] M. Cavo, M. Rivarolo, L. Gini, and L. Magistri, "An advanced control method for fuel cells - Metal hydrides thermal management on the first Italian hydrogen propulsion ship," *Int J Hydrogen Energy*, vol. 48, no. 54, pp. 20923–20934, Jun. 2023, doi: 10.1016/j.ijhydene.2022.07.223.
[56] M. Cavo *et al.*, "Thermal integration of PEM Fuel Cells and metal hydrides storage system for Zero Emission Ultimate Ship (ZEUS)," in *E3S Web of Conferences*, EDP Sciences, Jan. 2022. doi: 10.1051/e3sconf/202233404004.
[57] L. P. Barchewitz and J. R. Seume, "Dynamic Modelling and Controls of an Air Supply System for In-Flight Proton Exchange Membrane Fuel Cells (PEM-FC)," *Proceedings of the ASME Turbo Expo*, vol. 3, pp. 363–372, Mar. 2009, doi: 10.1115/GT2007-27900.
[58] F. Iester, L. Mantelli, M. Bozzolo, L. Magistri, and A. F. Massardo, "Performance Assessment of an Innovative Turbocharged Proton-Exchange Membrane Fuel Cell System," *Proceedings of the ASME Turbo Expo*, vol. 5, Sep. 2023, doi: 10.1115/GT2023-103513.
[59] M. Cavo, L. Mantelli, S. Crosa, M. Bozzolo, and L. Magistri, "Modelling and Control System Development of a Turbocharged Proton-Exchange Membrane Fuel Cell

System," *Proceedings of the ASME Turbo Expo*, vol. 5, Sep. 2023, doi: 10.1115/GT2023-102571.
[60] T. E. Springer, T. A. Zawodzinski, and S. Gottesfeld, "Polymer Electrolyte Fuel Cell Model," *J Electrochem Soc*, vol. 138, no. 8, pp. 2334–2342, Aug. 1991, doi: 10.1149/1.2085971/XML.
[61] D. Murschenhofer, D. Kuzdas, S. Braun, and S. Jakubek, "A real-time capable quasi-2D proton exchange membrane fuel cell model," *Energy Convers Manag*, vol. 162, pp. 159–175, Apr. 2018, doi: 10.1016/J.ENCONMAN.2018.02.028.
[62] H. Xu, B. Chen, J. Liu, and M. Ni, "Modeling of direct carbon solid oxide fuel cell for CO and electricity cogeneration," *Appl Energy*, vol. 178, pp. 353–362, Sep. 2016, doi: 10.1016/j.apenergy.2016.06.064.
[63] A. B. Stambouli and E. Traversa, "Solid oxide fuel cells (SOFCs): A review of an environmentally clean and efficient source of energy," *Renewable and Sustainable Energy Reviews*, vol. 6, no. 5. pp. 433–455, 2002. doi: 10.1016/S1364-0321(02)00014-X.
[64] J. Palsson, A. Selimovic, and L. Sjunnesson, "Combined solid oxide fuel cell and gas turbine systems for efficient power and heat generation," *J Power Sources*, vol. 86, no. 1, pp. 442–448, Mar. 2000, doi: 10.1016/S0378-7753(99)00464-4.
[65] J. Milewski, A. Miller, and J. Sałaciński, "Off-design analysis of SOFC hybrid system," *Int J Hydrogen Energy*, vol. 32, no. 6, pp. 687–698, May 2007, doi: 10.1016/j.ijhydene.2006.08.007.
[66] M. Henke, J. Kallo, K. A. Friedrich, and W. G. Bessler, "Influence of pressurisation on SOFC performance and durability: A theoretical study," in *Fuel Cells*, 2011, pp. 581–591. doi: 10.1002/fuce.201000098.
[67] P. Breeze, *Power generation technologies*. Elsevier, 2019. doi: 10.1016/C2017-0-03267-6.
[68] C. Bao, Y. Wang, D. Feng, Z. Jiang, and X. Zhang, "Macroscopic modeling of solid oxide fuel cell (SOFC) and model-based control of SOFC and gas turbine hybrid system," *Progress in Energy and Combustion Science*, vol. 66. Elsevier Ltd, pp. 83–140, May 01, 2018. doi: 10.1016/j.pecs.2017.12.002.
[69] K. Hassmann, "SOFC Power Plants, the Siemens-Westinghouse Approach," *Fuel Cells*, vol. 1, no. 1, pp. 78–84, May 2001, doi: 10.1002/1615-6854(200105)1:1<78::aid-fuce78>3.0.co;2-q.
[70] U. M. Damo, M. L. Ferrari, A. Turan, and A. F. Massardo, "Solid oxide fuel cell hybrid system: A detailed review of an environmentally clean and efficient source of energy," *Energy*, vol. 168, pp. 235–246, Feb. 2019, doi: 10.1016/j.energy.2018.11.091.
[71] C. L. DeBellis, "DE-FE0031180 Final Report - LGFCS Prototype System Testing - R0," Pittsburgh, PA, and Morgantown, WV (United States), Jan. 2019. doi: 10.2172/1493425.
[72] Mitsubishi Power, "Fuel Cells - Hybrid System of Solid Oxide Fuel Cells (SOFC) and Micro Gas Turbines (MGT)." [Online]. Available: https://power.mhi.com/products/sofc

[73] I. Rossi, A. Sorce, and A. Traverso, “Gas turbine combined cycle start-up and stress evaluation: A simplified dynamic approach,” *Appl Energy*, vol. 190, pp. 880–890, 2017, doi: 10.1016/j.apenergy.2016.12.141.
[74] V. Zaccaria, D. Tucker, and A. Traverso, “Transfer function development for SOFC/GT hybrid systems control using cold air bypass,” *Appl Energy*, vol. 165, pp. 695–706, Mar. 2016, doi: 10.1016/J.APENERGY.2015.12.094.
[75] C. Stiller, B. Thorud, O. Bolland, R. Kandepu, and L. Imsland, “Control strategy for a solid oxide fuel cell and gas turbine hybrid system,” *J Power Sources*, vol. 158, no. 1, pp. 303–315, Jul. 2006, doi: 10.1016/j.jpowsour.2005.09.010.
[76] K. Hauptmeier, M. Penkuhn, and G. Tsatsaronis, “Economic assessment of a solid oxide fuel cell system for biogas utilization in sewage plants,” *Energy*, vol. 117, pp. 361–368, Dec. 2016, doi: 10.1016/j.energy.2016.05.072.
[77] A. Abrassi, A. Traverso, D. Tucker, and E. Liese, “Impact of Different Volume Sizes on Dynamic Stability of a Gas Turbine-Fuel Cell Hybrid System,” *J Eng Gas Turbine Power*, vol. 142, no. 5, May 2020, doi: 10.1115/1.4045482.
[78] U. M. Damo, M. L. Ferrari, A. Turan, and A. F. Massardo, “Test rig for hybrid system emulation: New real-time transient model validated in a wide operative range,” *Fuel Cells*, vol. 15, no. 1, pp. 7–14, 2015, doi: 10.1002/fuce.201400046.
[79] M. L. Ferrari, M. Pascenti, R. Bertone, and L. Magistri, “Hybrid simulation facility based on commercial 100 kWe micro gas turbine,” *J Fuel Cell Sci Technol*, vol. 6, no. 3, pp. 0310081–0310088, Aug. 2009, doi: 10.1115/1.3006200.
[80] D. Tucker, L. Lawson, and R. Gemmen, “Preliminary results of a cold flow test in a fuel cell gas turbine hybrid simulation facility,” in *American Society of Mechanical Engineers, International Gas Turbine Institute, Turbo Expo (Publication) IGTI*, American Society of Mechanical Engineers Digital Collection, Feb. 2003, pp. 281–287. doi: 10.1115/GT2003-38460.
[81] M. Hohloch, A. Huber, and M. Aigner, “Experimental investigation of a sofc/mgt hybrid power plant test rig - impact and characterization of a fuel cell emulator,” in *Proceedings of the ASME Turbo Expo*, American Society of Mechanical Engineers (ASME), Sep. 2016. doi: 10.1115/GT2016-57747.
[82] M. Metten, M. Tomberg, M. P. Heddrich, and K. A. Friedrich, “Analysis of experimental results of a Pressurized Solid Oxide Fuel Cell System simulating a Hybrid Power Plant”, doi: 10.1051/e3sconf/201911302007.
[83] S. R. Oh, J. Sun, H. Dobbs, and J. King, “Performance evaluation of solid oxide fuel cell engines integrated with single/dual-spool turbochargers,” *J Fuel Cell Sci Technol*, vol. 8, no. 6, Dec. 2011, doi: 10.1115/1.4004471.
[84] K. Lee, S. Kang, and K. Y. Ahn, “Development of a highly efficient solid oxide fuel cell system,” *Appl Energy*, vol. 205, pp. 822–833, Nov. 2017, doi: 10.1016/j.apenergy.2017.08.070.
[85] Honeywell, “2018 Global Turbo Forecast,” 2018.
[86] R. H. Staunton and B. Ozpineci, “MICROTURBINE POWER CONVERSION TECHNOLOGY REVIEW,” 2003.

[87] W. P. J. Visser, S. A. Shakariyants, and M. Oostveen, “Development of a 3 kW microturbine for CHP applications,” *J Eng Gas Turbine Power*, vol. 133, no. 4, 2011, doi: 10.1115/1.4002156.
[88] “Mitsubishi Power | Fuel Cells.” Accessed: Mar. 18, 2024. [Online]. Available: https://power.mhi.com/products/sofc
[89] M. Liu, A. Lanzini, W. Halliop, V. R. M. Cobas, A. H. M. Verkooijen, and P. V. Aravind, “Anode recirculation behavior of a solid oxide fuel cell system: A safety analysis and a performance optimization,” *Int J Hydrogen Energy*, vol. 38, no. 6, pp. 2868–2883, Feb. 2013, doi: 10.1016/j.ijhydene.2012.12.070.
[90] K. Venkataraman, E. C. Wanat, and L. D. Schmidt, “Steam reforming of methane and water-gas shift in catalytic wall reactors,” *AIChE Journal*. 2003. doi: 10.1002/aic.690490518.
[91] A. Traverso, “TRANSEO code for the dynamic performance simulation of micro gas turbine cycles,” in *Proceedings of the ASME Turbo Expo*, 2005, pp. 45–54. doi: 10.1115/GT2005-68101.
[92] L. Magistri, R. Bozzo, P. Costamagna, and A. F. Massardo, “Simplified versus detailed solid oxide fuel cell reactor models and influence on the simulation of the design point performance of hybrid systems,” *J Eng Gas Turbine Power*, vol. 126, no. 3, 2004, doi: 10.1115/1.1719029.
[93] A. Greco, A. Sorce, R. Littwin, P. Costamagna, and L. Magistri, “Reformer faults in SOFC systems: Experimental and modeling analysis, and simulated fault maps,” *Int J Hydrogen Energy*, vol. 39, no. 36, 2014, doi: 10.1016/j.ijhydene.2014.09.063.
[94] A. Sorce, A. Greco, L. Magistri, and P. Costamagna, “FDI oriented modeling of an experimental SOFC system, model validation and simulation of faulty states,” *Appl Energy*, vol. 136, 2014, doi: 10.1016/j.apenergy.2014.03.074.
[95] M. L. Ferrari, M. De Campo, and L. Magistri, “Design and emulation of a turbocharged bio-fuelled sofc plant,” in *Proceedings of the ASME Turbo Expo*, 2018. doi: 10.1115/GT201875026.
[96] M. L. Ferrari, M. Pascenti, and A. F. Massardo, “Ejector model for high temperature fuel cell hybrid systems: Experimental validation at steady-state and dynamic conditions,” *J Fuel Cell Sci Technol*, vol. 5, no. 4, 2008, doi: 10.1115/1.2890102.
[97] A. Traverso, A. F. Massardo, and R. Scarpellini, “Externally Fired micro-Gas Turbine: Modelling and experimental performance,” *Appl Therm Eng*, vol. 26, no. 16, 2006, doi: 10.1016/j.applthermaleng.2006.01.013.
[98] M. Gallo, D. Kaza, F. D’Agostino, M. Cavo, R. Zaccone, and F. Silvestro, “Power plant design for all-electric ships considering the assessment of carbon intensity indicator,” *Energy*, vol. 283, p. 129091, Nov. 2023, doi: 10.1016/J.ENERGY.2023.129091.
[99] W. L. Becker, R. J. Braun, M. Penev, and M. Melaina, “Design and technoeconomic performance analysis of a 1 MW solid oxide fuel cell polygeneration system for combined production of heat, hydrogen, and power,” *J Power Sources*, vol. 200, 2012, doi: 10.1016/j.jpowsour.2011.10.040.

[100] J. Jia, Q. Li, M. Luo, L. Wei, and A. Abudula, “Effects of gas recycle on performance of solid oxide fuel cell power systems,” *Energy*, vol. 36, no. 2, 2011, doi: 10.1016/j.energy.2010.12.001.
[101] A. Afif, N. Radenahmad, Q. Cheok, S. Shams, J. H. Kim, and A. K. Azad, “Ammonia-fed fuel cells: a comprehensive review,” *Renewable and Sustainable Energy Reviews*, vol. 60, pp. 822–835, Jul. 2016, doi: 10.1016/J.RSER.2016.01.120.
[102] G. A. Birken, P. J. Fabri, and L. C. Carey, “Acute ammonia intoxication complicating multiple trauma,” *J Trauma*, vol. 21, no. 9, pp. 820–822, 1981, doi: 10.1097/00005373-198109000-00015.
[103] H. Jang *et al.*, “Regulatory gap analysis for risk assessment of ammonia-fuelled ships,” *Ocean Engineering*, vol. 287, p. 115751, Nov. 2023, doi: 10.1016/J.OCEANENG.2023.115751.
[104] S. S. Rathore, S. Biswas, D. Fini, A. P. Kulkarni, and S. Giddey, “Direct ammonia solid-oxide fuel cells: A review of progress and prospects,” *International Journal of Hydrogen Energy*, vol. 46, no. 71. Elsevier Ltd, pp. 35365–35384, Oct. 14, 2021. doi: 10.1016/j.ijhydene.2021.08.092.
[105] G. Cinti, G. Discepoli, E. Sisani, and U. Desideri, “SOFC operating with ammonia: Stack test and system analysis,” *Int J Hydrogen Energy*, vol. 41, no. 31, pp. 13583–13590, 2016, doi: 10.1016/j.ijhydene.2016.06.070.
[106] M. Ni, D. Y. C. Leung, and M. K. H. Leung, “Mathematical modeling of ammonia-fed solid oxide fuel cells with different electrolytes,” *Int J Hydrogen Energy*, vol. 33, no. 20, pp. 5765–5772, Oct. 2008, doi: 10.1016/j.ijhydene.2008.07.021.
[107] Q. Ma, J. Ma, S. Zhou, R. Yan, J. Gao, and G. Meng, “A high-performance ammonia-fueled SOFC based on a YSZ thin-film electrolyte,” *J Power Sources*, vol. 164, no. 1, pp. 86–89, Jan. 2007, doi: 10.1016/j.jpowsour.2006.09.093.
[108] S. S. Shy, S. C. Hsieh, and H. Y. Chang, “A pressurized ammonia-fueled anode-supported solid oxide fuel cell: Power performance and electrochemical impedance measurements,” *J Power Sources*, vol. 396, pp. 80–87, Aug. 2018, doi: 10.1016/j.jpowsour.2018.06.006.
[109] A. Perna, M. Minutillo, E. Jannelli, V. Cigolotti, S. W. Nam, and J. Han, “Design and performance assessment of a combined heat, hydrogen and power (CHHP) system based on ammonia-fueled SOFC,” *Appl Energy*, vol. 231, pp. 1216–1229, Dec. 2018, doi: 10.1016/j.apenergy.2018.09.138.
[110] Y. T. Hung and S. S. Shy, “A pressurized ammonia-fed planar anode-supported solid oxide fuel cell at 1–5 atm and 750–850°C and its loaded short stability test,” *Int J Hydrogen Energy*, vol. 45, no. 51, pp. 27597–27610, Oct. 2020, doi: 10.1016/j.ijhydene.2020.07.064.
[111] O. Siddiqui and I. Dincer, “A review and comparative assessment of direct ammonia fuel cells,” *Thermal Science and Engineering Progress*, vol. 5, pp. 568–578, Mar. 2018, doi: 10.1016/j.tsep.2018.02.011.
[112] D. S. Dhawale, S. Biswas, G. Kaur, and S. Giddey, “Challenges and advancement in direct ammonia solid oxide fuel cells: a review,” *Inorg Chem Front*, vol. 10, no. 21, pp. 6176–6192, Oct. 2023, doi: 10.1039/D3QI01557B.

[113] M. Ilbas, B. Kumuk, M. A. Alemu, and B. Arslan, “Numerical investigation of a direct ammonia tubular solid oxide fuel cell in comparison with hydrogen,” *Int J Hydrogen Energy*, vol. 45, no. 60, pp. 35108–35117, Dec. 2020, doi: 10.1016/j.ijhydene.2020.04.060.
[114] J. Yang, A. F. S. Molouk, T. Okanishi, H. Muroyama, T. Matsui, and K. Eguchi, “A Stability Study of Ni/Yttria-Stabilized Zirconia Anode for Direct Ammonia Solid Oxide Fuel Cells,” *ACS Appl Mater Interfaces*, vol. 7, no. 51, pp. 28701–28707, Dec. 2015, doi: 10.1021/ACSAMI.5B11122.
[115] Y. Luo *et al.*, “Coupling ammonia catalytic decomposition and electrochemical oxidation for solid oxide fuel cells: A model based on elementary reaction kinetics,” *J Power Sources*, vol. 423, pp. 125–136, May 2019, doi: 10.1016/j.jpowsour.2019.03.064.
[116] Y. Kalinci and I. Dincer, “Analysis and performance assessment of NH3 and H2 fed SOFC with proton-conducting electrolyte,” *Int J Hydrogen Energy*, vol. 43, no. 11, pp. 5795–5807, Mar. 2018, doi: 10.1016/j.ijhydene.2017.07.234.
[117] J. B. Hansen and P. V. Hendriksen, “The SOC4NH3 project. Production and use of ammonia by solid oxide cells,” *ECS Trans*, vol. 91, no. 1, pp. 2455–2465, Jul. 2019, doi: 10.1149/09101.2455ECST.
[118] K. H. M. Al-Hamed and I. Dincer, “A new direct ammonia solid oxide fuel cell and gas turbine based integrated system for electric rail transportation,” *eTransportation*, vol. 2, Nov. 2019, doi: 10.1016/j.etran.2019.100027.
[119] S. Di Micco, M. Minutillo, L. Mastropasqua, V. Cigolotti, and J. Brouwer, “Ammonia-based Solid Oxide Fuel Cell for zero emission maritime power: a case study”, doi: 10.1051/e3sconf/202233406007.
[120] O. A. Ojelade and S. F. Zaman, “Ammonia decomposition for hydrogen production: a thermodynamic study,” *Chemical Papers*, vol. 75, no. 1, pp. 57–65, Jan. 2021, doi: 10.1007/S11696-020-01278-Z.
[121] G. Jeerh, M. Zhang, and S. Tao, “Recent progress in ammonia fuel cells and their potential applications,” *J Mater Chem A Mater*, vol. 9, no. 2, pp. 727–752, Jan. 2021, doi: 10.1039/D0TA08810B.
[122] D. Cheddie and D. Cheddie, “Ammonia as a Hydrogen Source for Fuel Cells: A Review,” *Hydrogen Energy - Challenges and Perspectives*, Oct. 2012, doi: 10.5772/47759.
[123] A. W. LOGINOW and E. H. PHELPS, “Stress-Corrosion Cracking of Steels In Agricultural Ammonia,” *Corrosion*, vol. 18, no. 8, pp. 299t–309t, Aug. 1962, doi: 10.5006/0010-9312-18.8.299.
[124] D. S. Dhawale, S. Biswas, G. Kaur, and S. Giddey, “Challenges and advancement in direct ammonia solid oxide fuel cells: a review,” *Inorg Chem Front*, vol. 10, no. 21, pp. 6176–6192, Oct. 2023, doi: 10.1039/D3QI01557B.
[125] C. Zamfirescu and I. Dincer, “Using ammonia as a sustainable fuel,” *J Power Sources*, vol. 185, no. 1, pp. 459–465, Oct. 2008, doi: 10.1016/j.jpowsour.2008.02.097.